Theses and Dissertations

Fall 2014

Risk assessment for drug degradation products using physiologically-based pharmacokinetic models

Quynh Hoa Nguyen
University of Iowa

RISK ASSESSMENT FOR DRUG DEGRADATION PRODUCTS USING PHYSIOLOGICALLY-BASED PHARMACOKINETIC MODELS

by

Quynh Hoa Nguyen

A thesis submitted in partial fulfillment
of the requirements for the Doctor of
Philosophy degree in Pharmacy
in the Graduate College of
The University of Iowa

December 2014

Thesis Supervisor: Professor Lee E. Kirsch

CERTIFICATE OF APPROVAL

_____

PH.D. THESIS

_____

This is to certify that the Ph.D. thesis of

Quynh Hoa Nguyen

has been approved by the Examining Committee
for the thesis requirement for the Doctor of Philosophy
degree in Pharmacy at the December 2014 graduation.

Thesis Committee: _____
                   Lee E. Kirsch, Thesis Supervisor

                   _____
                   Maureen D. Donovan

                   _____
                   Aliasger K. Salem

                   _____
                   Jonathan A. Doorn

                   _____
                   Stephen D. Stamatis

To my parents and my beloved family, Trung Nguyen, Tri Nguyen and San Nguyen

The purpose of models is not to fit the data, but to sharpen the questions.

Samuel Karlin (1924), Evolutionary Geneticist

ACKNOWLEDGMENTS

Cuong and Hang.

Above all, none of this would have been possible without the love and encouragement of my family. My late parents, even without their presence, always cared and stood by me. My husband, with his constant source of love, was always there to cheer me up, supported me through the good and bad times. Words cannot express my love for my children, Tri and San, who are the motivation and joy of my life.

ABSTRACT

Degradation product toxicity is a critical quality issue for a small group of useful drug products—e.g. lidocaine, isoniazid, chlorhexidine, gabapentin. In the traditional risk assessment approaches, a no-observed-adverse-effect level (NOAEL) derived from animal data is determined with the use of generic (and arbitrary) uncertainty factors to obtain an acceptable daily intake. The effects of compound-specific biological complexities and pharmacokinetics are typically not part of the risk calculations. The selection of uncertainty factors that account for interspecies or intraspecies difference concerning biokinetics and biodynamics has also generally failed to consider chemical-specific mechanism information or pharmacokinetics data. The use of combining *in-vitro* biopharmaceutical characterization methods and physiologically-based pharmacokinetic modeling has undergone extensive study and validation for predicting clinical drug blood level time profiles. The rationale for the proposed research is that a PBPK modeling utilizing rat to human scaling for target tissue toxicity in combination with the Monte Carlo method for estimating human target exposure distributions provides a rational basis for assessing drug stability safety issues for drug substances that potentially degrade to toxic compounds.

PBPK models for rats and humans were developed to simulate drug exposure time profiles after oral administration of model compounds including aniline, p-chloroaniline, 2,6-xylidine, o-toluidine and p-aminophenol. The PBPK models were parameterized using a combination of literature values, computational models and standard in vitro experiments. Microsomal and hepatocyte metabolism studies were used to estimate the metabolic constants, and ultrafiltration was used to measure protein binding. Intestinal permeability was predicted using a set of related compound data to correlate measured Caco-2 permeability with molecular descriptors by multivariate regression. Sensitivity analyses were conducted to evaluate the impact of PBPK model parameters on plasma level predictions. To evaluate patient population effects on exposure profiles, the PBPK model parameters were varied in meaningful ways using Monte Carlo methods. Based on

population PBPK models, distributions of target tissue exposure in rats and humans were simulated and compared to derive human safe dose.

   As results, rat PBPK model-predicted aniline concentration time profiles were in reasonable agreement with published profiles. Distributions of target tissue exposure in rats and humans were generated and compared based on a criterion. A human reference dose was then selected at a value of 1% criteria. This approach was compared to traditional risk assessment calculations. In conclusion, the PBPK modeling approach resulted in drug degradation product risk specifications that were less stringent than those estimated by conventional risk assessment approach. The PBPK modeling approach provides a rational basis for drug instability risk assessment by focusing on target tissue exposure and leveraging physiological, biochemical, biophysical knowledge of compounds and species.

PUBLIC ABSTRACT

Patient safety risk due to toxic degradation products is a potentially critical quality issue for a small group of useful drug products (e.g. lidocaine, isoniazid, chlorhexidine, gabapentin). In recent years toxicity of unwanted components that remain with the active pharmaceutical ingredients, or arise during the manufacturing process and/or storage of the drug substance have received considerable attention industrial and regulatory scientists. Although the time course of potential toxic degradants in body will strongly affect product safety, these data are frequently unavailable in animal and impossible to safely obtain in human. The objective of this study is to incorporate the use of physiologically-based pharmacokinetic (PBPK) models in rats and humans for the development of rational degradant risk assessment procedures using a series of model drug degradants (substituted anilines). The PBPK models were parameterized using a combination of literature values, computational methods and standard experiments. Microsomal and hepatocyte metabolism studies were used to estimate the metabolic constants, and ultrafiltration was used to measure protein binding. The impact of the uncertainties and variability in parameter values on model predictions were analyzed. Human safe doses for model compounds were selected based on the comparison between predicted rat target tissue exposure at critical dose and human exposure at a series of predetermined doses. This approach was compared to traditional risk assessment calculations.

In conclusion, the PBPK modeling approach provides a rational basis for drug instability risk assessment by focusing on target tissue exposure and leveraging physiological, biochemical, biophysical knowledge of compounds and species.

TABLE OF CONTENTS

LIST OF TABLES

LIST OF FIGURES

CHAPTER 1.   INTRODUCTION

1.1. Potential risks of drug instability

A fundamental requirement for the licensure of pharmaceutical products is that their quality attributes (including potency and purity) are maintained throughout their manufacturing, shipping and storage. A drug substance may generate toxic impurities via hydrolytic and/or oxidative degradation, whereby, not only the rate of drug potency loss but also the rate of degradant accumulation and the potential safety/toxicity risks may be critical drug product stability determinants.

1.1.1. Concept of alerting structures

According to European Medicines Agency guideline (1) and U.S. FDA draft guidance (2), the use of chemical structural assessment is a valid means to predict the toxicity potential of drug impurities, including degradants. The concept of structural alerts was first elucidated by Ashby and Tennant (3-6) who investigated the correlation between chemical structure and DNA activity for about 300 compounds based on a Salmonella carcinogenicity assay. According to Ashby, structural alerts are structural features of a compound that correlate to carcinogenicity. They include primary or secondary aromatic amines (e.g. anilines, benzidines, 2-naphthylamine and its analogues), epoxides (e.g. ethylene oxide, styrene oxide), nitrosamines, hydrazines or azoxyalkyl compounds. Based on alerting structural analysis, Raillard and coworkers (7) conducted a study using a drug degradation database to evaluate the potential genotoxicity that may arise as a result of drug degradation. Approximately 70% of the structural alerts found in the degradant database were aldehydes, α,β-unsaturated carbonyls and primary aromatic amines.

For example, the primary degradant of acetaminophen was determined to be p-aminophenol (PAP) which contains a structural alert for an aromatic amine (8).

Consequently, the quantity of PAP is strictly controlled because of potential nephrotoxicity (9-12). Quantification of PAP is described in US Pharmacopeia (USP) 32–NF27 and limited to a level of 0.005% in acetaminophen bulk substance (13). The limits for PAP may vary in different products depending on the dosage form and formulation; the monograph of paracetamol tablets in British Pharmacopoeia (BP) allows 0.1% (14).

Chlorhexidine is an antiseptic antibacterial agent that can generate p-chloroaniline (PCA) via hydrolysis in aqueous solution (15, 16). The International Agency for Research on Cancer (IARC, 2006) categorizes PCA in their 2B Group, which means that this agent is possibly carcinogenic to humans (17). Chhabra and coworkers (18, 19) investigated toxicity of PCA in rats and mice and observed lesions in animals' kidney, spleen and liver. Toxicological profiles of PCA were also studied by other authors (20, 21) and indicate its primary toxicities include splenic fibrosis and sarcomas. Therefore, the limit of PCA in chlorhexidine gluconate oral rinse is set as 3 ppm by USP32-NF27 (13).

There are various commercially-available anesthetic products containing lidocaine, prilocaine, buvacaine, mepivacaine, or ropivacaine as active substances. During the storage of lidocaine preparations, 2,6-dimethylaniline (2,6-DMA), a potential carcinogenic agent (22-25), can be formed by lidocaine hydrolysis involving an intramolecular base-catalysis mechanism (26). Similarly, o-toluidine (o-TOL) can appear as a decomposition product during storage of drugs containing prilocaine (27). o-TOL can oxidize hemoglobin to methemoglobin and is known to cause bladder/spleen cancer in animal studies (28-30). By using electrochemical detection, Fijalek and coworkers (27, 31) developed an analytical method to determine low concentrations of 2,6-DMA and o-TOL based on their anodic oxidation reaction in various local anesthetic preparations. Quantification of the 2,6-DMA impurity in anesthetic products is also described by the European and British Pharmacopoeias. The BP 2003 allows for lidocaine and

bupivacaine injections and gels to contain not more than 400 ppm of 2,6-DMA, while for prilocaine, contents of o-TOL is limited to 1% of the active substance (27).

Other potentially toxic aromatic amines arising from the degradation of drug substances include 4-nitro-trifluoromethyl-aniline from non-steroidal anti-androgen flutamide (32) and 2,6-dichloroaniline from oxidative degradation of diclofenac (33-35).

1.1.2. Regulatory considerations

According to the International Conference on Harmonization (ICH) guidelines (36), impurities in pharmaceuticals are components that remain with the active pharmaceutical ingredients, or arise during the manufacturing process and/or storage of the drug substance. The performance of the pharmaceutical products may be influenced by the presence of these impurities, even in small amounts. The ICH and FDA have published guidelines for the identification and qualification of impurities in new drug substances and drug products (36-38). According to the guidelines, impurities can be characterized as organic or inorganic impurities and residual solvents. Organic impurities may include impurities in starting synthesis materials, synthesis by-products, degradation products and intermediates. For degradation products, the ICH Guidance Q3B (R2) (37) provides recommendations for reporting, control, identification and qualification in drug products. The critical values for *reporting, identifying and qualifying* impurities vary based on drug dosing regimens, and are shown in Table 1.1 (37).

Table 1.1- Thresholds for degradation products in new drug products

Reporting Thresholds

Maximum daily dose	Threshold
≤ 1 g	0.1%
> 1 g	0.05%

Table 1.2- Continued

Identification Thresholds

Maximum daily dose	Threshold
< 1 mg	1.0% or 5 µg TDI, whichever is lower
1 mg - 10 mg	0.5% or 20 µg TDI, whichever is lower
>10 mg - 2 g	0.2% or 2 mg TDI, whichever is lower
>2 g	0.10%

Qualification Thresholds

Maximum daily dose	Threshold
< 10 mg	1.0% or 50 µg TDI, whichever is lower
10 mg - 100 mg	0.5% or 200 µg TDI, whichever is lower
> 100 mg - 2 g	0.2% or 3 mg TDI, whichever is lower
> 2 g	0.15%

TDI: total daily intake of the degradation product

The critical value for *reporting* impurities ranges from 0.05% to 0.1%, and reporting an impurity may or may not require identification.

Identification is required for any degradation product observed in stability studies present at a level greater than the identification threshold. Identification requires assignment of a specific chemical composition of the impurity. The critical value for identification is typically between 0.1% and 0.5% depending on the daily drug dose. For low dose drugs (< 1mg per day), the identification threshold is 1% of the total daily intake (TDI) or 5 µg (whichever is lower).

Qualification is the process of evaluating safety data and establishing acceptance criteria for a degradation product. A degradation product should be qualified if it exceeds the limit which is the qualification threshold. Depending on the maximum daily dose, the critical range of the qualification threshold ranges from 0.15% to 1%.

As an example shown in Table 1.2, a drug product wherein the total daily dose was 50 mg is considered. In this case, the reporting, identification and qualification thresholds would be 50, 100 and 200 µg, respectively. In this hypothetical example, an

analytical procedure revealed the presence of four drug degradation products (A, B, C and D) with their corresponding analytical results listed in column 2 of Table 1.2. In this scenario, compound B, C and D appeared at levels greater than the reporting threshold; hence they require reporting in the registration application using conventional rules of rounding. Compound C and D require identification; therefore their chemical structure needs to be identified. Compound D requires qualification based on toxicity data in preclinical studies and/or a demonstration of clinical safety at the selected qualification threshold.

Table 1.3- Example of reporting, identifying and qualifying degradation products

Degradant	Amount observed (%)	TDI (rounded to μg)	Action		
			Reporting (Action, Result)	Identifying	Qualifying
A	0.04	20	No	No	No
B	0.2121	100	Yes, 0.2%	No	No
C	0.325	150	Yes, 0.3%	Yes	No
D	0.63	300	Yes, 0.6%	Yes	Yes

For a given degradation product, its acceptance criteria (allowable level) should be established no higher than its qualified level and along with safety considerations (38). In some cases, if the qualification thresholds are exceeded and adequate data are unavailable to qualify the degradation product, additional studies should be conducted on the drug product containing the degradant or isolated degradation products.

The guidance from FDA and ICH provides a convenient approach to control drug degradation products. However, it does not provide a rationale for establishing degradation product acceptance criteria for those exceeding qualification thresholds or for potentially toxic compounds.

1.2.Toxicity-based risk assessment

1.2.1 Traditional risk assessment

The goal of toxicity testing is to minimize potential adverse health impacts by setting safe human exposure levels for potentially toxic compounds. In the qualification of drug impurities, toxicity tests may include general toxicity or genotoxicity in animal models (38). The type of general toxicity tests may range from acute to subchronic and chronic studies. Traditionally, animal studies have served as the basis for most quantitative risk analysis and require interspecies extrapolation for human health evaluation. In the standard paradigm for non-cancer risk assessment, test animals are assigned to treatment (dose – level) and control groups. Dose amounts and route of administration are consistent with the intended use of the drug for humans. For each group, toxicity indicators such as body weight, biochemical parameters (e.g. albumin, glucose, and bilirubin) or adverse biological effects are measured. The result of a typical dose-response experiment is illustrated in Figure 1.1 wherein the percent of animals with critical adverse effect is displayed as function of different doses of toxicant. The statistically significant responses are determined by comparison of each treatment group to the control group. In Figure 1, point B is the highest non-statistically significant treatment group response compared with control group response, hence it is designated as the "no observed adverse effect level" (NOAEL) and in this hypothetical example, occurs at approximately 0.1 mg/kg body weight (39).

Reference dose (RfD) is the maximum acceptable human dose of a toxic substance calculated from NOAEL value in animals using the following Equation 1.1 (39):

$$RfD = \frac{NOAEL}{UF_1 \times UF_2 \times UF_{other}} \qquad (Eq.1.1)$$

6

Various uncertainty factors (UF_1, UF_2, UF_{other}) are used to account for potential sources of variability such as extrapolation from animals to humans, human population variability, extrapolation from short to long duration of exposure duration and database limitations due to experimental design or analytical techniques (40). Typically, each uncertainty factor is arbitrarily assigned a numerical value; a value of 10 is common. The selection of uncertainty factors typically does not consider chemical-specific toxicity mechanisms or pharmacokinetic data (40).
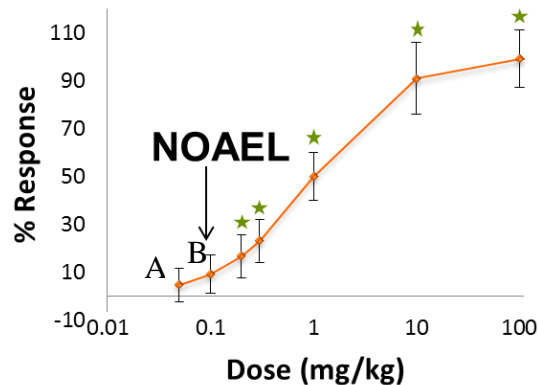
Figure 1.1- Hypothetical dose response curve. Points indicate mean responses at different doses. Symbol "☆" indicates responses for treatment groups that are statistically different than control group response

In the traditional paradigm for cancer risk assessment, dose–response modeling is used to calculate a carcinogenic potency based on tumor growth observed in animal bioassays. Quantitatively, in the guidelines for Carcinogen Risk Assessment by U.S.EPA (2005) (41), curve fitting is used on the animal bioassay data to estimate a point of departure (POD) (typically a 10% response) near the lower end of the observed range of the data to mark the beginning of extrapolation to lower doses. The extrapolation can be done with a linear or a non-linear model. When the mode of action information suggests

that the shape of the dose-response curve below the POD is linear, then linear extrapolation should be used. A linear extrapolation is conducted by drawing a straight line to the origin and calculating the unit risk at any given dose. Risk estimate using the linear low dose extrapolation is shown in Figure 1.2.
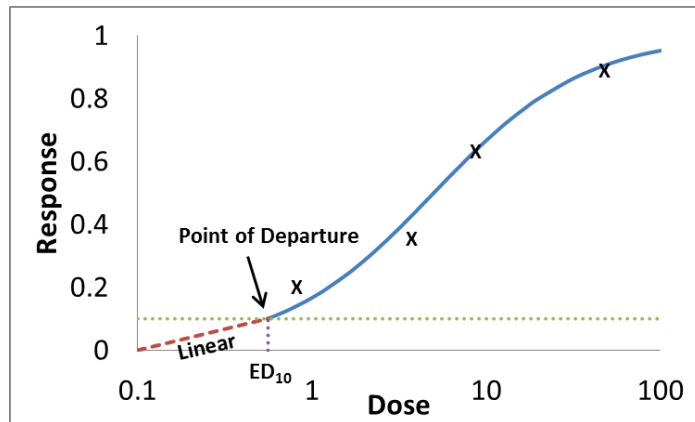
Figure 1.2- Linear low-dose extrapolation approach
from dose–response model

The extrapolation from the POD can also be done with the non-linear model which considers the overall database to determine if inclusion of an uncertainty factor is needed and to determine a safety margin between the estimated exposure level and the POD. In the case of insufficient data, linear extrapolation is used as a default approach and generally is recognized as a conservative and health–protective approach (42). Either linear extrapolation or non-linear threshold analysis approach for cancer risk assessment may require additional considerations of variability of the human population compared to the experimental animal population. The extrapolation of cancer response across doses, species, and routes continues to represent a challenge (42).

1.2.2 Uncertainty factor estimation

Until recently, drug/chemical risk assessment has relied on the traditional approach using uncertainty factors which can be applied across wide variety of

8

xenobiotics. As previously stated, these methods include little to no information about its chemical properties or toxicity mechanisms and require a number of conservative assumptions, estimates and rationalizations (43). It is generally recognized that inclusion of chemical–specific factors including pharmacokinetics, mechanism of toxicity and target population properties could significantly impact the risk estimates (44, 45).

In traditional risk assessment, 100-fold uncertainty factor is commonly applied to the NOAEL to derive safe levels of exposure in humans. This 100-fold safety factor consists of the product of two 10-fold factors for human variability and interspecies differences. The applicability of the default value of 10 for all xenobiotics, regardless of the extent of available information, to account for population variability in toxicokinetics, toxicodynamics or mode of action, lacks a clearly defined scientific basis. In an attempt to leverage available scientific data in a dose-response assessment, the International Program on Chemical Safety (46, 47) suggested the subdivision of these 10-fold factors to allow for variability in toxicokinetics and toxicodynamics. Values of $10^{0.6}$ (4) and $10^{0.4}$ (2.5), were proposed by Renwick (48) for species differences based on the analysis of small database, and equal values of $10^{0.5}$ (3.16) for human variability were adopted by a WHO task group on environmental health (46, 47). The aim of this subdivision of the 10-fold factors was to allow toxicokinetics and toxicodynamics to be considered separately and also to allow the incorporation of suitable chemical-specific data for one particular aspect of uncertainty to replace the relevant part of the overall default uncertainty factor (48). Recently, the analysis of Walton and coworkers (49) has suggested that the current interspecies toxicokinetic default uncertainty factor of 4.0 is inadequate for species differences due to the wide variability between both compounds and the individual species. This analysis indicated that there are significant differences between humans and the test species in the metabolic kinetics of investigated compounds, enzymes involved in the metabolic reactions, the route of excretion and oral bioavailability. These factors are

determinants that can influence the extent of the difference between humans and a test species in the target tissue dose of a toxicant. Ultimately this work supports the substitution of uncertainty factors from the risk assessment process by the use of compound-specific data (49).

Aside from the uncertainty associated with interspecies scaling, another challenging issue is the heterogeneity of the human population. This heterogeneity is produced by inter-individual variations in physiology, biochemistry, and molecular biology, and results in differences among individuals in the target tissue dose associated with exposure (pharmacokinetics) as well as the time-dependent response to a given tissue dose (pharmacodynamics) (45).

According to the IPCS framework, the factor of 10 can be subdivided by 3.16 to account for human variability in toxicokinetics, and another 3.16 to account for variability in dynamics (50). If there are adequate chemical-specific pharmacokinetic and pharmacodynamic data, they can be incorporated and replace these default uncertainty factors to better characterize human variability in dose–response assessment. Renwick and colleagues (51) used an extensive database to investigate the adequacy of the 10-fold factor and its subdivision for human variability. Data for the kinetics and clinical responses of 60 compounds were tabulated and the coefficients of variation were averaged for different studies. As a conclusion, analysis of kinetic data for subgroups of the population indicates that the standard default value of 3.16 for kinetics is not adequate for all subpopulations. The authors suggested that the uncertainty factor for inter-individual variability in kinetics could be selected based on the best information available. The standard default of 3.16 should be used only in the absence of relevant toxicokinetic information.

A recent approach has been developed to replace the default uncertainty factors using the pharmacokinetic and metabolism literature wherein compounds are classified

according to their metabolic route so that pathway-related uncertainty factors can be derived for interspecies and human variability. These pathway–related uncertainty factors were derived using probe substrates for the major human phase I metabolism (52), phase II conjugation reactions (53) and renal excretion (54). As a result, the magnitude of internal dose differences between species was found to exceed the four-fold default value in some cases (e.g. mouse, 10.6; rat, 5.4) and to be less than the default value in other cases (e.g. rabbit, 2.6; dog, 1.6) (52). Similarly, for compounds which are eliminated primarily by renal excretion in humans, the differences between humans and mice may exceed the four-fold default factor for toxicokinetics (54).

The uncertainty factors due to human variability were investigated by Dorne and Renwick (55) for substrates of phase I and phase II metabolism and renal excretion. The authors observed the human variability factors to be below the default uncertainty factor with a range between 1.6 and 2.2 for all pathways.

1.2.3 PBPK – based risk assessment

Quantitative methodologies that incorporate xenobiotic-specific pharmacokinetic data have been used in risk assessment. In particular, the application of physiologically-based pharmacokinetic (PBPK) modeling for toxicology risk assessment has been advocated as an alternative to traditional methods. The motivation for using PBPK models in risk assessment is to leverage knowledge about the biology of the test species and compound–specific properties into risk calculations, thereby reducing uncertainty in the human risk estimates. Moreover, because the parameters in a PBPK model have a biological correspondence, they provide a useful framework for evaluating the impact of physiological and pharmacokinetic factors on the variability of individual risks (56).

The use of internal dose or tissue exposure dose, instead of the administered dose, has been advocated as a way to provide better characterization of the dose-response relationship for toxic compounds (42, 57). Implementation of PBPK models in risk

11

assessment has been described elsewhere (40, 50, 57-59) and can be illustrated in the flowchart below:


```
┌─────────────────────────────────────┐
│        Problem Identification        │
└─────────────────────────────────────┘
                   ↓
┌─────────────────────────────────────────────────────┐
│              Available Data Evaluation                │
│  - The nature of the critical toxic effect            │
│  - The dose-response relationship for the critical    │
│    toxic effect                                       │
│  - Mode of action and nature of toxic moiety          │
│  - Processes involved in ADME of toxic moiety         │
│  - Biochemical characteristics of toxic moiety and    │
│    physiology of                                      │
└─────────────────────────────────────────────────────┘
                   ↓
┌─────────────────────────────────────────────────────┐
│      Model Structure and Parameter Specification      │
└─────────────────────────────────────────────────────┘
                   ↓
┌──────────────────┐  ┌─────────────────────────────────────┐
│ Model Refinement │  │ Mathematical and Computational       │
│                  │  │ Implementation                       │
└──────────────────┘  └─────────────────────────────────────┘
                   ↓
┌─────────────────────────────────────┐
│    Simulation of Toxic Moiety Exposure │
└─────────────────────────────────────┘
                   ↓
┌─────────────────────────────────────┐
│            Model Validation           │
└─────────────────────────────────────┘
                   ↓
┌─────────────────────────────────────┐
│           Model Application           │
└─────────────────────────────────────┘
```

One of the first PBPK models used for risk assessment extrapolations was developed for methylene chloride (60). This model was used to predict tissue exposures to highly reactive metabolites from oxidative and conjugative pathways resulting from several different exposure scenarios for both mice and humans. In this application, the tumor incidence was correlated with the amount of metabolites formed from the conjugative pathway. The PBPK analysis suggests that conventional risk analyses greatly overestimate the risk in humans to exposure from low methylene chloride concentrations.

Another example of a PBPK-based approach for environmental toxicants risk analysis was described by Leung and Paustenbach using 1,4-dioxane as a model

12

compound (61). The authors developed PBPK models for 1,4-dioxane to describe the time course of 1,4-dioxane in the blood and four tissue compartments for rats and humans receiving oral doses via drinking water. Due to the saturable metabolism of dioxane in both the rat and human, at low doses the metabolism appears to follow first-order kinetics, while at high doses the proportion of unmetabolized dioxane is increased. Nonlinear pharmacokinetics play an important role in the liver toxicity and subsequent carcinogenicity of 1,4-dioxane, especially at the high dose levels employed in the cancer bioassays. PBPK approaches can take into account saturation of metabolism at high doses when cancer risks observed in animals are extrapolated to humans. The tumor incidence was correlated with the tissue (liver) exposure dose. As a result, the risk - specific dose of dioxane for humans was found to be as much as 80 times higher than that calculated conventionally.

PBPK modeling can be used to quantify the impact of pharmacokinetic uncertainty and population variability in risk assessment (45, 62, 63). By using Markov Chain Monte Carlo (MCMC) sampling within a Bayesian statistical framework, a PBPK model for trichloroethylene (TCE) in rodents and humans was used to estimate of both variability between experimental groups and uncertainty in TCE toxicokinetics (64). The distribution of C_{max} values of TCE's metabolite for a continuous 1-ppm inhalation exposure of TCE in a human population was predicted, approximating a normal distribution (mean = 1.36, SD = 0.96).

The use of pharmacokinetic modeling in risk assessment provides a reliable method for incorporating cross-species, intra-species, cross-route, and dose regimen variability information. The use of physiologically-based pharmacokinetic predictions is especially appropriate when animal pharmacokinetics studies are unavailable and when human pharmacokinetic studies cannot be justified (as in the case for drug degradation compounds and many environment toxicants).

1.3. Project overview and research objectives

Appearance of drug degradation products during storage is a potentially important drug safety factor. To minimize toxicity risk, a critical level of a toxic degradant has to be identified as part of defining shelf-life. Conventional risk assessment practice estimates exposure risk for an average individual and typically applies a series of uncertainty factors to account for interspecies or intra-species differences associated with pharmacokinetics and pharmacodynamics. The effects of compound-specific properties are typically not part of the risk calculation.

The objective of this proposal is to develop a process for leveraging compound-specific pharmacokinetic information in the estimation of human safe dose for drug degradants using a series of chemically-related model drug degradants (substituted anilines). Our central hypothesis is that incorporation of PBPK modeling results in degradant risk specifications which are less stringent than those estimated by conventional risk assessment approach. The rationale for the proposed research is that a PBPK model utilizing rat to human scaling for target tissue toxicity in combination with Monte Carlo methods for estimating human reference dose provides a rational basis for assessing drug stability safety issues for drug substances that potentially degrade to toxic compounds.

The specific objectives of this project are the following:

- Determine pharmacokinetic parameters needed in PBPK simulations for model drug degradation compounds. A combination of literature and in vitro experimentation and prediction were used to obtain initial pharmacokinetic parameters.

- Construct PBPK models for the selected compounds in rats and humans for intravenous and oral exposure. Sensitivity and uncertainty analysis were used to evaluate the impact of model input parameters on model predictions. To evaluate

14

patient population effects on exposure profiles, the PBPK model parameters was varied in meaningful ways to reflect age and gender sources of patient variation using Monte Carlo methods.

- Derive human-equivalent-no-adverse-effect doses based on predicted degradant exposure in toxicity target tissues. Distributions of target tissue exposures in rats and humans were generated by application of Monte Carlo method and compared based on a critical value. A human no-adverse effect dose was then selected at a critical value of 1%.

- Finally, the PBPK-based risk assessment was compared to the traditional risk assessment approach using standard uncertainty factors.

1.4. Whole body physiologically - based pharmacokinetic models

Whole body PBPK modeling provides a quantitative description of the absorption, distribution, metabolism and excretion of drug substances to predict the concentration - time profiles of compounds administered through any route of interest in many different species (65). Whereas classical pharmacokinetics attempts to describe concentrations of drug in plasma/blood, PBPK modeling attempts to accurately predict drug profiles for body tissues by incorporating physiological and compound-specific properties into a mathematical framework. In other words, contrary to descriptive traditional pharmacokinetic models derived from empirical data, PBPK modeling is intended to leverage prior information of the system to predict an outcome. Since classical PK models do not incorporate anatomy, physiology, and biochemistry of the species of interest, interspecies predictions are limited to allometric scaling of individual pharmacokinetic parameters. PBPK models attempt to incorporate relevant biological and mechanistic information, enabling them to be used with limited animal experimentation for extrapolation of the kinetic behavior of chemicals from high dose to low dose, from

one exposure route to another, and from test animal species to humans (66).

1.4.1 Modeling Methodology

1.4.1.1 Structure of the generic whole body PBPK model

A whole body PBPK model represents the body as a collection of physiologically realistic compartments including organs (e.g. heart, lung), eliminating organs (e.g. gut, liver, kidney), distribution tissues (muscle, skin, adipose) and specific biophase organs (e.g. sites of toxicity or pharmacodynamic effects). These compartments are linked together by the arterial and venous blood flows. The need to represent a particular organ or tissue as a separate compartment is determined based on its relevance to target organ toxicity, mode of action, elimination pathways, distribution pathways and administration route. Model complexity and number of compartments are consistent with chemical characteristics, intended purpose and available pharmacokinetic data (50). The generic structure of whole body PBPK model is depicted in Figure 1.3.
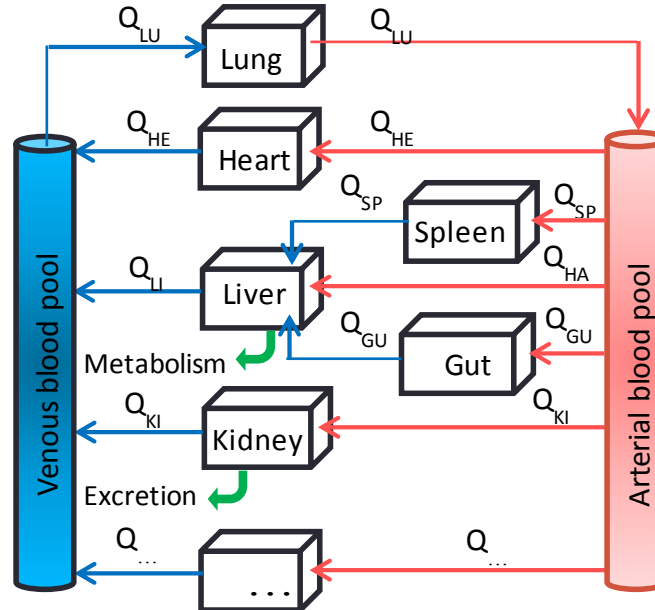
Figure 1.3- Conceptual representation of a Whole Body PBPK Model. Blood flow rates associated with the compartments is represented by Q. Subscripts LU, HE, LI, KI, SP, and GU mean lung, heart, liver, kidney, spleen and gut. Q_{HA} refers to the blood flow rate from the hepatic artery. Elimination is depicted as occurring from liver and kidney.

16

1.4.1.2 Model parameters and methods of parameter estimation

Model parameters: The characteristics of organ, tissues and drug are described by physiological and compound-specific parameters. **Physiological Parameters** include arterial and venous blood flows, tissue volumes, tissue blood flow rates and tissue composition (lipid, phospholipids, and water). Comprehensive sets of the physiological parameters for humans and common laboratory animals are available in the literature (67-71). **Compound-specific Parameters** include physicochemical properties (e.g. logP, pKa, dissolution rate) and biochemical/ biophysical properties (e.g. V_{max}, K_m, and permeability, fraction unbound in plasma or tissues, blood to plasma ratio). **PK-derived Parameters** are computed by combining compound-specific and physiological parameters, such as tissue-to-plasma partition coefficients (Kpu) estimated from logP, pKa and tissue composition and intrinsic clearance (CL_{int}) derived from V_{max}, K_m and amount of liver microsomal protein.

Methods of parameter estimation: In addition to literature resources, model parameters can be determined by the following methods:

- *In vitro* assay: for example, binding to plasma protein, intrinsic clearance, metabolic constants (V_{max}, K_m) can be determined using microsomes or hepatocytes (72).

- *In silico* calculation: for example, tissue-to-plasma partition coefficients estimated by tissue composition-based approach or effective permeability can be predicted using Quantitative Structure Activity Relationship (QSAR) method (73-75).

- *In vivo* experiment: critical PK parameters can be determined by experimentation and parameter estimation / optimization methods based pharmacokinetic data.

Tissue distribution is an important pharmacokinetics process. In the PBPK model,

a key characteristic is the affinity of drugs for specific tissues, which is defined by the tissue-to-plasma partition coefficient. Tissue-to-plasma partition coefficients (Kpu) can be measured experimentally (76-78) using tissue homogenates, tissue slices or isolated perfused organs based on steady state approaches. Determination of Kpu values by drug infusion to animals and assay of blood and tissues is quite laborious and time consuming, and therefore various methods have been proposed to predict Kpu from the physicochemical characteristics of the drug and the physiological composition of the tissues (73, 74, 79, 80). DeBuck and colleagues (81) compared two different methods for predicting tissue partition coefficients (73, 74, 79, 80) by computing the volume of distribution at steady state (V_{ss}) based on predicted Kpu values. They found that the methods of Rodgers and Rowland yielded the most accurate predictions of V_{ss} wherein 80% of the predicted values for a diverse set of 50 compounds were within a two-fold range of the experimentally-measured values.

For the majority of drugs, the liver is the major organ of drug metabolism. Hence, prediction of hepatic drug clearance has been investigated using various *in vitro* metabolizing systems. Metabolic parameters can be obtained with microsomes or hepatocytes either through substrate disappearance or initial rate of metabolite formation. The first step is to estimate *in vitro* intrinsic clearance based on estimated Michaelis - Menten constants (V_{max}, K_m) ($CL_{int,in\ vitro} = V_{max}/K_m$; in μL/min/mg microsomal protein or μL/min/10^6 hepatocyte cells) (82-84). The second step is to estimate *in vivo* clearance from *in vitro* parameters. Scaling factors used to estimate *in vivo* intrinsic clearance include microsomal protein in liver, nonspecific binding to biological material, and liver weight (85).

The binding parameters (e.g. fraction unbound in blood and tissues, blood to plasma ratio) are determined by established methods, such as equilibrium dialysis, ultrafiltration, and ultracentrifugation (86). Equilibrium dialysis separates molecules

18

across a semipermeable membrane according to molecular size by utilizing the driving force of concentration differential between solutions on each side of the membrane. Ultrafiltration is a method that rapidly (usually within 10 min) separates free small molecules from protein-bound ones using a membrane. Between these two methods, equilibrium dialysis suffers from relatively long analysis time. The analytical procedure needs to be capable of determining the free drug concentration, non-specific binding of drugs onto the membrane, and possible leakage of bound drug through the membrane.

In vitro methods are available for estimating drug permeability, such as immobilized artificial membrane (IAM) high-performance liquid chromatography (HPLC), cell layer (Caco-2) permeability, and parallel artificial membrane permeability assay (PAMPA). The IAM and PAMPA methods model only passive diffusion. The Caco-2 method models passive diffusion, active uptake transport, efflux, and paracellular permeability (86). The permeability of compounds can also be predicted by *in silico* models which describe the Quantitative Structure and Activity Relationship (QSAR) between permeability and compound physicochemical descriptors (87) .

Mathematical description of PBPK models

PBPK modeling describes the physical, biochemical and biophysical processes that determine the fate of a drug in the body: dissolution/drug release, absorption, distribution and elimination.

Oral drug absorption: Oral administration is the most popular and convenient route of drug administration. A drug administered orally needs to get absorbed into systemic circulation by passing from the gastrointestinal lumen, through the intestinal wall and through the liver before entering systemic circulation. Therefore, drug oral bioavailability is the product of the fraction of the dose which enters the gut wall (F_a), the fraction of drug which escapes metabolism in the gut wall and enters the portal vein (F_g), and the fraction of the drug that escapes hepatic first-pass metabolism (F_h).

$$F = F_a \times F_g \times F_h$$

Several factors can affect the processes involved in drug oral absorption such as dissolution rate, drug physicochemical properties (solubility, lipophilicity, pKa) and physiological factors (e.g. gastric emptying, intestinal transit time, GI fluid pH, intestinal blood flow, transporters, enzymes). All these components can be incorporated in PBPK model to provide realistic prediction of drug absorption kinetics (88, 89).

Drug distribution refers to the reversible partitioning of a drug into the various tissues of the body from the systemic circulation, driven by blood flow rates and drug permeation across membrane barriers. The rate and extent of drug distribution into tissues is determined by several factors, such as blood flow rates, drug permeability, concentration of plasma proteins, hematocrit and membrane transporters. Other compound-dependent factors are responsible for the distribution of drug in the body such as membrane permeability, tissue partition coefficients, blood-plasma ratios and drug affinity to influx or efflux transporter proteins. These parameters represent the characteristics of the distribution process and can be integrated into a PBPK model for distribution. For example, for a non-eliminating tissue (e.g. brain, adipose, heart, muscle, spleen), the rate of change of drug concentration in the tissue (dC_{tis}/dt) is described by the differential equation below (Equation 1.2):

$$V_{tis}\frac{dC_{tis}}{dt} = Q_{tis}\left(C_{Ar} - \frac{C_{tis}\times K_{B/P}}{fu_p\times Kpu^{tis}}\right) \qquad \text{(Eq. 1.2)}$$

It is assumed that that distribution of drug into tissue is limited by the blood flow rate to the tissue. Q_{tis} is the blood flow rate into the tissue, V_{tis} is the volume of the tissue, C_{Ar} is concentration of drug in arterial blood, fu_p is the unbound fraction in plasma, $K_{B/P}$ is blood-plasma concentration ratio and Kpu is tissue-plasma partition coefficient defined as the ratio of concentration of test compound in the tissue to unbound compound in plasma at steady state.

The volume of distribution cannot be considered as a constant due to the fact that the proportion of the drug in different tissues changes with time (90). By determining the partitioning to various tissues, volume of distribution of drugs can be estimated using the following Equation 1.3

$$Vd_{ss} = V_{plasma} + V_{RBC} \times \frac{K_{B/P} - (1-H)}{H} + \sum_{tissues} V_i . Kp_i \qquad (Eq.1.3)$$

Where, Vd_{SS} refers to volume of distribution at steady state. V_{plasma}, V_{RBC} and V_i are volume of plasma, erythrocyte and tissue, respectively. $K_{B/P}$ and H are blood to plasma ratio and hematocrit value. Kp_i is tissue-to-plasma partition coefficient.

Drug elimination: The process of drug elimination includes metabolism (enzymatic biotransformation) and excretion, typically via the biliary and/or renal route. As with other PK parameters, drug metabolism and excretion are influenced by both the physiology of the species and compound properties. Equation 1.4 is an example used in PBPK modeling to describe the nonlinear drug elimination process, in which V_{max} and K_m are maximal velocity and Michaelis constant from the Michaelis-Menten equation. Kpu^{Liver} is liver-unbound plasma partition coefficient.

$$V_{Liver} \frac{dC_{Liver}}{dt} = Q_{Liver} \left(C_{Ar} - \frac{C_{Liver} \times K_{B/P}}{fu_p \times Kpu^{Liver}} \right) - \frac{V_{max} \times \frac{C_{Liver}}{Kpu^{Liver}}}{K_m + \frac{C_{Liver}}{Kpu^{Liver}}} \qquad (Eq.1.4)$$

The entire PBPK model can be built by coupling differential equations for all selected compartments to describe the time course of a drug in the body using mass balance for venous blood (Equation 1.5):

$$V_{Ven} \frac{dC_{Ven}}{dt} = \sum \frac{Q_{tis} \times C_{tis} \times K_{B/P}}{fu_p \times Kpu^{tis}} - Q_{Ven} \times C_{Ven} \qquad (Eq.1.5)$$

Certain constraints need to be maintained in parameterizing these equations. For example, the sum of blood flow rates to all tissues adds up to the total cardiac output. The weights of individual tissues should be less than or equal to the body weight. The total

administered dose of test compound should be equal to the sum of the amount absorbed plus its amount in the body and amount eliminated. The equations above, with appropriate parameter values and initial conditions, form a system of differential equations that can be solved to predict the time profile of drug concentrations in each tissue compartment. Implementations in R or MATLAB can be used for extensive model evaluation associated with MCMC sampling.

<u>Model evaluation</u>

Once the initial parameter values have been estimated, they are incorporated into a system of differential equations that are numerically integrated to predict plasma, blood and tissue concentration time profiles. These predicted profiles are compared with experimentally observed concentrations to evaluate the model. During this model refinement process, the model structure and parameters need to be physiologically and biochemically realistic and appropriate. In PBPK modeling, predictions that are within a factor of 2 of the experimental data have frequently been considered adequate (50) . Once a PBPK model has been validated, model simulation may be performed for a given set of initial conditions, such as species of interest, dosing route, dosing levels, and applied for a specific purpose.

1.4.2 Uncertainty and Variability

In their review, Bois and coworkers (62) distinguished uncertainty from variability by defining variability as a product of inter-individual differences. Uncertainty is lack of knowledge and may have various sources. For example, uncertainty results from experimental error in measuring the ''true'' value of a response. Overall, uncertainty is a defect in knowledge that typically can be reduced by additional experimentation, while variability is a fact of life that can only be better characterized by additional experiment. Figure 1.4 illustrates the sources of uncertainty and variability consideration in PBPK modeling.

In conventional risk assessment methods, a single value estimate of risk has often been used to depict the expected risk for an "average" person. A more logical representation of risk for a population with various subpopulations (e.g. neonates, adults, and the elderly) should be a value that incorporates inter-individual variations. Physiological, anatomical and biochemical variation is inherent to any population. It cannot be minimized, for example, by experimental design and therefore must be quantitatively characterized in describing risk. Similarly, compound-specific PBPK parameters are subject to inherent population variability, but also are imbued with uncertainty associated with measurement inaccuracies and imprecision. Therefore, both uncertainty and variability are relevant to risk assessment. Monte Carlo methods coupled with the PBPK models can be used to evaluate uncertainty and variability (57). Generally, in Monte Carlo analysis, parameters are repeatedly sampled from distributions to generate output distributions after a large number of model iterations.

In order to perform model parameter analysis, coefficient of variation of parameters and their distributional forms must be obtained for model simulations. Physiological parameter variabilities are often based on estimates of standard error included in a review of the physiological literature (67). Biochemical and PK parameter variability can be measured directly from experimental data (91).

Using sensitivity analysis, model parameters can be evaluated to determine which one has the most influence on model predictions (92, 93). There are two approaches: local sensitivity and global sensitivity analysis. Local sensitivity is the sensitivity of the model output about a specific point in parameter space. In contrast, global sensitivity analysis determines the effect of simultaneous parameter variation on model outcome response by sampling predefined parameter distributions (94).
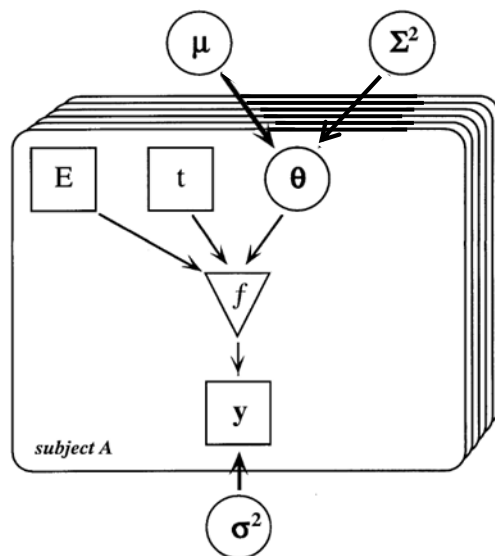
Figure 1.4- Illustration of uncertainty and variability in pharmacokinetic population models. At the individual level, blood concentrations (y) are measured experimentally with the residual error variance σ^2 (uncertainty). The PBPK model is a function (f) of exposure level (E), time (t), a set of parameters (θ). The population level contained prior distributions (P) for the population mean (μ) and population variance (Σ^2) - variability for each PBPK model parameter.
(Figure adapted from [61])

1.4.3   Limitations of PBPK Modeling

Although numerous studies on the use of PBPK modeling in human health risk assessment have been appeared in literature, this approach has some practical limitations and issues. McLanahan (95) emphasized the need of standardized model evaluation criteria and a thorough and efficient review process to prepare a model for application. Other issues include model code availability, portability, and validity. Probabilistic (e.g., population-based) PBPK models and evaluation of critical parameter values are needed to fully characterize population variability.

During PBPK model development, model parameters can be obtained via available data or *in vitro* and *in vivo* experimentation. Due to a large number of unknown model parameters, the need of improving their quality, as well as a sensitivity analysis of
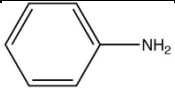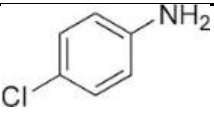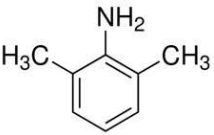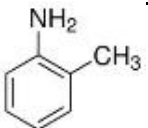
parameter impact on the dose metric, is essential. Another issue is the diversity of human population (e.g.,young, elderly, obese, pregnant and health status), thus, careful consideration of the variability associated with subpopulation is needed for meaningful population risk assessment.

1.5.Model compounds

1.5.1 Selection of model compounds

In order to investigate the utility of the proposed risk assessment procedure, a series of substituted anilines was chosen to be the subject of our investigations (Table 1.3). These compounds were selected because they are reported degradants in commercially-available drug products, known or potential toxicants, and structurally-similar to aniline which has been the subject of some detailed environmental toxicology studies.

Table 1.4- Model drug degradant and parent API

Degradant	Structure	API
Aniline		n/a
p-chloroaniline		Chlorhexidine
p-aminophenol		Acetaminophen
2,6-xylidine		Lidocaine Bupivacaine Prilocaine
2-methylaniline		Lidocaine Bupivacaine Prilocaine

1.5.2   Critical effect of model compounds

The acute toxicity of aniline and structurally-related aromatic amines are associated with their ability to form methemoglobin, increase splenic weight and damage to erythrocytes (96-98). The formation of methemoglobin results from the oxidation of hemoglobin by phenylhydroxylamine, the N-oxidation product of aniline (21). In a long-term feeding study, aniline and structurally-related compounds (p-chloroaniline, o-toluidine) produced spleen tumors in rats given high doses of compound in 2-year bioassay studies (99-101). According to chronic animal bioassays in the same strain of rats, the tumorigenic response induced by aniline and p-chloroaniline appears to be non-linearly related to dose (21). The mechanism of splenic toxicity of aniline and structurally-related compounds results from their erythrocyte toxicity and is due to the scavenging of chemically-damaged red blood cells by the spleen, leading to the development of spleen tumors (21, 96, 102-104).

Aniline-induced splenic toxicity has been quantified in several dose-response studies (98, 105, 106). Jenkins and colleagues (98) investigated the effect of single oral doses of aniline in the rat and in humans. Oral doses of 5, 15 and 25 mg aniline, respectively, were administered on three successive days to each of 20 volunteers ranging in age from 22 to 45 years old. Male rats (Colworth-Wistar albino strain) were given aniline in isotonic saline by injection into the tail vein or by stomach tube. Isotonic saline was administered instead of aniline to control animals. Blood samples were obtained after each dose of aniline and were subject to the estimation of methemoglobin. Doses of 5 and 15 mg aniline produced no significant increase of methemoglobin in 20 subjects, but a significant increase followed the administration of 25 mg aniline and higher doses. In the rat, the no-effect oral dose (NOAEL) was approximately 10 mg/kg body weight to produce methemoglobinemia. In addition to the increase in percentage of methemoglobin, the authors also observed increases in splenic weight of rats fed diets

containing aniline.

Chhabra and Thompson (18) conducted a toxicity study to characterize p-chloroaniline (PCA) toxicity in rats (Fisher 344/N), including the identification of target organs and the establishment of dose-response relationships (Figure 1.5). The weights of brain, liver, thymus, kidney, heart, lung and testis for dosed groups were not significantly different from those of the vehicle controls. However, spleen weights were increased in PCA-treated groups, and a clear dose response relationship was observed in both sexes.
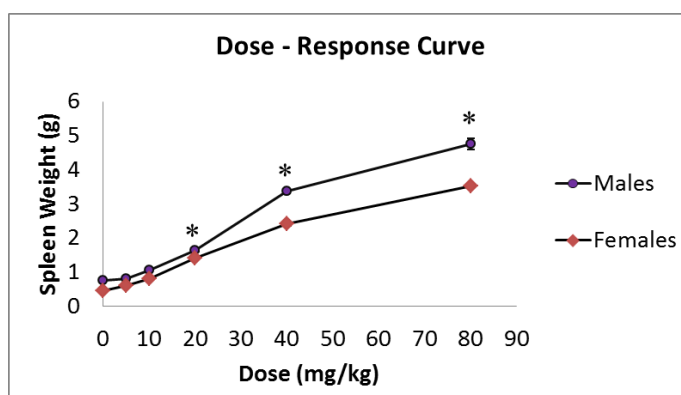
Figure 1.5- Spleen weights for rats in a 13-week gavage study of p-chloroaniline hydrochloride. (Those points marked with asterisks differ significantly from the corresponding control value).

p-Aminophenol (PAP) is a nephrotoxicant in the rat which has been shown to produce selective necrosis to renal proximal tubules (11, 12, 107-109). In the study of Newton el al. (110), male F344 rats received various doses of PAP hydrochloride in aqueous solution (0 to 200 mg/kg). Each group contained four rats. After 24 hr of PAP administration, blood was collected and the resulting renal function measurements indicated damage. Blood urea nitrogen (BUN) was elevated at doses of PAP as low as 100 mg/kg. Based on the effect of PAP on renal function, the NOAEL of PAP was detected at the dose of 25 – 50 mg/kg PAP (Figure 1.6).
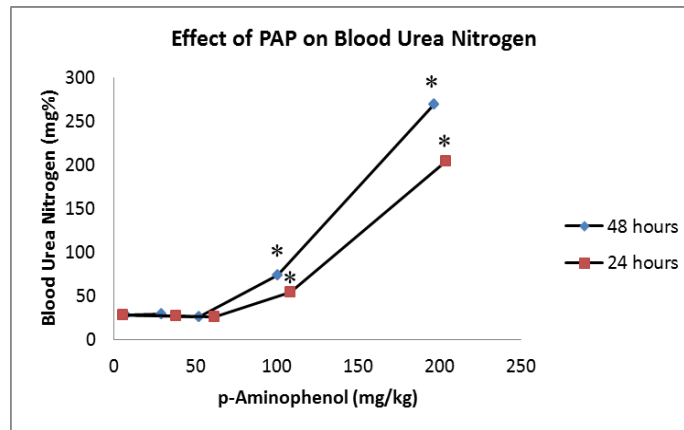
Figure 1.6- Effect of p-aminophenol on blood urea
nitrogen in Fisher F344 rats. * Significantly different
from control (0 mg/kg PAP), $p < 0.05$

Harada and colleagues (111) conducted a reproductive and developmental toxicity screening study of PAP in rats. Twelve male and female rats per group were given PAP by gavage at 0, 20, 100, or 500 mg/kg/day. The study's findings show that PAP is a general and reproductive/developmental toxic, but it is unlikely to be teratogenic in rats. These findings indicated that the NOAEL of PAP for general toxicity is considered to be 20 mg/kg/day.

In the 2-year studies of 2,6-dimethylaniline (2,6-DMA) conducted in Charles River CD rats, decreases in erythrocyte counts, accompanied by decreases in hemoglobin and hematocrit levels, were observed (112). Investigators reported anemia and methemoglobinemia in rats exposed to 2,6-DMA (113). In a dietary rat study as part of the National Toxicology Program (112), 2,6-DMA has been shown to cause significant increases in the incidence of carcinomas in the nasal cavity of both male and female rats when provided in the diet at 3000 ppm for 2 years. The rat oral chronic lowest-observed-adverse-effect level (LOAEL) of 2,6-DMA was reported as 15 mg/kg.

There are numerous reports on the toxic and carcinogenic effects of o-toluidine (o-TOL) (28, 30, 100, 114). Increased incidence of bladder cancer among workers employed in dyestuff factories which use o-TOL was found (115, 116) . Hecht et al. [4]

investigated the carcinogenicity of o-TOL and of one of its metabolites, o-nitrosotoluene, in rats. They found that both compounds induced comparable numbers of peritoneal tumors and fibroma of the skin and the spleen. A sub-acute (14 days) feeding study in male and female Fischer rats (n = 5 per sex and group) with doses of 0, 500, 3000, 6000 ppm was performed to investigate the urinary bladder toxicity of o-TOL (117). Statistically significant and dose-related increases in methemoglobin production were found in all treated animals. Therefore a NOAEL could not be established. The LOAEL based on methemoglobinemia (male and females) and decreased body weight gain (females) was 500 ppm (23.7 mg/kg/day for males and app. 25.5 mg/kg/day for females after adjusting to the test substance stability).

1.5.3 Mode of action of toxicity

The biotransformation of aniline compounds occurs via N-oxidation to form phenylhydroxylamines, oxidation of the phenyl ring to form phenols, acetylation of the amino group to form acetanilides, and sulfate and glucuronide conjugation of oxidative metabolites (118, 119). Harrison and co-authors (119) found the major metabolic pathways involved ring oxidation to yield 4-aminophenol, as the major metabolite and, after acetylation, 4-hydroxyacetanilide (acetaminophen).

An additional dead-end pathway leads to phenylhydroxylamine, which in the red blood cell forms a redox pair with nitrosobenzene. Pathways of aniline metabolism in rats were depicted in Figure 1.7.
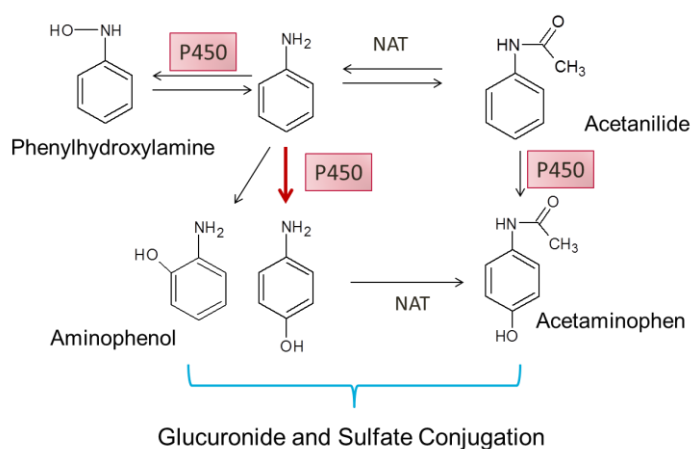
Figure 1.7- Metabolic scheme of aniline in rat liver

29

The data from Harrison indicates that phenylhydroxylamine is largely responsible for the damage to red blood cells which results in the hemolytic anemia associated with aniline exposure in animals. Side reactions may occur within erythrocytes including binding of phenylhydroxylamine to erythrocytic protein (9), and binding of both nitrosobenzene and phenylhydroxylamine to sulfhydryl groups in glutathione or protein.

Khan's studies of aniline exposure in rats (103, 105, 120) demonstrated an association between erythrocyte damage and the severity of the splenotoxicity. Since one of the major functions of the spleen is to remove damaged erythrocytes, aniline-damaged erythrocytes would be expected to be scavenged by the spleen, especially by phagocytes. The deposition and subsequent breakdown of damaged erythrocytes will not only release aniline and/or its metabolites, but, most importantly, will also result in accumulation of iron in the spleen which may catalyze the generation of tissue-damaging oxygen radicals and subsequently results in lipid peroxidation and protein oxidation. During the scavenging of damaged erythrocytes, the splenic phagocytes can become activated and release reactive oxygen species (ROS) which could further contribute to the oxidation leading to tissue injury.

1.5.4 Pharmacokinetic data for model compounds

Aniline is lipophilic base, with a pKa of 4.6, and would be expected to be rapidly and completely absorbed from the small intestine. Kao and coauthors (121) observed that urinary elimination of metabolized aniline in sheep and rat was extensive and no free aniline was detected in the urine. In rats, sulfate conjugates were the major metabolites (77%). The concentration ratios of aniline and phenolic aniline metabolites in plasma from spiked blood samples, as compared to similarly spiked water samples, was 1:1, indicating that the compounds were distributed equally in plasma and erythrocytes, and that plasma levels of these compounds were reflective of total blood levels. The time course of aniline in rat blood after i.p. administration (119) is shown in Figure 1.8.
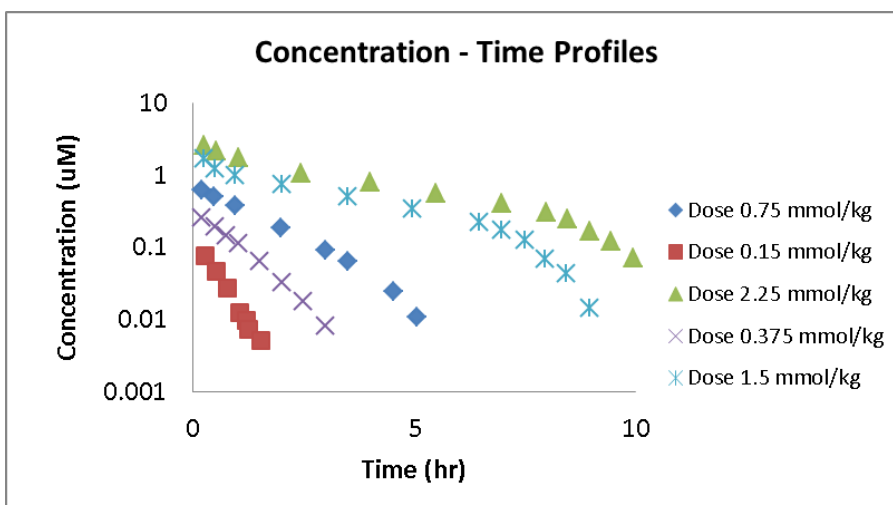
Figure 1.8- Blood concentration time profiles of aniline administered
intraperitoneally in rats

More than 90% of PCA was excreted into the urine (18, 122). Very little PCA was eliminated unchanged and no p-chloroacetanilide was observed. Instead, two major components were observed: 2-amino-5-chlorophenylsulfate and p-chloro-oxanilic acid, along with other minor metabolites. PCA is rapidly absorbed after oral administration. The orally-administered HCl salt would be neutralized in the small intestine, and the free base form of chloroaniline would be absorbed into the systemic circulation.

According to the IARC Monographs (123) on the evaluation of carcinogenic risks to humans from 2,6-DMA exposure, the absorption half-time of 2,6-DMA was rapid (14.4 min). The metabolism of 2,6-DMA was examined qualitatively in rats, and 4-hydroxy-2,6-dimethylanilne and 3-methyl-2-aminobenzoic acid were identified as major and minor urinary metabolites, respectively. Short el al. (124) concluded that p-hydroxylation was the major metabolism pathway of 2,6-DMA in rats.

Metabolism of o-TOL was assessed in male F344 rats (125). Following a single dose (400 mg/kg subcutaneously) of radioactive o-TOL, > 80% of the radioactivity appeared in the urine and < 3.5% in feces after 48 hours. Major routes of metabolism were N-acetylation and hydroxylation at the 4-position. Minor pathways included

hydroxylation at the 6-position, oxidation of the methyl group, and oxidation of the amino group.

p-Aminophenol metabolism was investigated by Yan et al. using rat hepatocytes (126). PAP was found to be metabolized predominantly to PAP-S-glutathione conjugates and accounts for > 50% of the metabolites identified in hepatocytes. *In vitro* biotransformation of PAP was conducted in human hepatocytes (127). The authors concluded that human hepatocytes mainly converted PAP to sulfate or glucuronic acid conjugates of N-acetyl-p-aminophenol or PAP. The pharmacokinetics and metabolism of PAP after dermal exposure to PAP were investigated in rats by Dressler et al. (128). Blood and plasma samples were analyzed for radioactivity and the presence of metabolites. However, no free PAP was detected in the plasma.

CHAPTER 1 LITERATURE CITED

1. Committee for Medicinal Products for Human Use (CHMP), European Medicines Agency (EMEA). London, 28 June 2006. Guideline on the limits of genotoxic impurities, CPMP/SWP/5199/02, EMEA/CHMP/QWP/251344/2006.

2. FDA Center for Drug Evaluation and Research. Guidance for Industry (Draft). 03 December 2008. Genotoxic and carcinogenic impurities in drug substances and products: Recommended approaches.

3. Ashby J. 1978. Structural analysis as a means of predicting carcinogenic potential. *British Journal of Cancer.* 37 : 904

4. Ashby J. 1985. Fundamental structural alerts to potential carcinogenicity or noncarcinogenicity. *Environmental Mutagenesis.* 7 : 919-21

5. Ashby J, Tennant RW. 1988. Chemical structure, salmonella mutagenicity and extent of carcinogenicity as indicators of genotoxic carcinogenesis among 222 chemicals tested in rodents by the U.S. NCI/NTP. *Mutation Research/Genetic Toxicology.* 204 : 17-115

6. Ashby J, Tennant RW, Zeiger E, Stasiewicz S. 1989. Classification according to chemical structure, mutagenicity to salmonella and level of carcinogenicity of a further 42 chemicals tested for carcinogenicity by the U.S. national toxicology program. *Mutation Research/Genetic Toxicology.* 223 : 73-103

7. Raillard S.P. 2010. Prediction of drug degradation pathways leading to structural alerts for potential genotoxic impurities. *Organic Process Research & Development.* 14 : 1015

8. Koshy KT, Lach JL. 1961. Stability of aqueous solutions of N-acetyl-p-aminophenol. *Journal of Pharmaceutical Sciences.* 50 : 113-8

9. Kiese M, Szinicz L, Thiel N, Weger N. 1975. Ferrihemoglobin and kidney lesions in rats produced by 4-aminophenol or 4-dimethylaminophenol. *Archives of Toxicology.* 34 : 337-40

10. Davis JM, Kerry RE, Ronald SS. 1983. Early functional and morphological changes in renal tubular necrosis due to p-aminophenol. *Kidney International.* 24 : 740-7

11. Lock EA, Cross TJ, Schnellmann RG. 1993. Studies on the mechanism of 4-aminophenol-induced toxicity to renal proximal tubules. *Human & Experimental Toxicology.* 12 : 383-8

12.   Green CR, Kathryn NH, TangeJD. 1969. Kidney lesions induced in rats by P-aminophenol. *British Medical Journal.* 1 : 162-4

13.   US Pharmacopeial convention. 2009. *United States Pharmacopeia and National Formulary (USP 32-NF 27),* Rockville, MD:

14.   British Pharmacopoeia. 2004. Paracetamol tablets. In Stationery Office, London, UK

15.   Zhixin Z, Kirsch LE. 2012. Studies on the instability of chlorhexidine, part I: Kinetics and mechanisms. *Journal of Pharmaceutical Sciences.* 101 : 2417-27

16.   Thomas JE, Sem DS. 2010. An in vitro spectroscopic analysis to determine whether para-chloroaniline is produced from mixing sodium hypochlorite and chlorhexidine. *Journal of Endodontics.* 36 : 315-7

17.   International Agency for Research on Cancer. 2006. IARC monography on the evaluation of carcinogenic risks to human. *World Health Organization.* 86 : 1-25

18.   Chhabra RS, Thompson M, Elwell MR, Gerken DK. 1990. Toxicity of p-chloroaniline in rats and mice. *Food and Chemical Toxicology.* 28 : 717-22

19.   Chhabra RS, Huff JE, Haseman JK, Elwell MR, Peters AC. 1991. Carcinogenicity of p-chloroaniline in rats and mice. *Food and Chemical Toxicology.* 29 : 119-24

20.   Goodman DG, Ward JM, Reichardt WD. 1984. Splenic fibrosis and sarcomas in F344 rats fed diets containing aniline hydrochloride, p-chloroaniline, azobenzene, o-toluidine hydrochloride, 4,4'-sulfonyldianiline, or D & C red no. 9. *Journal of the National Cancer Institute.* 73 : 265-73

21.   Bus JS, Popp JA. 1987. Perspectives on the mechanism of action of the splenic toxicity of aniline and structurally-related compounds. *Food and Chemical Toxicology.* 25 : 619-26

22.   Kornreich M, Montgomery CA. 1990. *Toxicology and carcinogenesis studies of 2,6-dimethylaniline. Rep. 90-2534,* National Institutes of Health, US

23.   Koujitani T, Yasuhara K, Kobayashi H, Shimada A, Onodera H, et al. 1999. Tumor-promoting activity of 2,6-dimethylaniline in a two-stage nasal carcinogenesis model in N-bis(2-hydroxypropyl)nitrosamine-treated rats. *Cancer Letters.* 142 (2) : 161 (Abstr.)

24.   Magnusson G, Majeed SK, Down WH, Sacharin RM, Jorgeson W. 1979. Hepatic effects of xylidine isomers in rats. *Toxicology.* 12 : 63-74

25. Kirkland D, Ballantyne M, Harlfinger S, Will O, Jahnel U, et al. 2012. Further investigations into the genotoxicity of 2,6-xylidine and one of its key metabolites. *Regulatory Toxicology and Pharmacology*. 62 : 151-9

26. Powell MF. 1987. Stability of lidocaine in aqueous solution: Effect of temperature, pH, buffer, and metal ions on amide hydrolysis. *Pharmaceutical Research*. 4 : 42-5

27. Fijałek Z, Baczyński E, Piwońska A, Warowna-Grześkiewicz M. 2005. Determination of local anaesthetics and their impurities in pharmaceutical preparations using HPLC method with amperometric detection. *Journal of Pharmaceutical and Biomedical Analysis*. 37 : 913-8

28. Hecht SS, El-Bayoumy K, Rivenson A, Fiala E. 1982. Comparative carcinogenicity of o-toluidine hydrochloride and o-nitrosotoluene in F-344 rats. *Cancer Letters*. 16 : 103-8

29. Freudenthal RI, Anderson DP. 1995. A reexamination of recent publications suggesting o-toluidine may be a human bladder carcinogen. *Regulatory Toxicology and Pharmacology*. 21 : 199-202

30. Danford N. 1991. The genetic toxicology of ortho-toluidine. *Mutation Research/Reviews in Genetic Toxicology*. 258 : 207-36

31. Baczynski E, Piwonska A. 2002. Determination of 2,6 dimethylaniline and o-toluidine impurities in preparations for local anaesthesia by the HPLC methodwith emperometric detection. *Acta Poloniac Pharmaceutica Drug Research*. 59 : 333-9

32. Sternal R, Nugara N. Flutamide. In *Analytical Profiles of Drug Substances and Excipients,* Volume 27 : 115-57. Academic Press

33. Vogna D, Marotta R, Napolitano A, Andreozzi R, d'Ischia M. 2004. Advanced oxidation of the pharmaceutical drug diclofenac with UV/H2O2 and ozone. *Water Research*. 38 : 414-22

34. Kubala T, Gambhir B, Borst SI. 1993. A specific stability indicating hplc method to determine diclofenac sodium in raw materials and pharmaceutical solid dosage forms. *Drug Development and Industrial Pharmacy*. 19 : 749-57

35. Hartmann J, Bartels P, Mau U, Witter M, Tümpling Wv, et al. 2008. Degradation of the drug diclofenac in water by sonolysis in presence of catalysts. *Chemosphere*. 70 : 453-61

36. International Conference on Harmonization (ICH). June 2008. Guidance for industry Q3A impurities in new drug substances.

37.   International Conference on Harmonization (ICH). June 2006. Impurities in new products Q3B (R2).

38.   U.S. FDA. 2010. *Guidance for Industry ANDAs: Impurities in drug products.* Center for Drug Evaluation and Research (CDER), U.S

39.   Curtis DK, ed. 2008. *Casarett and Doull's Toxicology the Basic Science of Poisons,* McGraw Hill Professional. 1280 pp. 7th ed.

40.   Kannan Krishnan, Melvin E. Andersen, ed. 2010. *Quantitative Modeling in Toxicology,* John Wiley & Sons. 485 pp. 1st ed.

41.   U.S. EPA. 2005. *Guidelines for carcinogen risk assessment. Rep. EPA/630/P-03/001F,* U.S. Environmental Protection Agency, Washington, DC

42.   Ching-Hung Hsu, Todd Stedeford, eds. 2010. *Cancer Risk Assessment, Chemical Carcinogenesis, Hazard Evaluation, and Risk Quantificatioin,* Vol. Chapter 21. United States of America: John Wiley & Sons. 824 pp

43.   Clewell HJ. 2002. A consistent approach for the application of pharmacokinetic modeling in cancer and noncancer risk assessment. *Environmental Health Perspectives.* 110 : 85

44.   Clewell III HJ, Andersen ME, Blaauboer BJ. 2008. On the incorporation of chemical-specific information in risk assessment. *Toxicology Letters.* 180 : 100-9

45.   Lipscomb JC, Meek ME, Krishnan K, Kedderis GL, Clewell H, Haber L. 2004. Incorporation of pharmacokinetic and pharmacodynamic data into risk assessments. *Toxicology Mechanisms and Methods.* 14 : 145-58

46.   WHO. 1994. *Assessing human health risks of chemicals: Derivation of guidance values for health-based exposure limits (International Programme on Chemical Safety, Environmental Health Criteria, 170).* Geneva, Switzerland, World Health Organization

47.   WHO. 1999. *Principles for the assessment of risks to human health from exposure to chemicals (international programme on chemical safety, environmental health criteria 210).* Geneva, Switzerland, World Health Organization,

48.   Renwick A. 1993. Data-derived safety factors for the evaluation of food additives and environmental contaminants. *Food Additives & Contaminants.* 10 : 275-305

49.   Walton K, Dorne JC, Renwick AG. 2001. Default factors for interspecies differences in the major routes of xenobiotic elimination. *Human and Ecological Risk Assessment: An International Journal.* 7 : 181-201

50.   WHO. 2010. *Characterization and application of physiologically based pharmacokinetic models in risk assessment. IPCS harmonization project.* Vol. No.9. Ottawa, Canada: . 97pp

51.   Renwick AG, Lazarus NR. 1998. Human variability and noncancer risk assessment— an analysis of the default uncertainty factor. *Regulatory Toxicology and Pharmacology.* 27 : 3-20

52.   Walton K, Dorne J, Renwick A. 2001. Uncertainty factors for chemical risk assessment: Interspecies differences in the in vivo pharmacokinetics and metabolism of human CYP1A2 substrates. *Food and Chemical Toxicology.* 39 : 667-80

53.   Walton K, Dorne J, Renwick A. 2001. Uncertainty factors for chemical risk assessment: Interspecies differences in glucuronidation. *Food and Chemical Toxicology.* 39 : 1175-90

54.   Walton K, Dorne J, Renwick A. 2004. Species-specific uncertainty factors for compounds eliminated principally by renal excretion in humans. *Food and Chemical Toxicology.* 42 : 261-74

55.   Dorne JLCM, Renwick AG. 2005. The refinement of uncertainty/safety factors in risk assessment by the incorporation of data on toxicokinetic variability in humans. *Toxicological Sciences.* 86 : 20-6

56.   Clewell III HJ, Andersen ME. 1996. Use of physiologically based pharmacokinetic modeling to investigate individual versus population risk. *Toxicology.* 111 : 315-29

57.   Clewell RA, Clewell III HJ. 2008. Development and specification of physiologically based pharmacokinetic models for use in risk assessment. *Regulatory Toxicology and Pharmacology.* 50 : 129-43

58.   U.S. EPA. 2006. *Approaches for the application of physiologically based pharmacokinetic (PBPK) models and supporting data in risk assessment (final report).* U.S. Environmental Protection Agency, Washington, D.C., EPA/600/R-05/043F,

59.   Lipscomb JC, Haddad S, Krishnan K. 2012. Physiologically based pharmacokinetic model (PBPK) in toxicity testing and risk assessment. In *New Technologies for Toxicity Testing,* eds. M Balls, RD Combes, Chapter 6 : 76-95. Springer Science

60.   Andersen ME, Clewell HJ, Gargas ML, Smith FA, Reitz RH. 1987. Physiologically based pharmacokinetics and the risk assessment process for methylene chloride. *Toxicology and Applied Pharmacology.* 87 : 185-205

61.   Hon-Wing L, Paustenbach DJ. 1990. Cancer risk assessment for dioxane based upon a physiologically-based pharmacokinetic approach. *Toxicology letters*. 51 : 147-62

62.   Bois FY, Jamei M, Clewell HJ. 2010. PBPK modelling of inter-individual variability in the pharmacokinetics of environmental chemicals. *Toxicology*. 278 : 256-67

63.   Gelman A, Bois F, Jiang J. 1996. Physiological pharmacokinetic analysis using population modeling and informative prior distributions. *Journal of the American Statistical Association*. 91 : 1400-12

64.   Bois FY. 2000. Statistical analysis of clewell et al. PBPK model of trichloroethylene kinetics. *Environmental Health Perspectives*. 108(Suppl 2) : 307-16

65.   Peters SA., 2012. *Physiologically-based pharmacokinetic (PBPK) modeling and simulations: Principles, methods, and applications in the pharmaceutical industry,* America: John Wiley & Sons

66.   Reisfeld B, Mayeno AN, Lyons MA. 2007. Physiologically based pharmacokinetic and pharmacodynamic modeling. In *Computational Toxicology: Risk Assessment for Pharmaceutical and Environmental Chemicals,* ed. S Ekins, 33-68. John Wiley & Sons, Inc.

67.   Brown RP, Delp MD, Lindstedt SL, Rhomberg LR, Beliles RP. 1997. Physiological parameter values for physiologically based pharmacokinetic models. *Toxicology and Industrial Health*. 13 : 407-84

68.   Gentry PR, Haber LT, McDonald TB, Zhao Q, Covington T, Nance P, Clewell HJ, III, Lipscomb JC, Barton HA. Data for physiologically based pharmacokinetic modeling in neonatal animals: Physiological parameters in mice and sprague-dawley rats. *Journal of Children's Health*. 363-411

69.   Price PS, Conolly RB, Chaisson CF, Gross EA, Young JS, 2003. Modeling interindividual variation in physiological factors used in PBPK models of humans. *Critical Reviews in Toxicology*. 33 : 469-503

70.   Thompson CM, Johns DO, Sonawane B, Barton HA, Hattis D, 2009. Database for physiologically based pharmacokinetic (PBPK) modeling: Physiological data for healthy and health-impaired elderly. *Journal of Toxicology & Environmental Health: Part B*. 12 : 1-24

71.   Davies B, Morris T. 1993. Physiological parameters in laboratory animals and humans. *Pharmaceutical Research*. 10 : 1093-5

72. Brian Houston J, Carlile DJ. 1997. Prediction of hepatic clearance from microsomes, hepatocytes, and liver slices. *Drug Metab. Rev.* 29 : 891-922

73. Rodgers T, Leahy D, Rowland M. 2005. Physiologically based pharmacokinetic modeling 1: Predicting the tissue distribution of moderate-to-strong bases. *Journal of Pharmaceutical Sciences.* 94 : 1259-76

74. Rodgers T, Rowland M. 2006. Physiologically based pharmacokinetic modelling 2: Predicting the tissue distribution of acids, very weak bases, neutrals and zwitterions. *Journal of Pharmaceutical Sciences.* 95 : 1238-57

75. Hou TJ, Zhang W, Xia K, Qiao XB, Xu XJ. 2004. ADME evaluation in drug discovery. 5. correlation of caco-2 permeation with simple molecular properties. *Journal of Chemical Information and Computer Sciences.* 44 : 1585-600

76. Sweeney LM, Thrall KD, Poet TS, Corley RA, Weber TJ. 2008. Physiologically based pharmacokinetic modeling of 1,4-dioxane in rats, mice, and humans. *Toxicological Sciences.* 101 : 32-50

77. Murphy JE, Janszen DB, Gargas ML. 1995. An in vitro method for determination of tissue partition coefficients of non-volatile chemicals such as 2,3,7,8-tetrachlorodibenzo-p-dioxin and estradiol. *Journal of Applied Toxicology.* 15 : 147-52

78. Lin JH, Sugiyama Y, Awazu S, Hanano M. 1982. *In vitro* and *in vivo* evaluation of the tissue-to-blood partition coefficient for physiological pharmacokinetic models. *Journal of Pharmacokinetics and Pharmacodynamics.* 10 : 637-47

79. Poulin P, Theil F. 2002. Prediction of pharmacokinetics prior to in vivo studies. 1. mechanism-based prediction of volume of distribution. *Journal of Pharmaceutical Sciences.* 91 : 129-56

80. Poulin P, Theil F. 2000. A priori prediction of tissue:Plasma partition coefficients of drugs to facilitate the use of physiologically-based pharmacokinetic models in drug discovery. *Journal of Pharmaceutical Sciences.* 89 : 16-35

81. De Buck SS, Sinha VK, Fenu LA, Gilissen RA, Mackie CE, Nijsen MJ. 2007. The prediction of drug metabolism, tissue distribution, and bioavailability of 50 structurally diverse compounds in rat using mechanism-based absorption, distribution, and metabolism prediction tools. *Drug Metabolism and Disposition.* 35 : 649-59

82. Brian Houston J. 1994. Utility of in vitro drug metabolism data in predicting in vivo metabolic clearance. *Biochemical Pharmacology.* 47 : 1469-79

83. Obach RS. 1999. Prediction of human clearance of twenty-nine drugs from hepatic microsomal intrinsic clearance data: An examination of in vitro half-life approach and nonspecific binding to microsomes. *Drug Metabolism and Disposition.* 27 : 1350-9

84. Obach RS, Reed-Hagen AE. 2002. Measurement of michaelis constants for cytochrome P450-mediated biotransformation reactions using a substrate depletion approach. *Drug Metabolism and Disposition.* 30 : 831-7

85. Barter ZE, Bayliss MK. 2007. Scaling factors for the extrapolation of in vivo metabolic drug clearance from in vitro data: Reaching a consensus on values of human microsomal protein and hepatocellularity per gram of liver. *Current Drug Metabolism.* 8 : 33-45

86. Kerns EH, Li Di. 2008. *Drug-like properties: Concepts, structure design and methods from ADME to toxicity optimization,* Elsevier. 552pp

87. Nordqvist A, Nilsson J, Lindmark T, Eriksson A, Garberg P, Kihlén M. 2004. A general model for prediction of caco-2 cell permeability. *QSAR & Combinatorial Science.* 23 : 303-10

88. Yu LX, Amidon GL. 1999. A compartmental absorption and transit model for estimating oral drug absorption. *International Journal of Pharmaceutics.* 186 : 119-25

89. Agoram B, Woltosz WS, Bolger MB. 2001. Predicting the impact of physiological and biochemical processes on oral drug bioavailability. *Advanced Drug Delivery Reviews.* 50 : S41-67

90. Jamei M, Dickinson GL, Rostami-Hodjegan A. 2009. A framework for assessing inter-individual variability in pharmacokinetics using virtual human populations and integrating general knowledge of physical chemistry, biology, anatomy, physiology and genetics: A tale of'bottom-up'vs' top-down'recognition of covariates. *Drug Metabolism and Pharmacokinetics.* 24 : 53-75

91. Gearhart JM, Mahle DA, Greene RJ, Seckel CS, Flemming CD, et al. 1993. Variability of physiologically based pharmacokinetic (PBPK) model parameters and their effects on PBPK model predictions in a risk assessment for perchloroethylene (PCE). *Toxicology Letters.* 68 : 131-44

92. Clewell HJ, Lee T, Carpenter RL. 1994. Sensitivity of physiologically based pharmacokinetic models to variation in model parameters: Methylene chloride. *Risk Analysis.* 14 : 521-31

93.   Gueorguieva I, Nestorov I, Rowland M. 2006. Reducing whole body physiologically based pharmacokinetic models using global sensitivity analysis: Diazepam case study. *Journal of Pharmacokinetics and Pharmacodynamics.* 33 : 1-27

94.   Soetaert K, Petzoldt t. 2010. Inverse modelling, sensitivity and Monte Carlo analysis in R using package FME. *Journal of Statistical Software.* 33 : 1-28

95.   McLanahan ED, El-Masri HA, Sweeney LM, Kopylev LY, Clewell HJ. 2012. Physiologically based pharmacokinetic model use in risk Assessment—Why being published is not enough. *Toxicological Sciences.* 126 : 5-15

96.   Khan MF, Wu X, Kaphalia BS, Boor PJ, Ansari GAS. 1997. Acute hematopoietic toxicity of aniline in rats. *Toxicology Letters.* 92 : 31-7

97.   Short CR, King C, Sistrunk PW, Kerr KM. 1983. Subacute toxicity of several ring-substituted dialkylanilines in the rat. *Fundamental and Applied Toxicology.* 3 : 285-92

98.   Jenkins FP, Robinson JA, Gellatly JBM, Salmond GWA. 1972. The no-effect dose of aniline in human subjects and a comparison of aniline toxicity in man and the rat. *Food and Cosmetics Toxicology.* 10 : 671-9

99.   National Cancer Institute. 1978. *Bioassay of aniline hydrochloride for possible carcinogenicity. Technical Report Series. Rep. No 130,* US Department of Health, Education, and Welfare, NIH

100.   National Cancer Institute. 1979. *Bioassay of o-toluidine hydrochloride for possible carcinogenicity. Technical Report Series. Rep. No. 153,* US. Department of Health, Education, and Welfare, NIH

101.   National Cancer Institute. 1979. *Bioassay of p-chloroaniline for possible carcinogenicity. Technical Report Series. Rep. No 189,* US. Department of Health, Education, and Welfare, NIH

102.   Albert MA, Weinberger RH, Montgomery SB. 1985. Splenotoxicity associated with splenic sarcomas in rats fed high doses of D & C red no. 9 or aniline hydrochloride. October:

103.   Ansari MFK, G.A.S. 2000. Contribution of nitrosobenzene to splenic toxicity of aniline. *Journal of Toxicology and Environmental Health, Part A.* 60 : 263-73

104.   Wu X, Kannan S, Ramanujam VM-S, Khan MF. 2005. Iron release and oxidative DNA damage in splenic toxicity of aniline. *Journal of Toxicology and Environmental Health, Part A: Current Issues.* 68 : 657

105.   Khan MF, Boor PJ, Gu Y, Nancy WA, Ansari GAS. 1997. Oxidative stress in the splenotoxicity of aniline. *Toxicological Sciences.* 35 : 22-30

106.   Mellert W, Deckardt K, Gembardt C, Zwirner-Baier I, Jäckh R, van Ravenzwaay B. 2004. Aniline: Early indicators of toxicity in male rats and their relevance to spleen carcinogenicity. *Human & Experimental Toxicology.* 23 : 379-89

107.   Crowe CA, Yong AC, Calder IC, Ham KN, Tange JD. 1979. The nephrotoxicity of p-aminophenol. I. the effect on microsomal cytochromes, glutathione and covalent binding in kidney and liver. *Chemico-biological interactions.* 27 : 235-43

108.   Gartland KR, Bonner F, Timbrell J, Nicholson J. 1989. Biochemical characterisation of para-aminophenol-induced nephrotoxic lesions in the F344 rat. *Archives of Toxicology.* 63 : 97-106

109.   Klos C, Koob M, Kramer C, Dekant W. 1992. p-aminophenol nephrotoxicity: Biosynthesis of toxic glutathione conjugates. *Toxicology and Applied Pharmacology.* 115 : 98-106

110.   Newton JF, Kuo CH, Gemborys MW, Mudge GH, Hook JB. 1982. Nephrotoxicity of p-aminophenol, a metabolite of acetaminophen, in the fischer 344 rat. *Toxicology and Applied Pharmacology.* 65 : 336-44

111.   Harada T, Kimura E, Hirata-Koizumi M, Hirose A, Kamata E, Ema M. 2008. Reproductive and developmental toxicity screening study of 4-aminophenol in rats. *Drug and Chemical Toxicology.* 31 : 473-86

112.   National Toxicology Program (NTP). 1990. *Toxicology and carcinogenesis studies of 2,6-xylidine (2,6-dimethylaniline) in charles river CD rats (feed studies). NTP Technical Report. Rep. No. 278,* US Department of Health and Human Services, Public Health Service, National Institutes of Health, Bethesda,

113.   Lindstrom HV, Hansen WH, Nelson AA, Fitzhugh OG. 1963. The metabolism of FD&C red no. 1. II. the fate of 2, 5-para-xylidine and 2, 6-meta-xylidine in rats and observations on the toxicity of xylidine isomers.*. Journal of Pharmacology and Experimental Therapeutics.* 142 : 257-64

114.   Sellers C, Markowitz S. 1992. Reevaluating the carcinogenicity of ortho-toluidine: A new conclusion and its implications. *Regulatory Toxicology and Pharmacology.* 16 : 301-17

115.   Ward E, Carpenter A, Markowitz S, Roberts D, Halperin W. 1991. Excess number of bladder cancers in workers exposed to ortho-toluidine and aniline. *Journal of the National Cancer Institute.* 83 : 501-6

116. Acquaveixa JF, Wilson JD, C.,P., B, J. 1991. An alternative hypothesis for bladder cancer among workers exposed to ortho-toluidine and aniline. *Journal of the National Cancer Institute.* 83, no.22 : 1686

117. Dupont. *Urinary bladder toxicity - 14-day feeding study with o-tuluidine in rats.* Report DuPont HLR 699-93, TS0557449, as cited in OECD, 2006; Screening Information Data Set for o-Toluidine.

118. Grossman SJ, Jollow DJ. 1986. Use of the NIH shift to determine the relative contribution of competing pathways of aniline metabolism in the rat. *Drug Metabolism and Disposition.* 14 : 689-91

119. Harrison JH, Jollow DJ. 1986. Role of aniline metabolites in aniline-induced hemolytic anemia. *Journal of Pharmacology and Experimental Therapeutics.* 238 : 1045-54

120. Khan MF, Wu X, Boor PJ, Ansari GA. 1999. Oxidative modification of lipids and proteins in aniline-induced splenic toxicity. *Toxicological Sciences.* 48 : 134-40

121. Kao J, Faulkner J, Bridges JW. 1978. Metabolism of aniline in rats, pigs and sheep. *Drug Metabolism and Disposition.* 6 : 549-55

122. Dial LD, Anestis DK, Kennedy SR, Rankin GO. 1998. Tissue distribution, subcellular localization and covalent binding of 2-chloroaniline and 4-chloroaniline in fischer 344 rats. *Toxicology.* 131 : 109-19

123. International Agency for Research on Cancer. 1993. 2, 6-dimethylaniline (2, 6-xylidine). *IARC Monographs on the Evaluation of Carcinogenic Risks to Humans. Occupational Exposures of Hairdressers and Barbers and Personal Use of Hair Colourants; Some Hair Dyes, Cosmetic Colourants, Industrial Dyestuffs and Aromatic Amines.* 57 : 323-35

124. Short CR, Hardy ML, Barker SA. 1989. The in vivo oxidative metabolism of 2, 4- and 2, 6-dimethylaniline in the dog and rat. *Toxicology.* 57 : 45-58

125. Soon Son O, Everett D, Fiala E. 1980. Metabolism of o-[methyl-14C] toluidine in the F344 rat. *Xenobiotica.* 10 : 457-68

126. Yan Z, Nikelly JG, Killmer L, Tarloff JB. 2000. Metabolism of para-aminophenol by rat hepatocytes. *Drug Metabolism and Disposition.* 28 : 880-6

127. Nohynek GJ, Duche D, Garrigues A, Meunier P, Toutain H, Leclaire J. 2005. Under the skin: Biotransformation of para-aminophenol and para-phenylenediamine in reconstructed human epidermis and human hepatocytes. *Toxicology Letters.* 158 : 196-212

128.   Dressler WE, Appelqvist T. 2006. Plasma/blood pharmacokinetics and metabolism after dermal exposure to para-aminophenol or para-phenylenediamine. *Food and Chemical Toxicology*. 44 : 371-9

CHAPTER 2. PBPK MODEL PARAMETERIZATION

2.1.Introduction

PBPK models aim to describe the pharmacokinetics of drugs within the body in relation to blood flows, tissue volumes, along with routes of administration, biotransformation pathways, and interactions with the tissue or organ. As mentioned in Chapter 1, PBPK models consist of a number of biological, physiological and compound-specific parameters which are obtained either experimentally, by calculation, or from the literature to predict drug concentration time profiles in blood/plasma and tissues. In this chapter, the studies used to estimate initial model parameter values needed in PBPK simulations for drug degradation model compounds are presented. A combination of literature, *in vitro* experimentation and *in silico* prediction were used to obtain initial model parameters.

2.1.1. Physiological parameters

The values for physiological parameters used in PBPK modeling (e.g. tissue volumes, rates of tissue blood flow, cardiac output, tissue composition) have been published in a number of references (1-6) but still represent a diverse quality of data. In the majority of the published resources, the authors provided point estimates for the mean value of specific parameters. Occasionally, some studies reported the biological and experimental variability associated with these estimates. Representation of the variability associated with these parameters is essential for population-based PBPK simulation using Monte Carlo methods (2). For example, the publication from the International Commission on Radiological Protection (ICRP) - "Basic Anatomical and Physiological Data for Use in Radiological Protection: Reference Values" presents age- and gender - specific reference values for anatomical and physiological parameters which can be used to estimate radiation doses for humans (1). Data from Western European and North American populations were used to define ICRP reference values because these

populations have been well-studied with respect to anatomy, body composition, and physiology. This report also provided information on individual variation associated with several parameters due to differences in age, gender, race, such as the mass of the stomach, small intestine, large intestine, kidneys and bone and their corresponding standard deviations in males and females. Another useful study by Brown et al (2) contained an extensive compilation of physiological parameter values from open resources for commonly used laboratory animals and humans. Some parameter estimates from this study were used to provide variability estimates for model parameter sensitivity analysis.

2.1.2. Tissue to plasma partition coefficients

In addition to physiological and anatomical parameters, tissue-to-plasma partition coefficients are key biochemical parameters that determine the rate and extent of tissue distribution. These parameters are estimated by various methods. For example, Poulin and Thiel (7) and Rodgers and Rowland (8, 9) derived prediction equations for tissue partition coefficients based on physicochemical properties of drug molecules, protein binding and the composition of specific tissues.

The model proposed by Poulin and Thiel considered drug solubility in lipids and water and its binding to macromolecules. Model assumptions include steady-state, uniform distribution within a tissue and passive diffusion based on lipophilicity of unbound, unionized drug. However, this model does not consider paracellular permeability, which is important for small, hydrophilic molecules such as group of substituted anilines, nor does it consider transporter-mediated distribution. Additionally, no distinction was made between acids, bases and neutral compounds with regard to interaction with tissue components. Rodgers and Rowland (8) extended the model to reflect the significance of electrostatic interactions between moderate to strong bases and Type 1 zwitterions (at least one basic $pK_a \geq 7$) and acidic phospholipids. A separate

model (9) was also developed for very weak bases, neutral compounds, acids and Type 2 zwitterions (no $pK_a > 7$) to address their bindings to extracellular proteins such as albumin and lipoprotein. Mathematically, the model of Rodgers and Rowland for acids, neutral compounds and very weak bases was derived as described as follows:

Kpu is the ratio of concentration of unbound drug in tissues (C_T) to unbound drug in plasma (Cu_P) at steady state. The total concentration of drug in tissues is the sum of concentration in each component (Equation 2.1):

$$C_T = Cu_{IW} \times f_{IW} + (Cu_{EW} + C_{PR,EW}) \times f_{EW} + C_{NL} \times f_{NL} + C_{NP} \times f_{NP} \quad (Eq.2.1)$$

Where f refers to fractional tissue volume; and IW, EW, NL, NP and PR refer to intracellular water, extracellular water, neutral lipid, neutral phospholipid and protein, respectively.

For very weak monoprotic bases, X and Y are defined as the inverse fractions of weak base unionized in intracellular water and plasma, respectively:

$$X = 1 + 10^{pK_a - pH_{IW}} ; Y = 1 + 10^{pK_a - pH_P}$$

For monoprotic acids, X and Y are inverse fractions of monoprotic acid unionized in intracellular water and plasma, respectively:

$$X = 1 + 10^{pH_{IW} - pK_a} ; Y = 1 + 10^{pH_P - pK_a}$$

For neutral compounds: $\quad X = Y = 1$

The concentration in the different cellular components in Equation 2.1 was calculated as below:

- The first term is the concentration of drug in intracellular water:
$$Cu_{IW} \times f_{IW} = Cu_P \times \frac{X}{Y} \times f_{IW} \quad (Eq. 2.2)$$

- The second term is the concentration of drug in extracellular water:
$$(Cu_{EW} + C_{PR,EW}) \times f_{EW} = (Cu_P + Cu_P \times Ka_{PR} \times [PR]_{EW}) \times f_{EW}$$

$$= Cu_P \times (f_{EW} + Ka_{PR} \times [PR]_T) \quad (Eq. 2.3)$$

Where, Ka_{PR} is the association constant of acids and very weak bases for albumin,

47

and neutral drugs for lipoproteins. Ka_{PR} is assumed to be identical in all tissues, and can be calculated as Equation 2.4:

$$Ka_{PR} = \left[\frac{1}{fu} - 1 - \left(\frac{P \times f_{NL,P} + (0.3P + 0.7) \times f_{NP,P}}{Y}\right)\right] \times \frac{1}{[PR]_P} \qquad (Eq.2.4)$$

[PR] refers to albumin or lipoprotein concentration in tissue ($[PR]_T$) or plasma ($[PR]_P$). $P_{o/w}$ is the octanol/water partition coefficient which is used to describe partitioning for non-adipose tissues. $P_{vo/w}$ is the vegetable oil / water coefficient which is used to describe partitioning for adipose tissue, based on the study of Poulin et al. which indicated that vegetable oil was a better surrogate than n-octanol for neutral lipid such as adipose tissue (10).

- The third term is the concentration of drug in neutral lipids

$$C_{NL} \times f_{NL} = \frac{Cu_P \times P}{Y} \times f_{NL} \qquad (Eq.2.5)$$

- The fourth term is the concentration of drug in neutral phospholipids:

$$C_{NP} \times f_{NP} = \frac{Cu_P}{Y}(0.3P + 0.7) \times f_{NP} \qquad (Eq.2.6)$$

Substitution of the drug concentrations in various tissue components (Eq. 2.2 – 2.6) into equation 2.1 and Kpu can be obtained as Equation 2.7:

$$Kpu = \frac{C_T}{Cu_P} = \frac{X}{Y} \times f_{IW} + f_{EW} + \left[\frac{1}{fu} - 1 - \left(\frac{P \times f_{NL,P} + (0.3P + 0.7) \times f_{NP,P}}{Y}\right)\right] \times \frac{[PR]_T}{[PR]_P}$$
$$+ \frac{P \times f_{NL} + (0.3P + 0.7) \times f_{NP}}{Y}$$

$$(Eq.2.7)$$

2.1.3. *In vitro* methods for determination of metabolic constants

The group of model drug degradants (Table 1.3) has been reported to be metabolized mainly in the liver. Hence, in order to express the rate and extent of metabolism in PBPK model, metabolic parameters, such as intrinsic clearance (CL_{int}), the maximum metabolic rate (V_{max}) and the Michaelis constant (K_m - the value for substrate concentration at the half-maximal velocity) need to be estimated. Intrinsic clearance CL_{int}

is defined as the ratio of V_{max} and K_m of all enzymes involved in its metabolism, provided that the substrate concentration is well below the K_m of the metabolizing system (11). Assessment of the underlying primary parameters, V_{max} and K_m, enables the prediction of non-linear kinetics which may improve the accuracy of the prediction of *in vivo* pharmacokinetics (12). V_{max} and K_m are typically determined using *in vitro* experiments to measure metabolism rates, such as liver microsomes, hepatocytes and cytosol (13, 14). In general, these parameters can be estimated by measuring the rate of metabolite appearance or rate of substrate depletion. Metabolic pathway specificity plays an important role in metabolite appearance rate whereas depletion rates represent the summation of all metabolic pathways and therefore are potentially more useful in estimating overall intrinsic clearance.

Depending upon the ratio of the initial substrate concentration to the Michaelis constants, the substrate depletion profile will reflect first order, zero order or mixed order. Therefore, depletion profiles are typically evaluated by using initial rate conditions wherein the final substrate concentration is within 20% of the initial concentration and the rate can be estimated by linear regression of the substrate concentration versus time. Under these conditions:

$$[S_t] = [S_0] - k_0 \times t$$

$$\upsilon = -\frac{d[S]}{dt} = k_0$$

$$v = \frac{V_{max} \times [S_0]}{K_m + [S_0]}$$

S_t is the substrate concentration at time t and S_0 is initial substrate concentration. And k_0 is the zero order rate (also the rate constant).

2.1.4. Plasma and microsomal protein binding

Plasma protein binding impacts both the pharmacokinetics and pharmacodynamics of a compound. Only the unbound fraction of a drug in plasma is

available for many pharmacokinetic and pharmacodynamic processes, such as membrane permeation and receptor binding. If the drug molecules are highly bound to plasma protein, they may have restricted distribution into target tissue and will be retained in plasma. High plasma protein binding also can cause decreases in drug metabolism, clearance and prolong drug half-life (15). Consequently, the determination of the plasma protein binding properties of a compound is essential during PBPK model development. Albumin and acid glycoprotein are responsible for most plasma binding of drug molecules. Some lipophilic drugs also extensively bind to plasma lipoproteins (8, 9). The model degradation products (substituted anilines) are weak bases and hence primarily bind to albumin (8, 9).

Prediction of the *in vivo* metabolic clearance of compounds has been investigated using variety of *in vitro* metabolizing systems, such as liver microsomes, hepatocytes and cytosol. Nonspecific microsomal binding in the *in vitro* metabolic assays can significantly affect the observed kinetics of metabolism and reduce the accuracy of the clearance prediction (16). Therefore, estimated metabolism parameters need to be corrected for the unbound drug fraction (fu_{mic}) to predict *in vivo* clearance.

The extent of protein binding in plasma and microsomes can be determined using the ultrafiltration technique. Ultrafiltration relies on centrifugal force to drive the unbound test compound through a size-selective membrane. Ultrafiltration methods are generally less time-consuming than other protein binding determination methods such as equilibrium dialysis. However, non-specific binding of the test compounds to the ultrafiltration device components should be determined for plasma protein binding calculations (17).

2.1.5. Prediction of Caco-2 permeability using molecular descriptors

The permeability of a drug across cell membranes is an important determinant of both the rate and extent of absorption following oral administration. In PBPK modeling

for orally administered compounds, effective intestinal permeability coefficients must be determined. The *in vitro* permeability across monolayers of the human colon carcinoma cell line (Caco-2), cultured on permeable supports are commonly used to predict the absorption of orally administered drugs. Recently, computational methods (Quantitative Structure Activity Relationship – QSAR) have been developed to predict permeability using various molecular descriptors (18-24). In this approach, several molecular descriptors that may influence the permeation of drugs through biological membranes by a passive diffusion mechanism such as solubility, lipophilicity, polarity molecular size and hydrogen bonding capability are used to construct a multivariate correlation. In the context of model selection, Bayesian information criterion (BIC) provides a means for selecting the best model from a set of candidate models when addressing the issue of over-fitting in regression. Given two candidate models, the model with the lower value of BIC is the one to be preferred (25)

Palm and coworkers (19) found a good correlation between dynamic surface properties of the β-receptor blocking agents and their permeability coefficients in monolayers of human intestinal epithelial Caco-2 cells. This finding indicated that the dynamic polar surface area is an important factor in passive transcellular transport across cell membranes. Waterbeemd and Camenisch (18) investigated a number of different calculated molecular size and hydrogen-bonding descriptors with respect to membrane permeation. A linear combination of suitable molecular size and hydrogen bonding was found to provide reasonable estimates of permeability by multiple linear or partial least squares regression. Hou et al. (20) included 100 drug molecules with various descriptor sets to generate models with coefficient of determination R^2 ranging from 0.1 to 0.72. The authors identified that Caco-2 permeation depends primarily on distribution coefficient (logD), highly-charged polar surface areas and the radius of gyration.

51

2.1.6. The Bayesian approach and Markov Chain Monte Carlo simulation

As with other approaches to statistics, the object of analyzing data is to make inferences about some unknown parameters. In the Bayesian approach, inference is a process of learning from data (26). In this process, prior information is incorporated, then observations are made and the prior knowledge is updated to create posterior information. Both the prior and posterior knowledge in the Bayesian framework are described as probability distributions. The aim of Bayesian analysis is to obtain the posterior distribution of the parameter of interest instead of a point estimate. The basic tool of the Bayesian approach is Bayes' theorem, which is the formula for deriving the posterior distribution. It can be simply expressed as:

$$p(\theta|y) \sim p(\theta) \times p(y|\theta)$$

In which, $p(\theta|y)$ is the posterior density, whereas $p(\theta)$ is the prior density. The other term, $p(y|\theta)$, is the probability distribution for the data, conditional on the parameter θ, and is referred to as the likelihood function. If the observed data is normally distributed, a likelihood function can be expressed in Equation 2.8:

$$L(y_i|f_i,\sigma_i^2) = \prod_{i=1}^{n} \frac{1}{\sigma_i\sqrt{2\pi}} \exp\left(-\frac{(y_i - f_i)^2}{2\sigma_i^2}\right) \qquad \text{(Eq.2.8)}$$

In this equation, y_i is observed data, f_i is predicted value for a specific model, and n is the number of observations. The variance σ_i^2 of the error in the data can be constant (σ^2) (homoscedatic) or can be treated as heteroscedatic by multiplicative and additive error models.

The theorem states that the posterior density is proportional to the product of the prior density and the likelihood. In the Bayesian approach, the posterior combines information in both a priori knowledge from literature and information in experimental data. This results in the posterior distribution for a specific parameter that leverages both prior knowledge and observation, thereby providing a narrower range of possible values

52

for θ (26).

Typically, the Markov chain Monte Carlo (MCMC) method is used to make inferences about model parameters and to make predictions. MCMC is based on drawing values for parameter θ (Monte Carlo) from approximate distributions and then adjusting the random selections to better approximate the target posterior distribution $p(\theta|y)$ via Markov chains (27). The Metropolis-Hastings algorithm is useful for drawing samples from Bayesian posterior distributions. This algorithm is an adaption of a random walk that uses an acceptance/rejection rule to converge to a specified target distribution (27). Generally, model parameters are assigned initial values by random sampling from prior distribution or may be based on maximum likelihood estimate. When the Metropolis-Hastings algorithm is used, each component θ_k of the parameter vector θ is updated at each iteration step according to an acceptance/rejection rule. The algorithm usually requires several thousand iterations. The MCMC inputs require observed data, a model for data prediction, a likelihood function, prior distributions and initial values for model parameters.

Proof of convergence to a target distribution can be assessed by convergence diagnostics, such as history plots. A history plot shows the trajectories of sampler output for each model parameter from every iteration. It can quickly reveal failure or success of MCMC samplers to reach the target distribution. In general practice, the initial iterations which are the first half of the iteration sequence need to be discarded so that the remaining samples are drawn from a distribution close enough to the true stationary distribution to be usable for estimation and inference (27).

2.1.7. Data analysis in R using deSolve and FME packages

R is an open source data analysis system which has been widely used (28). In R, 'deSolve' is an add-on package for solving a system of differential equations (29). A system of ordinary differential equations was formulated as the mathematical description

53

of PBPK models and solved by numerical integration using deSolve's integration function `ode`.

Another package used for PBPK model development is FME (30). FME is an R-package that contains functions to run complex applications of models, such as parameter estimation, sensitivity and Monte Carlo analysis. It can be applied to perform global sensitivity analysis to investigate the impact of parameter variation on model outputs. It can run the MCMC to estimate parameter uncertainties. The function `modMCMC` is used to run a MCMC by implementing the delayed rejection-adaptive Metropolis algorithm.

2.2. Materials and Methods

2.2.1 Materials

Aniline (Lot # 68396APV), p-chloroaniline (PCA) (Lot # 12131JJV), 2,6-dimethylaniline (DMA) (Lot# STBB2839V), o-toluidine (o-TOL) (Lot# MKBL4145V), p-aminophenol (PAP) (Lot # SZBB2860V), and aniline metabolites which are 2-aminophenol (2-AP) (Lot # 2107X), 3-aminophenol (3-AP) (Lot # 02922PA) and acetaminophen (APAP)) were purchased from Sigma-Aldrich (USA). Methanol (chromatographic grade), acetonitrile, potassium phosphate monobasic and dibasic (analytical grade) were purchased from Fisher Scientific (New Jersey, USA). Sprague Dawley rat liver microsomes, NADPH regenerating system solution A (26 mM NADP$^+$, 66 mM glucose-6-phosphate, and 66 mM MgCl$_2$ in H$_2$O) (Lot # 29850) & solution B (40 U/mL glucose-6-phosphate dehydrogenase in 5 mM sodium citrate) (Lot # 28594), potassium phosphate (0.5M, pH 7.4) (Lot # 28589) were obtained from BD Biosciences (Massachusetts, USA). Cryopreserved Sprague-Dawley rat and Rodent Hepatocyte Isolation Kits were purchased from Xenotech LLC (Lenexa, KS). Rat plasma and blood (Sprague Dawley) were purchased from Bioreclamation LLC (New York, USA).

2.2.2. Physiological and physicochemical parameters

Physiological parameters

Reported organ tissue volumes and blood flows for each organ were incorporated into differential equations that describe the fate of a compound within a specific tissue. These parameters were obtained from the literature for a 250 g rat, a 60 kg adult healthy woman and a 70 kg man. Organ volumes in the rat were taken from Brown and colleagues (2), except for adipose tissue (31), bone (32) and artery and vein blood volumes (33). Blood flows in rat were taken from Brown et al. (2) and Delp et al. (31) and other sources (33-35). The mean value of cardiac output in rats was reported as 110.4 ± 15.60 (ml/min) (2). Physiological parameters in rats were presented in Table 2.1.

Table 2.1- Physiological parameters for rats

Organ	Organ weight [a] (% body weight)		Blood flow [e] (% of cardiac output)	
	Mean	SD	Mean	SD
Adipose Tissue	5.55[b]	0.18[b]	1.03[f]	0.2[f]
Bone	4.77[c]	0.17[c]	12.2	1.1
Brain	0.57	0.14	2.0	0.3
Stomach	0.46	0.06	1.8[g]	0.5[g]
Gut	2.24	0.39	11.6[h]	1.7[h]
Heart	0.33	0.04	4.9	0.1
Kidneys	0.73	0.11	14.1	1.9
Liver	3.66	0.65	18.3	-
Lungs	0.50	0.09	2.1	0.4
Muscle	40.43	7.17	27.8	2.9
Pancreas	0.32	0.07	0.8[i]	0.5[i]
Skin	19.03	2.62	5.8	0.62
Spleen	0.20	0.05	1.0	0.6
Thyroid	0.005	0.002	1.0	-
Artery	2.24[d]	-		
Vein	4.52[d]	-		

[a] Organ volumes in the rat were taken from Brown et al. (2) . [b] Volume of adipose tissue from Delp et al. (31). [c] Volume of bone from MacPherson (32). [d] Artery and vein blood volumes from Bernareggi et al. (33). [e] Blood flows in rat were taken from Brown et al. (2). [fh] Blood flow of adipose and gut were taken from Delp et al. (31). [g] Stomach blood flow was from Idvall (34). Pancreas blood flow was taken from Sasaki (35).

The mean values and standard deviations of organ weights (percent of body weight) for adult healthy males (70 kg) and females (60 kg) were taken from ICRP Publication 89 (1) and de la Grandmaison et al. (36) (Table 2.2). The blood flow rates for human model were obtained from ICRP Publication 89 (1). Adults are generally considered to be in the age range of 20–50 years and the reference values were obtained from Western Europeans and North American populations.

Table 2.2- Organ weight (percent of body weight - % BW) and blood flow rate (percent of cardiac output - % CO) for human males and females

Organ	Males [a]			Females [a]		
	Organ weight (% BW)		Blood Flow (% CO)	Organ weight (% BW)		Blood Flow (% CO)
	Mean	SD	Mean	Mean	SD	Mean
Heart	0.54	0.10	4.3	0.54	0.13	5.3
Left lung	0.86	0.32	100	0.81	0.30	100
Right lung	0.98	0.35	100	0.94	0.36	100
Spleen	0.23	0.13	3.2	0.24	0.13	3.2
Thymus	0.04	0.02	1.6	0.03	0.02	1.6
Liver	2.47	0.58	27.2	2.54	0.62	29.5
Kidney	0.44	0.11	20.1	0.45	0.13	18.3
Stomach	0.21	0.06	1.1	0.23	0.03	1.1
Small Intestine	0.89	0.11	10.6	1.00	0.12	11.8
Large Intestine	0.51	0.10	4.3	0.60	0.08	5.3
Pancreas [b]	0.21	0.06	1.1	0.21	0.06	1.1
Vein	5.11	-	100	4.56	-	100
Artery	2.56	-	100	2.28	-	100
Adipose	20.00	-	5.3	30.00	-	9.1
Muscle	39.70	-	18.1	29.20	-	12.8
Skin	4.52	-	5.3	3.83	-	5.3
Brain	1.99	-	12.8	2.17	-	12.8
Bone	14.38	-	5.3	13.00	-	5.3
Hepatic Artery	-	-	6.9	-	-	7

[a] Values from ICRP Publication 89 (1)
[b] Pancreas weight for males and females were from de la Grandmaison et al. (36).

The fractional volumes for vascular space and interstitial fluid were obtained from the literature (37) and displayed in Table 2.3. As common assumption used in Rodger and Rowland approach, (38) for each tissue, these fractional volumes measured in rats were assumed to be the same as those in humans.

Table 2.3- Fractional volume of vascular and interstitial space in various organs of mammals (37)

Name	Vascular	Interstitial space
Adipose	0.010	0.135
Muscle	0.026	0.120
Skin	0.019	0.302
Brain	0.037	0.004
Heart	0.262	0.100
Lung	0.262	0.188
Pancreas	0.180	0.120
Spleen	0.282	0.150
Bone	0.041	0.100
Thymus	0.030	0.150
Liver	0.115	0.163
Kidney	0.105	0.200
Stomach	0.032	0.100
Gut	0.024	0.094

Other physiological parameters, such as gastric emptying rate, small intestine transit rate, pH of the gastrointestinal compartments and radius of small intestine were obtained from Peters (39).

The primary factors controlling the distribution of drug between blood and tissues are plasma protein, extracellular water, intracellular water, acidic phospholipids, neutral lipids and neutral phospholipids (8). In order to predict tissue-to-plasma partition coefficients in rats and humans using Equation 2.7, the residual blood adjusted rat tissue composition data were taken from literature for both species (8, 9, 40, 41). Tissue composition parameters for rats are shown in Table 2.4.

Table 2.4-Mean value of rat tissue composition parameters for the mechanistic equations used to predict Kpu values

Organ	Fractional Tissue Volume					Tissue-plasma albumin ratio	Tissue-plasma lipoprotein ratio
	Neutral Lipid	Neutral Phospholipid	Extracellular Water	Intracellular Water	Acidic Phospholipid*		
Adipose	0.853	0.0016	0.135	0.017	0.40	0.049	0.068
Bone	0.0174	0.0016	0.100	0.346	0.67	0.100	0.050
Brain	0.0391	0.0015	0.162	0.620	0.40	0.048	0.041
Gut	0.0375	0.0124	0.282	0.475	2.41	0.158	0.141
Heart	0.0135	0.0106	0.320	0.456	2.25	0.157	0.160
Kidney	0.0121	0.0240	0.273	0.483	5.03	0.130	0.137
Liver	0.0135	0.0238	0.161	0.573	4.56	0.086	0.161
Lung	0.0215	0.0123	0.336	0.446	3.91	0.212	0.168
Muscle	0.0100	0.0072	0.118	0.630	1.53	0.064	0.059
Pancreas	0.0403	0.0090	0.120	0.664	1.67	0.060	0.060
Skin	0.0603	0.0044	0.382	0.291	1.32	0.277	0.096
Spleen	0.0071	0.0107	0.207	0.579	3.18	0.097	0.207
Thymus	0.0168	0.0092	0.150	0.626	2.30	0.075	0.075
Stomach**	0.0182	0.0338	0.282	0.475	2.41	0.158	0.141
Blood cells	0.0017	0.0029	-	0.603	0.50	0.603	0.500
Plasma	0.0032	0.0021	-	-	-	-	-

* Concentration of acidic phospholipids (mg/g); ** Stomach values of neutral lipid, neutral phospholipid obtained from Peters (37); other stomach components assumed to be the same as gut components. All other parameters were obtained from Rodgers and Rowland (8,9)

58

Physicochemical parameters

Aniline, o-toluidine, p-chloroaniline and 2,6-dimethylaniline are aromatic amines and act as weak bases in aqueous solution. 4-Aminophenol is amphoteric with both aromatic amine and phenolic hydroxyl groups. The acidity of the hydroxyl function is depressed by the presence of an amino group on the benzene ring and the amino group behaves as a weak base. The physicochemical parameters such as pKa and logP values are necessary for the prediction of tissue to plasma partition coefficients using Equation 2.7. The experimental pKa values (25ºC) of model compounds determined using potentiometric or spectrophotometric methods were taken from literature (Table 2.5).

Table 2.5- pKa and logP$_{o/w}$ of model compounds

Compound	pKa ± SD (reference)	logP$_{o/w}$ (reference)
Aniline	4.596 ± 0.002 (42); 4.72 ± 0.02 (43); 4.62 ± 0.003 (44) 4.56 (45); 4.58 (46, 47); 4.6(48); 4.62 (49, 50); 4.63 (51)	0.90 (52); 0.94 ± 0.006 (53); 0.90 (54); 0.98 (54); 0.90 ± 0.01 (55)
p-Chloroaniline	3.98 (47, 48); 4.05 (56)	1.88 ± 0.014 (53); 1.83 (54)
2,6-Dimethylaniline	3.91 ± 0.05 (44); 3.95 (57)	1.815 (60)
o-Toluidine	4.447 ± 0.001 (42); 4.45 ± 0.03 (44); 4.39 (58); 4.45 (48); 4.53 (56)	1.29 (54), 1.32 (54)
p-Aminophenol	5.65 (56); 5.5 (47); 5.48 (59); 10.46 (60)	0.04 (54)

2.2.3. Tissue-plasma partition coefficients

In order to predict the venous blood drug concentration leaving a tissue, the partition coefficient of drug between the tissue and blood (Kpu) needs to be estimated. The mechanistic tissue composition-based equation (Eq. 2.7) for acids, very weak bases, neutral compounds, and some zwitterions from the model of Rodgers and Rowland (52) was utilized to predict the Kpu values for model compounds. The assumption of passive drug distribution is reasonable based on based on the absence of evidence for specific

transporters (61). The Kpu values in rats and humans were estimated for 14 tissues (adipose, bone, brain, gut, heart, kidney, liver, lung, muscle, pancreas, skin, spleen, stomach and thymus) using residual blood adjusted rat tissue composition data for both species along with fraction unbound in plasma and blood to plasma ratio values. Blood to plasma ratio of aniline in rats was obtained from literature (62, 63), which is equal to 1. Other model compounds (such as PCA, o-TOL, 2,6-DMA and PAP) were assumed to distribute equally in plasma and erythrocytes.

LogP$_{vo/w}$ was calculated from logP$_{o/w}$ using the following relationship based on a linear regression analysis obtained between experimental data on logP$_{vo/w}$ and logP$_{o/w}$ of several organic chemicals including weak acids, bases and unchanged molecules (64)

$$\text{LogP}_{vo/w} = 1.115 \times \text{LogP}_{o/w} - 1.35 \qquad (n = 104, r = 0.99) \qquad \text{(Eq.2.9)}$$

The predictions of tissue-to-plasma partition coefficients were used to determine whole body unbound volume of distribution at steady state in rats and humans (Vd$_{u,ss}$). The Vd$_{u,ss}$ values were computed by inserting the appropriate Kpu values into equation 2.10 and converted into L/kg by dividing by 250 g in rats and 70 kg in humans.

$$\text{Vd}_{u,ss} = \frac{V_{plasma}}{fu_p} + \frac{V_{RBC}}{fu_p} \times \frac{K_{B/P} - (1-H)}{H} + \sum_{tissues} V_i . Kpu_i \qquad \text{(Eq.2.10)}$$

Vd$_{u,ss}$ refers to unbound volume of distribution at steady state which is in equilibrium between unbound concentration in plasma and tissues. V$_{plasma}$, V$_{RBC}$ and V$_i$ are volume of plasma, erythrocyte and ith tissue, respectively. K$_{B/P}$ and H are blood to plasma ratio and hematocrit value. Kpu$_i$ is ith unbound tissue-to-plasma partition coefficient.

2.2.4. Metabolic rate constants

In order to parameterize metabolic clearance in rat PBPK model, the maximal velocity (V$_{max}$) and Michaelis constant (K$_m$) values were determined by measuring the rate of substrate depletion in *in vitro* metabolizing systems.

Substrate depletion in rat liver microsomes

Aniline was reported to be mainly metabolized in liver, by acetylation and hydroxylation pathway (65). The hydroxylation by CYP 450 is major pathway of aniline metabolism and aminophenol is major metabolite of aniline. Therefore, pooled rat liver microsomes were used to investigate the metabolic kinetics of substituted anilines.

General incubation conditions and sample treatment: Substrate was incubated with 100 mM potassium phosphate buffer pH 7.4 and NADPH-generating system in a shaking water bath at 37ºC. After thawing microsomes, the reaction was initiated with the addition of 25 μL microsomes giving a final incubation volume of 1mL and 0.5 mg/mL microsome concentration. At times of zero, 10, 20, 30, 40, 50, 60 minutes, aliquots (0.12 mL) were removed and quenched with the addition of 0.12 mL ice-cold methanol. The sample tubes were centrifuged for 5 minutes at 10,000 g, and the supernatant was pipetted into HPLC vials for analysis. Substrate depletion experiments were conducted at 5 or 6 substrate concentrations in triplicate. Concentration ranges used for each model compound were as following: aniline, 10 to 1000 μM; PAP, 2 to 2000 μM; 2,6-DMA, 10 to 1000 μM; o-TOL, 3 to 1250 μM.

Substrate depletion in rat hepatocytes

p-Aminophenol has been reported to be mainly converted by human hepatocytes to sulfate and glucuronic acid conjugates of both APAP and PAP (66). Therefore, hepatocytes were chosen to investigate enzyme kinetics of PAP and obtain the depletion profiles of PAP.

Cryopreserved rat hepatocytes and hepatocyte isolation kits were purchased from XenoTech LLC (Lenexa, KS); the cells were stored in the vapor phase of liquid nitrogen until use. Immediately before use, vials of hepatocytes were rapidly thawed in a shaking water bath (37°C; 1 – 1.5 min) or until the frozen cell pellet move freely when the cryotube was inverted. In a biological cabinet, the frozen pellet containing the

hepatocytes was slowly transferred to the 30% isotonic Percoll solution (Tube A of the Rodent Hepatocyte Isolation Kits). The tube was inverted horizontally and mixed until the pellet was completely suspended in the solution. The hepatocytes were isolated via centrifugation using Eppendorf centrifuge rotor 5810 R at 100g for 5 minutes at room temperature. The supernatant was removed and the pellet of hepatocytes was resuspended by gentle inversion in prewarmed Hepatocyte Incubation Media (Waymouth's media, pH 7.4; 1–2 ml). The cell number and viability were determined by the trypan blue exclusion assay (67) prior to substrate incubations.

Stock solutions of PAP were prepared freshly in methanol and diluted with Hepatocyte Incubation Media. The initial PAP concentration was twice the desired final concentration in reaction mixture. The initial substrate concentration range was 500 to 3000 μM. In a microcentrifuge tube, 500 μL of PAP in media was added and preincubated in the shaking water bath at 37°C, gassed with the mixture of 95% O_2 and 5% CO_2 for 5 min. The reaction was initiated by adding 500 μL of hepatocyte suspension (final concentration $1x10^6$ cells/mL). After incubation at 37°C for various time periods, the metabolism of PAP were quenched by the addition of acetonitrile. The quenched reaction mixtures were centrifuged at 10,000g for 5 min, and an aliquot of the supernatant was injected into an HPLC for measuring the unchanged compound concentration. Assays were performed in triplicate depending on cell availability.

<u>Analytical Assays</u>

HPLC methods for the measurement of unchanged model compound concentrations in liver microsomes, hepatocytes after centrifugation to precipitate protein were developed. Samples were analyzed by a Thermo Spectrum HPLC System (P4000 pump, AS3000 auto injector, and UV 6000 LP photodiode array detection system). Chromatographic data were analyzed and stored using PC1000 chromatography data system software. The elution of aniline, PCA, 2,6-DMA, and o-TOL was accomplished

using a 4.6x150 mm Symmetry C18 5 μm column (Waters Corporation). PAP was eluted using an XBridge^{TM} C18 5μm 4.6x150 mm column (Waters Corporation). Analytical wavelength used was 230 nm, flow rate was 1 ml/min. The mobile phase for the analysis of each model compound is listed in the following Table 2.6.

Table 2.6- Mobile phase for each model compound

Compound	Mobile phase
Aniline	methanol: phosphate buffer 5 mM pH 7.4 (25:75)
PCA	methanol: phosphate buffer 10 pH 7.4 (40:60)
2,6-DMA	methanol: phosphate buffer 10 mM pH 7.4 (40:60)
o-TOL	methanol: phosphate buffer 10 mM pH 7.4 (40:60)
PAP	acetonitrile: phosphate buffer 25 pH 7.4 (5:95)

Method validation

To determine system suitability, a stock solution of aniline and its major metabolites (2-AP, 3-AP, PAP, and acetaminophen) was prepared in 50 mL of methanol. The stock solution was then diluted with mobile phase for system suitability standards. The separation of aniline and metabolites was accomplished using a 150 mm Symmetry C18 5 μm column (Waters Corporation), using a flow rate of 1.0 ml/min with methanol: phosphate buffer 5mM pH 7.4 (25:75) as mobile phase. System suitability was determined from six replicate injections of the standards before sample analysis. Analytical parameters including theoretical plates, asymmetry and resolution between aniline and other metabolites were evaluated. Three acceptance criteria for aniline were peak area RSD $\leq$ 2%, column plates $>$ 2000 and asymmetry value $<$ 3. The results were used to monitor critical operational parameters of the chromatographic system to confirm that the resolution and precision were adequate for sample analysis.

To assess linearity of the analytical method for aniline, standard calibration curves were prepared using substrate solutions with concentrations range of 5 – 1500 μM. The peak areas versus concentrations were evaluated using linear regression analysis.

63

Analytical methods for the other model compounds were carried out using the same procedure except the analytical concentration ranges were adjusted based on the initial concentration ranges used in the substrate depletion studies (as described above).

Data Analysis

Enzyme kinetic parameters (V_{max}, K_m) were estimated by fitting the Michaelis-Menten equation to all depletion curves simultaneously with Bayesian parameter estimation via MCMC sampling. The starting values for V_{max} and K_m were obtained from nonlinear least square estimates by fitting the Michaelis-Menten equation to initial rates versus substrate concentrations using nonlinear regression. The prior distributions for the metabolic parameters were non-informative which expresses negligible prior knowledge relative to the data. The MCMC simulation using the Metropolis-Hastings algorithm was performed using software R and the FME package. In the MCMC process, 10,000 iterations were run for convergence and 50,000 iterations were burned-in to make inference. The protein content in micrososmes was determined based on the manufacturer information of material supply.

After the MCMC sampler converged, the posterior distributions of V_{max} and K_m were used to estimate the mean and 95% confidence intervals of the initial reaction velocities based on Michaelis-Menten model predictions. The observed and predicted metabolic rates were compared to evaluate model structure and reliability.

2.2.5. Microsomal and plasma protein binding

Microsomal and plasma protein unbound fractions were measured using ultrafiltration techniques. The determination of microsomal binding was necessary to correct the Michaelis constant, K_m, for the fraction of drug concentration unbound in metabolic assay using liver microsomes. Plasma protein binding was used as input parameter for tissue to plasma partition coefficient prediction using the tissue composition-based equation (Eq. 2.7).

General procedure: Protein binding was determined in the Sprague Dawley rat microsomal incubation media (BD Biosciences) by an ultrafiltration method. Stock solutions of substrates were added to rat microsomes suspended in 0.1 M potassium phosphate buffer, pH 7.4 (0.5 mg/mL microsomal protein) at 37ºC in shaking water bath to give final concentrations containing less than 1% methanol (v/v). After 20 min of equilibration, aliquots (1 mL, in triplicate) of these samples were added to ultrafiltration tubes (Centrifree, Millipore). Then 100 μL of samples were withdrawn and centrifuged at 10,000 g for 5 min (Eppendorf) to measure the actual total concentration added into the incubation mixture. The remaining medium in tubes was separated from proteins and other cellular material by centrifugation at 1000 g, 37ºC for 30 min. The filtrate was analyzed by HPLC-UV to measure the unbound drug concentration. To evaluate the nonspecific binding to the ultrafiltration tube, concentrations of compounds were measured in filtered and unfiltered 0.1 M potassium phosphate buffer, pH 7.4. Fraction unbound of unbound substrate to microsomes was then calculated with correction of nonspecific binding to ultrafiltration tube. The experiment was conducted at 3 to 5 substrate concentrations.

The fraction of substrate unbound to plasma protein was determined using similar procedure wherein plasma was substituted for microsomes as a source of substrate binding. Frozen plasma was thawed at room temperature and then centrifuged in 5 min at 2000 g (Eppendorf) to remove fibrous precipitate. Defrosted plasma was measured and adjusted pH to 7.4 by adding small amounts of sodium phosphate dibasic. Stock solutions were added to plasma in microcentrifuge tube, mixed and incubated at 37ºC for 20 min in shaking water bath. After incubation, a 1 mL aliquot was added to ultrafiltration tubes and the free fraction was separated and analyzed as above. The total substrate concentration added into the plasma incubation was computed from stock solutions instead of measuring.

The concentration ranges for individual substrates were as follows: aniline, 2 – 1000 µM; PCA, 10 – 2000 µM; 2,6-DMA, 20 – 1000 µM, o-TOL, 20 – 1000 µM; PAP, 10 – 3000 µM.

The filtrate of each model compound was analyzed by HPLC-UV with the chromatographic conditions similar to those for the metabolic assays described above. The fraction unbound was calculated by dividing the substrate concentration after filtration ([Cu]), corrected for nonspecific binding to ultrafiltration device (fu$_{device}$) , with total substrate concentration [C] (Equation 2.11):

$$fu_p = \frac{[Cu]}{[C]_{total} \times fu_{device}}$$
(Eq. 2.11)

2.2.6. Effective intestinal permeability

The jejunal effective permeability (logP$_{eff}$) of model compounds for absorption rate calculation was estimated using QSAR method wherein two correlations were used to estimate *in vivo* permeability from molecular properties of the individual model compounds. The first correlation was used to establish a relationship between molecular descriptors and Caco-2 permeability. A second correlation model was then developed to relate Caco-2 permeability to *in vivo* permeability. The specific procedures are described below:

Correlation of Caco-2 permeation with molecular properties

The first correlation was developed for Caco-2 cell permeability (logP$_{app}$) and molecular descriptors using multivariate regression analysis. A set of 22 structurally-related aromatic amines which contain one benzene ring were selected to build the model. The compounds included aspirin, alprenolol, aminopyrine, atenolol, clonidine, dopamine, ibuprofen, ephedrine, metopropol, hydroquinone, oxeprenolol, practolol, salicylic acid, terbutaline, acetaminophen, procaine, amphetamine, ethionamide, acebutolol, guanabenz, epinephrine and lidocaine. For each compound, two sets of data were compiled: the

molecular descriptors including topological indices, structural keys, E-state indices obtained from the Molecular Operating Environment (MOE) software (68) and literature reported Caco-2 cell permeabilities. A list of the molecular descriptors is tabulated in Table 2.7.

Table 2.7- Code of molecular descriptors considered in the Caco-2
cell model

Code	Description
b_rotR	Fraction of rotatable bonds
rgyr	Radius of gyration.
a_acc	Number of hydrogen bond acceptor atoms
a_don	Number of hydrogen bond donor atoms
E_sol	Solvation energy
E_tor	Torsion (proper and improper) potential energy
E_vdw	van der Waals component of the potential energy
VSA	van der Waals surface area
TPSA	Topological polar surface area
apol	Sum of the atomic polarizabilities
SMR	Molecular refractivity
logS	Log of solubility
logP(o/w)	Log of the octanol/water partition coefficient
MW	Molecular weight

Caco-2 permeability values were obtained from literature (20, 21, 69-71). Most of the Caco-2 values were taken from Hou et al. (20) and presented as mean values obtained from various literature sources. The molecular descriptors and Caco-2 permeabilities for all compounds are shown in Table 2.8.

Table 2.8- Molecular descriptors (obtained from MOE software) and Caco-2 permeabilities of 22 aromatic amines

Compound	b_rotB	rgyr	a_acc	a_don	E_sol	E_tor	E_vdw	VSA	TPSA	apol	SMR	logS	logP(o/w)	MW	logPapp
aspirin	0.23	2.47	3	2	-11.19	7.444	21.10	194.75	63.60	24.38	4.47	-1.71	1.51	180.16	-5.06
alprenolol	0.44	4.09	3	2	-13.46	-11.37	34.33	320.42	41.49	44.44	7.50	-2.81	2.62	249.35	-4.62
aminopyrine	0.11	3.08	1	0	-7.930	11.25	32.41	270.03	26.79	38.32	6.81	-1.94	1.35	231.30	-4.44
atenolol	0.42	4.72	4	3	-25.61	-5.766	32.27	322.29	84.58	43.92	7.40	-1.97	0.73	266.34	-6.50
clonidine	0.13	2.80	1	2	-14.24	15.80	18.14	225.29	36.42	29.50	6.04	-3.14	2.47	230.10	-4.59
dopamine	0.18	2.73	3	3	-13.23	-6.452	20.60	181.45	66.48	24.12	4.25	-0.39	0.67	153.18	-5.03
ibuprofen	0.27	3.34	2	2	-9.243	-0.584	26.17	262.05	37.30	36.49	6.10	-3.64	3.61	206.29	-4.28
ephedrin	0.25	2.70	2	2	-9.147	-6.418	25.09	214.27	32.26	29.50	5.00	-1.25	1.58	165.24	-4.99
metopropol	0.47	4.97	3	1	-8.834	-12.67	36.56	352.93	30.49	48.87	7.98	-2.44	3.25	265.40	-4.59
hydroquinon	0.00	1.99	2	2	-10.52	-4.253	10.52	136.10	40.46	17.50	3.05	-0.10	0.51	112.13	-4.80
oxeprenolol	0.47	4.14	4	2	-16.26	-11.81	35.75	333.91	50.72	45.24	7.68	-2.20	2.07	265.35	-4.68
practolol	0.42	4.76	4	3	-21.45	-8.454	34.05	321.24	70.59	43.92	7.54	-1.86	0.99	266.34	-6.05
salicylic acid	0.10	2.14	3	3	-9.764	1.808	19.32	147.92	57.53	18.73	3.51	-0.99	1.27	138.12	-4.79
terbutaline	0.25	3.47	4	4	-16.52	-9.635	31.76	266.98	72.72	37.30	6.26	-1.18	1.82	225.29	-6.38
acetaminophen	0.18	2.65	2	2	-14.51	4.473	20.07	175.24	49.33	22.79	4.24	-1.23	0.89	151.17	-4.63
procaine	0.41	3.98	2	1	-3.886	-5.149	32.77	292.13	55.56	40.02	6.89	-2.04	1.73	236.32	-5.71
amphetamine	0.20	2.50	1	1	-6.927	-7.430	20.63	187.89	26.02	25.61	4.38	-1.44	1.71	135.21	-4.39
ethionamide	0.18	2.71	2	1	-11.27	1.504	21.48	196.29	71.00	25.85	4.95	-1.95	0.61	166.25	-4.40
acebutolol	0.46	5.07	5	3	-23.89	-9.949	43.41	405.59	87.66	55.76	9.46	-2.89	1.80	336.43	-5.83
guanabenz	0.14	3.07	2	2	-17.86	6.564	23.33	229.35	76.76	28.17	5.99	-3.39	3.43	231.09	-4.50
epinephrine	0.23	3.02	4	4	-14.03	-1.338	23.50	214.55	72.72	28.01	4.88	-0.20	0.53	183.21	-6.02
lidocaine	0.35	3.18	2	1	-9.576	-0.462	35.32	296.11	32.34	42.31	7.23	-2.46	2.22	234.34	-4.21

The entire data set of the compounds was randomly divided into a training set of 17 compounds and a test set of 5 compounds. From the training set, all combinations of molecular descriptors were investigated using multiple-linear regression. The best model was selected based on the BIC criterion. The reliability of the model was assessed by using the test set of compounds wherein the Caco-2 permeability values were compared to the model predicted values. The model was deemed to be reliable if the predicted values were overall within 0.5 log limits. After being evaluated for its reliability, the model for Caco-2 permeability prediction was used to predict apparent Caco-2 permeability coefficients for model drug degradants.

Conversion of apparent Caco-2 permeability to *in vivo* permeability

The estimates of Caco-2 permeability were then converted to *in vivo* permeability ($logP_{eff}$) using a second model that was developed by linear regression to correlate Caco-2 permeability to measured human jejunum permeability. Human $logP_{eff}$ data based on direct, *in vivo* determinations in the human GI tract with a single pass perfusion were available for a few compounds, which served as the basis for model construction. Caco-2 permeability and human $logP_{eff}$ values were obtained from Alsenz (72) in Table 2.9.

Table 2.9- Reported human $logP_{eff}$ and Caco-2 cell permeability (72)

Compound	P_{eff} human perfusion ($\times 10^{-4}$ cm/s)	P_{app} ($\times 10^{-6}$ cm/s) (pH 7.4 donor)
Antipyrine	4.50	54.30 (± 2.98)
Atenolol	0.20	1.730 (± 0.66)
Carbamazepine	4.30	62.23 (± 3.98)
Cimetidine	0.30	0.590 (± 0.35)
Creatinine	0.30	1.550 (± 0.72)
Desipramine	4.40	43.00 (± 2.01)
Enalaprilat	0.20	1.850 (± 0.79)
Furosemide	0.05	0.310 (± 0.09)
Hydrochlorothiazide	0.04	0.420 (± 0.33)
Ketoprofen	8.40	24.36 (± 1.82)

Table 2.10- Continued

Compound	P_{eff} human perfusion $(\times 10^{-4}$ cm/s$)$	P_{app} $(\times 10^{-6}$ cm/s$)$ (pH 7.4 donor)
L-Leucine	6.20	15.50 ($\pm$1.68)
Lisinopril	0.33	1.270 ($\pm$0.83)
Naproxen	8.30	53.07 ($\pm$2.91)
PEG400	0.56	3.120 ($\pm$1.53)
Phenoxymethylpenicillin	0.26	1.900 ($\pm$1.19)
Phenylalanine	3.40	18.34 ($\pm$3.16)
Piroxicam	7.80	28.85 ($\pm$2.81)
Propranolol	2.90	47.20 ($\pm$2.56)
Ranitidine	0.27	0.670 ($\pm$0.39)
Terbutaline	0.30	1.710 ($\pm$0.79)
Urea	1.40	4.820 ($\pm$1.12)
Verapamil	6.70	44.67($\pm$3.61)

2.3.Results

2.3.1. Tissue-to-plasma partition coefficients

The estimated tissue-to-plasma partition coefficient values for rats and humans are presented in Table 2.10. As a small molecule with low lipophilicity, aniline distributes equally between tissues and plasma with most of Kpu values close to 1. The PCA and 2,6-DMA Kpu values suggest that these compounds are predicted to partition to greater extent into adipose (4.603 and 4.366, respectively) or brain (3.615 and 3.450, respectively) compared to bone tissue (1.986 and 1.791, respectively) as expected. PAP has a greater extent of binding to plasma proteins; which results in smaller volume of distribution. Overall, PCA and 2,6-DMA area predicted to have about 2-fold higher tissue affinity values than aniline, therefore they have larger volumes of distribution. For example, the aniline $Vd_{u,SS}$ values were 0.72 L/kg in both rats and humans. For PCA, the volumes of distribution estimated in rats and humans were 2.40 L/kg and 2.74 L/kg, respectively. For 2,6-DMA, the volumes of distribution estimated in rats and humans were 2.16 L/kg and 2.42 L/kg.

Table 2.11- Tissue-to-plasma partition coefficients predicted
using the Eq. 2.7 from model of Rodgers and Rowland

Organ/Tissue		Aniline	PCA	2,6-DMA	o-TOL	PAP
Adipose		0.555	4.603	4.366	1.255	0.213
Bone		0.602	1.986	1.791	0.857	0.508
Brain		1.106	3.615	3.450	1.584	0.854
Gut		1.114	4.073	3.736	1.666	0.874
Heart		0.936	2.429	2.150	1.205	0.864
Kidney		0.943	2.507	2.263	1.229	0.848
Liver		0.927	2.430	2.250	1.206	0.813
Lung		1.017	3.193	2.810	1.412	0.900
Muscle		0.859	1.787	1.660	1.030	0.800
Pancreas		1.142	3.895	3.704	1.666	0.870
Skin		1.201	5.755	5.188	2.047	0.844
Spleen		0.888	1.811	1.638	1.055	0.849
Thymus		0.949	2.352	2.192	1.210	0.841
Stomach		1.026	3.218	2.910	1.430	0.875
$Vd_{u,ss}$	Rat	0.72	2.40	2.16	1.08	0.67
(L/kg)	Human	0.72	2.71	2.42	1.09	0.63

2.3.2. Metabolic rate constants

Analytical system suitability

Aniline: The absorbance spectrum of aniline was determined for 0.2 mM aniline solution in 0.1M potassium phosphate buffer and shown in Figure 2.1 below. The spectra range from 200 nm to 380 nm. The wavelength of maximum absorbance for aniline is 230 nm.
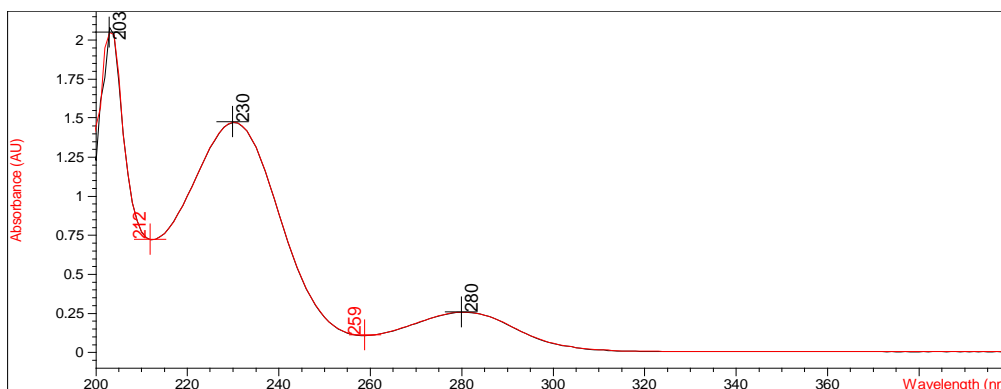
Figure 2.1- Absorbance spectrum of aniline

The analytical system suitability was determined by analyzing the chromatograms of aniline and its identified metabolites obtained from PC1000 chromatography data system software. The estimated analytical system suitability parameters are summarized in Table 2.11 and an example of chromatogram is displayed in Figure 2.2.

Table 2.12- Chromatographic parameters for aniline obtained from PC1000 software

Parameter	Aniline	2-AP	3-AP	4-AP	APAP	Criteria
Repeatability - retention time (RSD%)	0.032	0.050	0.048	0.055	0.037	X < 1%
Repeatability - area (RSD%)	0.625	0.760	0.719	0.787	0.567	X < 1%
Theoretical plates	5269	3852	3561	2762	3595	N > 2000
Resolution	4.24	4.34	3.28	NA	2.74	R > 1.5
Asymetry	1.23	1.52	1.19	1.23	1.16	T < 2

Analyst: System
Sample ID: mix05   Vial: A06   Injection Volume: 20
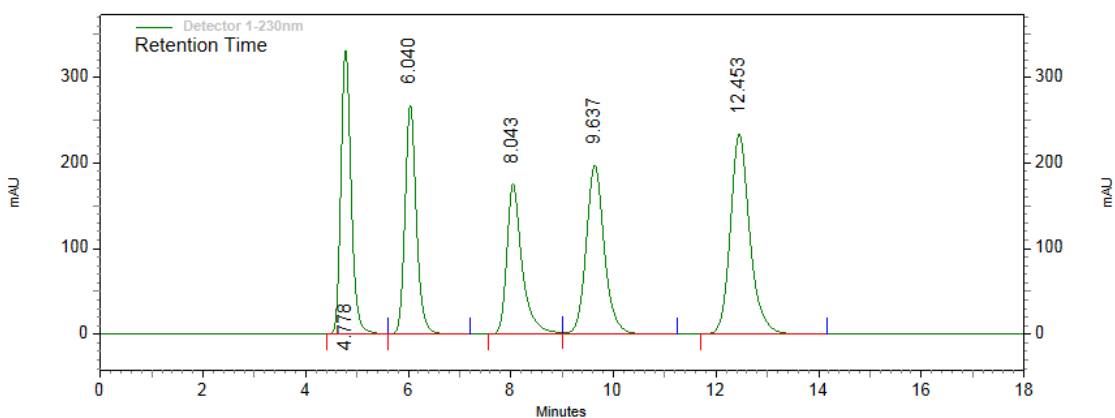
Figure 2.2- Sample chromatogram of aniline and its metabolites. Retention times of 4-AP, 3-AP, 2-AP, acetaminophen and aniline are 4.78, 6.04, 8.04, 9.67, and 12.45, respectively.

The relative standard deviations (RSD) for retention times of aniline and metabolites were observed less than 1%. Similarly, the relative standard deviation for peak area ranges from 0.57% to 0.78%. Theoretical column plates were greater than 2000; resolution between aniline and its metabolites was 2.7 as the least value and most

of peak symmetry measures are close to 1. The results were used to verify that the resolution and reproducibility of the chromatographic system are adequate for analytical studies.

Linearity of the method was confirmed by preparing standard curves of aniline for the analytical range of 5 – 1500 μM. The results, summarized in Tables 2.12, show a good correlation between analyte peak area and concentration of aniline within the analytical range with $R^2 \geq 0.99$. Standard curve for aniline used in the microsomal study of 150 μM aniline incubation are shown in Figure 2.3.

PCA; 2,6-DMA, o-TOL and PAP: The analytical system suitability parameters are shown in Table 2.13. The representative chromatograms of samples incubated with microsomes or hepatocytes after centrifugation are displayed in Figures 2.4 – 2.7, for PCA, 2,6-DMA, o-TOL and PAP, respectively. The results of linear regression for standard curves of PCA, 2,6-DMA, o-TOL and PAP were shown in Table 2.14, 2.15, 2.16, and 2.17, respectively.

Table 2.13- Linearity testing of HPLC analytical system for aniline

Standard curve	Analytical range	Calibrators	Slope	y-intercept	R^2 value
Set 1	5 - 15 μM	5	802.6	-27.13	0.990
Set 2	25 - 125 μM	5	797.8	-670.2	1.00
Set 3	500 - 1500 μM	5	800.3	15190.2	1.00
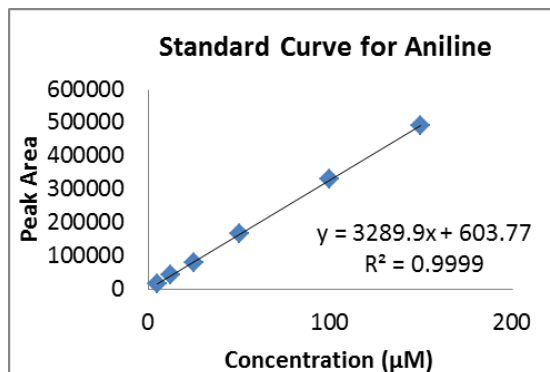
Figure 2.3- Standard curve for aniline from microsomal study using 150 μM aniline

73

Table 2.14- System suitability parameters for model compounds

Parameter	PCA	2,6-DMA	o-TOL	PAP	Criteria
Repeatability - retention time (RSD%)	0.06	0.34	0.06	0.02	X < 1%
Repeatability - area (RSD%)	0.27	0.42	0.68	0.52	X < 1%
Theoretical plates	6452	7255	5688	2483	N > 2000
Asymmetry	1.06	1.26	1.30	1.26	T < 2
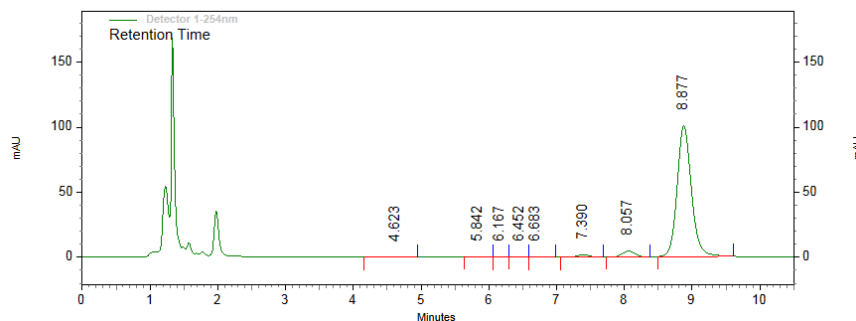
Figure 2.4- Chromatogram of p-chloroaniline from microsomal study for metabolic parameters determination
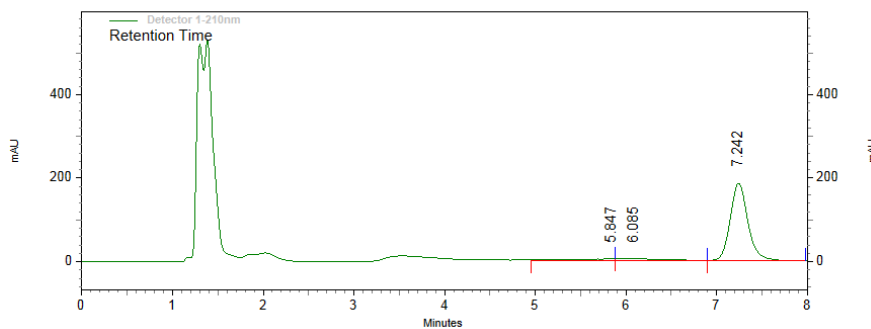
Figure 2.5- Chromatogram of 2,6-dimethylaniline from microsomal study for metabolic parameters determination
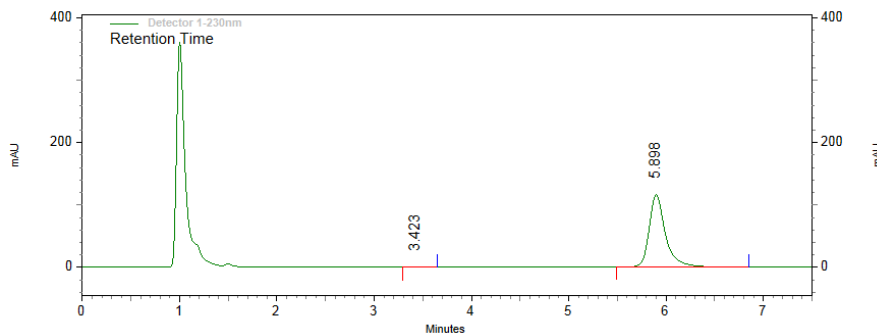
Figure 2.6- Chromatogram of o-toluidine from microsomal study for metabolic parameters determination
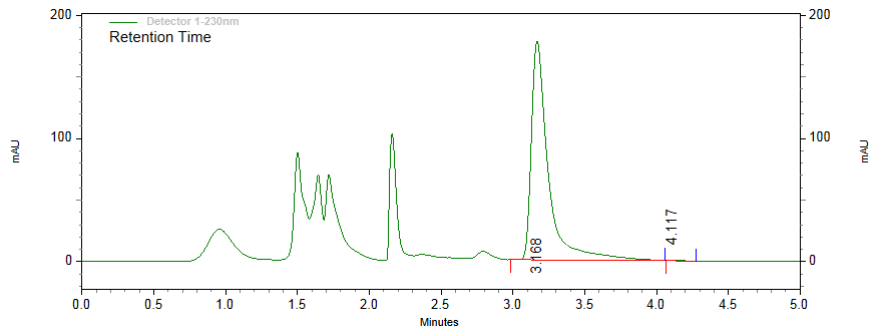
Figure 2.7- Chromatogram of p-aminophenol from hepatocyte study for metabolic parameters determination

Table 2.15- Linearity testing of HPLC analytical system for p-chloroaniline

Standard curve	Analytical range	Calibrators	Slope	y-intercept	R^2 value
Set 1	10 − 100 µM	5	4047.28	707.82	0.9996
Set 2	200 − 600 µM	5	2028.43	-588.87	0.9997
Set 3	1000 − 2000 µM	5	2044.93	-471.67	0.9992

Table 2.16- Linearity testing of HPLC analytical system for 2,6-dimethylaniline

Standard curve	Analytical range	Calibrators	Slope	y-intercept	R^2 value
Set 1	5 − 12 µM	5	31582	4010.4	0.997
Set 2	375 − 550 µM	5	5090.85	146288.3	0.998
Set 3	625 − 1250 µM	5	5414.65	118692.1	0.997

Table 2.17- Linearity testing of HPLC analytical system for o-toluidine

Standard curve	Analytical range	Calibrators	Slope	y-intercept	R^2 value
Set 1	5 − 12.5 µM	5	21746.4	1085.3	0.999
Set 2	60 − 125 µM	5	9322.4	-23480.5	0.999
Set 3	650 − 1300 µM	5	4161.0	62396.2	0.995

Table 2.18- Linearity testing of HPLC analytical system for p-aminophenol

Standard curve	Analytical range	Calibrators	Slope	y-intercept	R^2 value
Set 1	10 – 50 μM	5	9076.7	988.9	0.997
Set 2	100 – 500 μM	5	7847.2	579.7	0.998
Set 3	2625 – 4200 μM	5	4131.5	18978.4	0.994

Estimation of initial rates from depletion profiles

Concentration-time profiles of aniline, PCA, 2,6-DMA, o-TOL and PAP depletion in rat liver microsomes and hepatocyte suspension are shown in Figures 2.8 – 2.12 . In the hepatocyte study of PAP, viability of cells was determined to be 75% - 87% for each experiment.

For each depletion profile, linear regression was used to estimate the initial rate of substrate loss for a 20% decrease in concentration. Slopes, standard error of slopes and correlation coefficient R^2 of aniline, PCA, 2,6-DMA, o-TOL and PAP disappearance curves obtained by linear regression are shown in Tables 2.18 – 2.22.
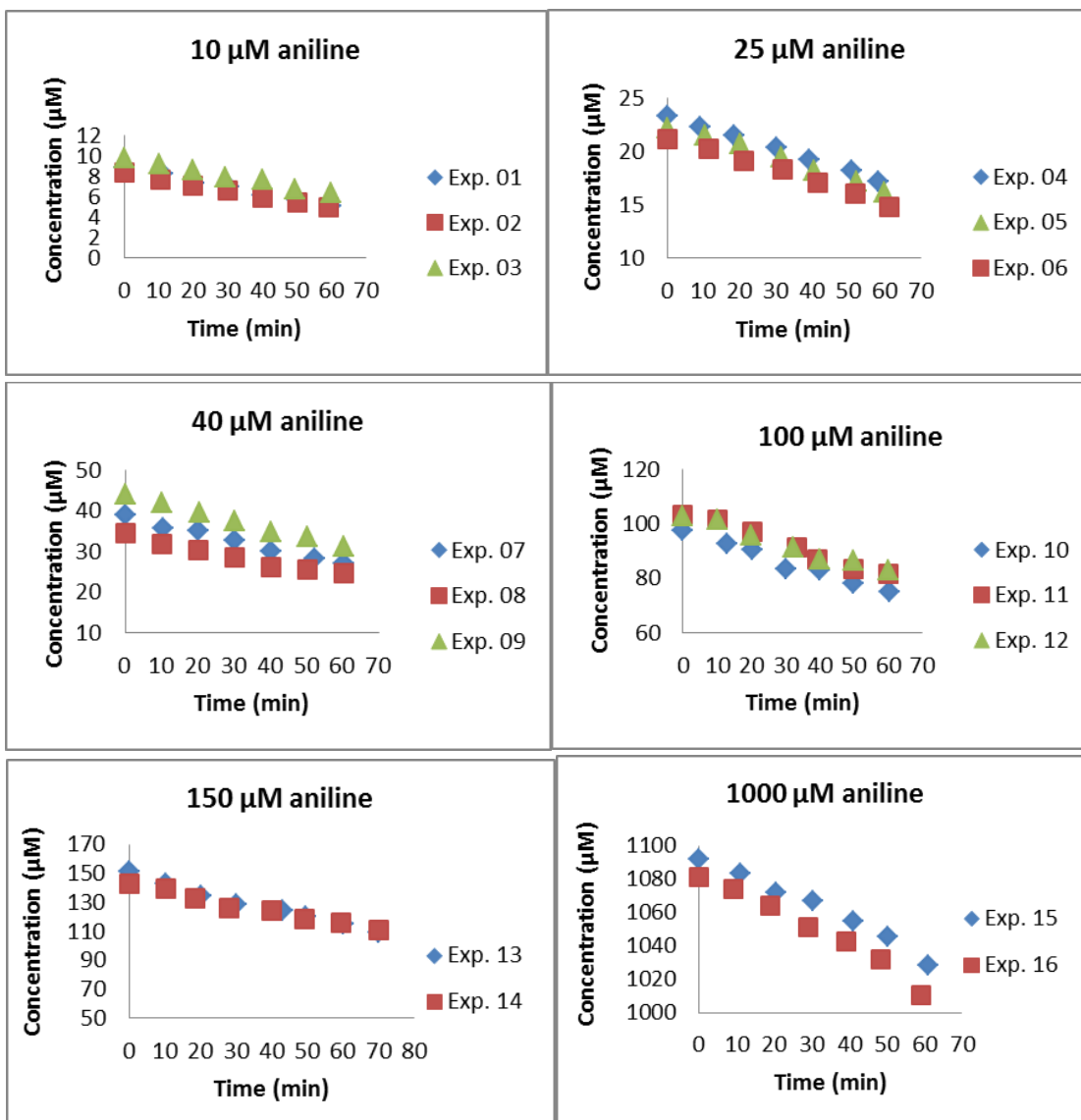
Figure 2.8- Aniline depletion plots from rat liver microsomal studies. Each "Exp." represents a single study. Points correspond to observed concentrations.

77
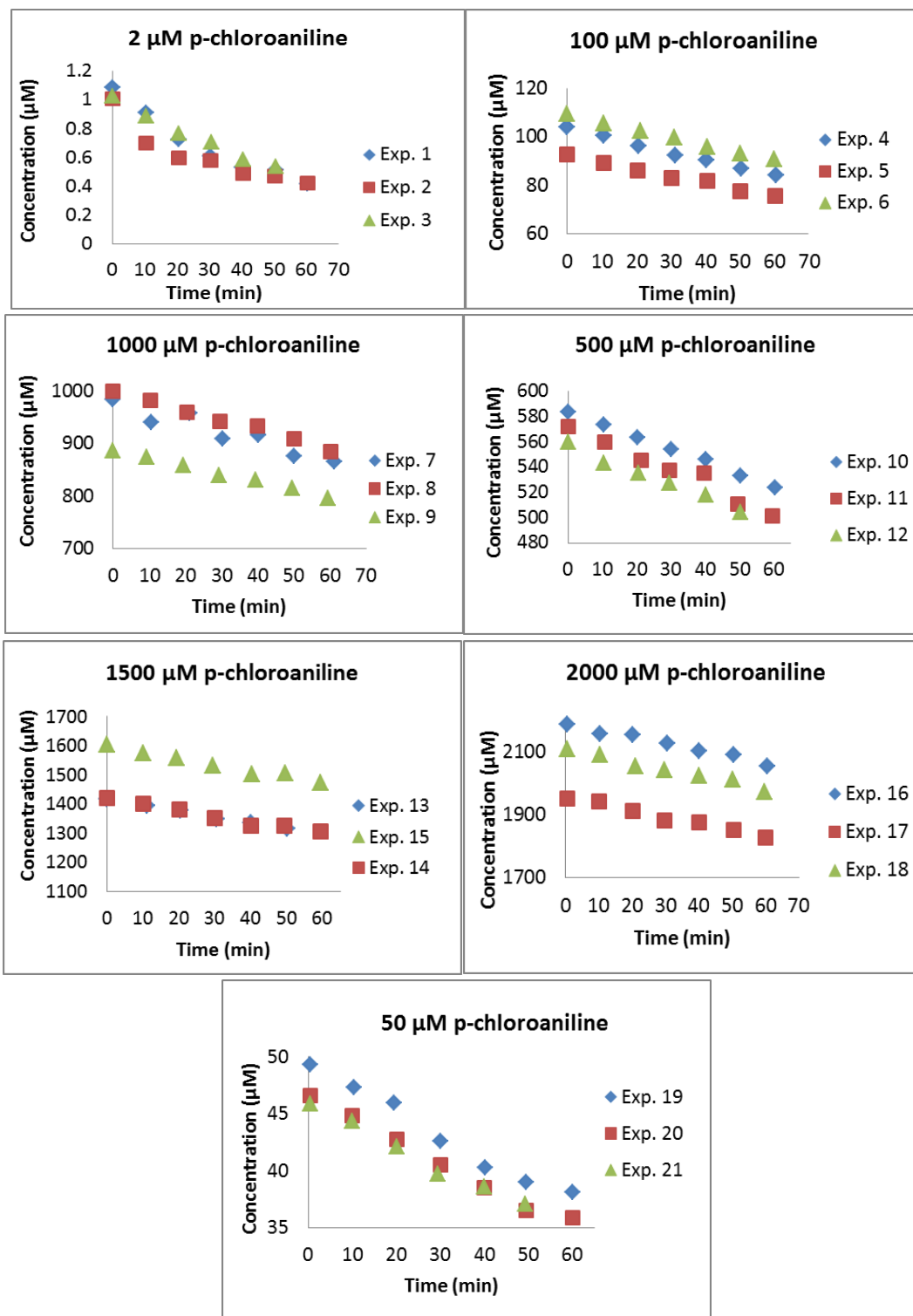
Figure 2.9- p-Chloroaniline depletion plots from rat liver microsomal studies. Each "Exp." represents a single study. Points correspond to observed concentrations.
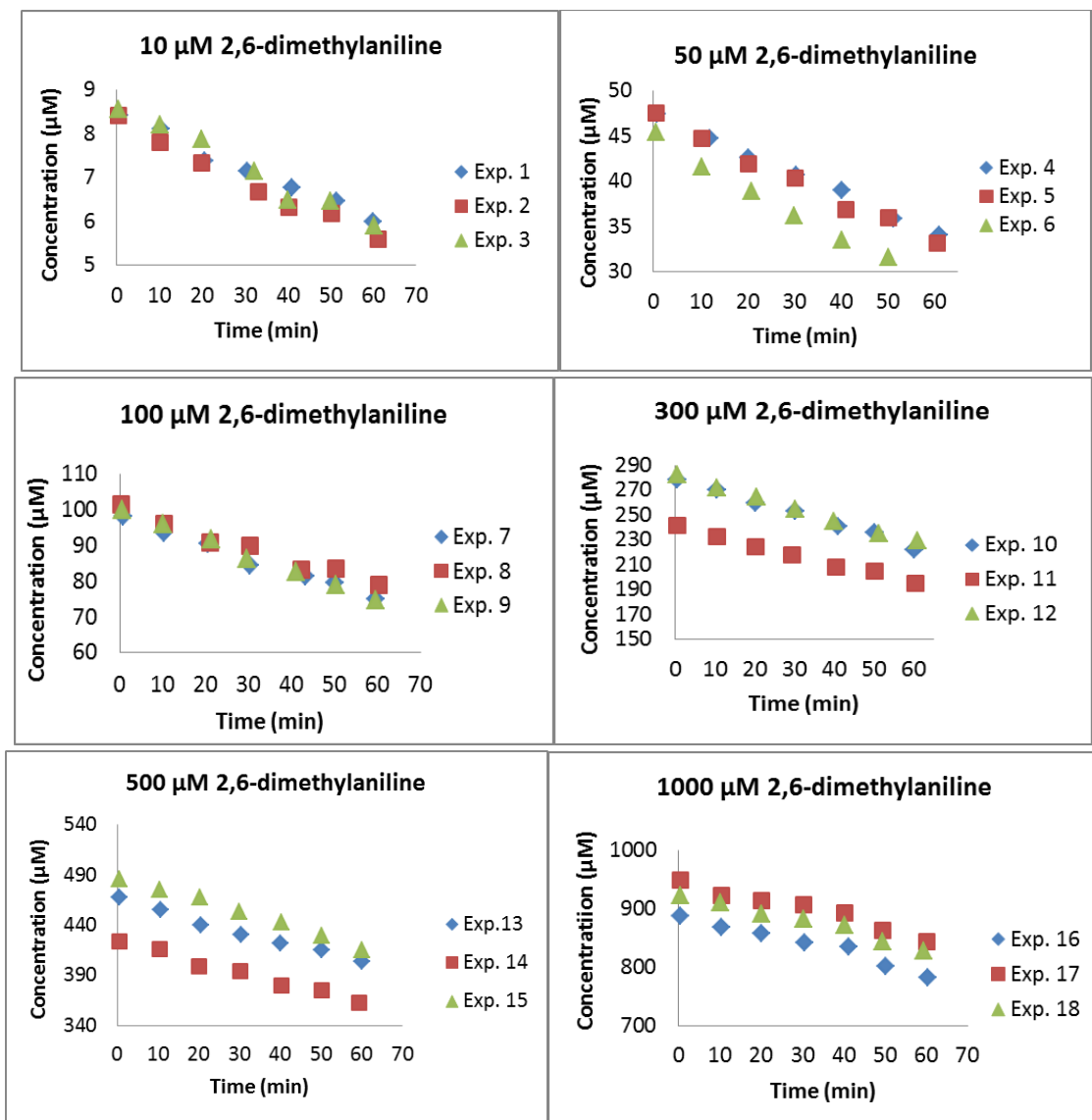
Figure 2.10- 2,6-dimethylaniline depletion plots from rat liver microsomal studies. Each "Exp." represents a single study. Points correspond to observed concentrations.
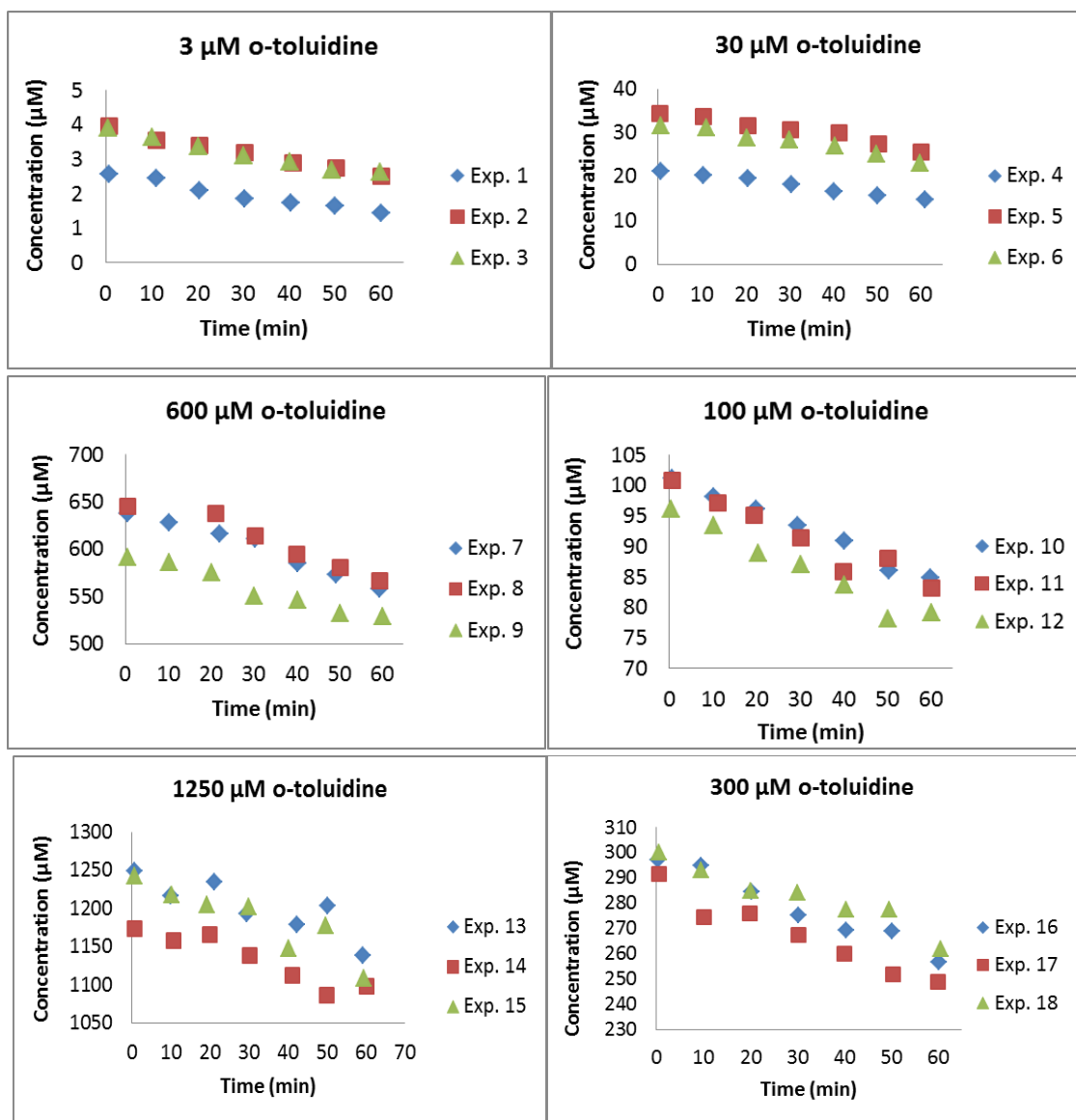
Figure 2.11- o-toluidine depletion plots from rat liver microsomal studies. Each "Exp." represents a single study. Points correspond to observed concentrations.

80
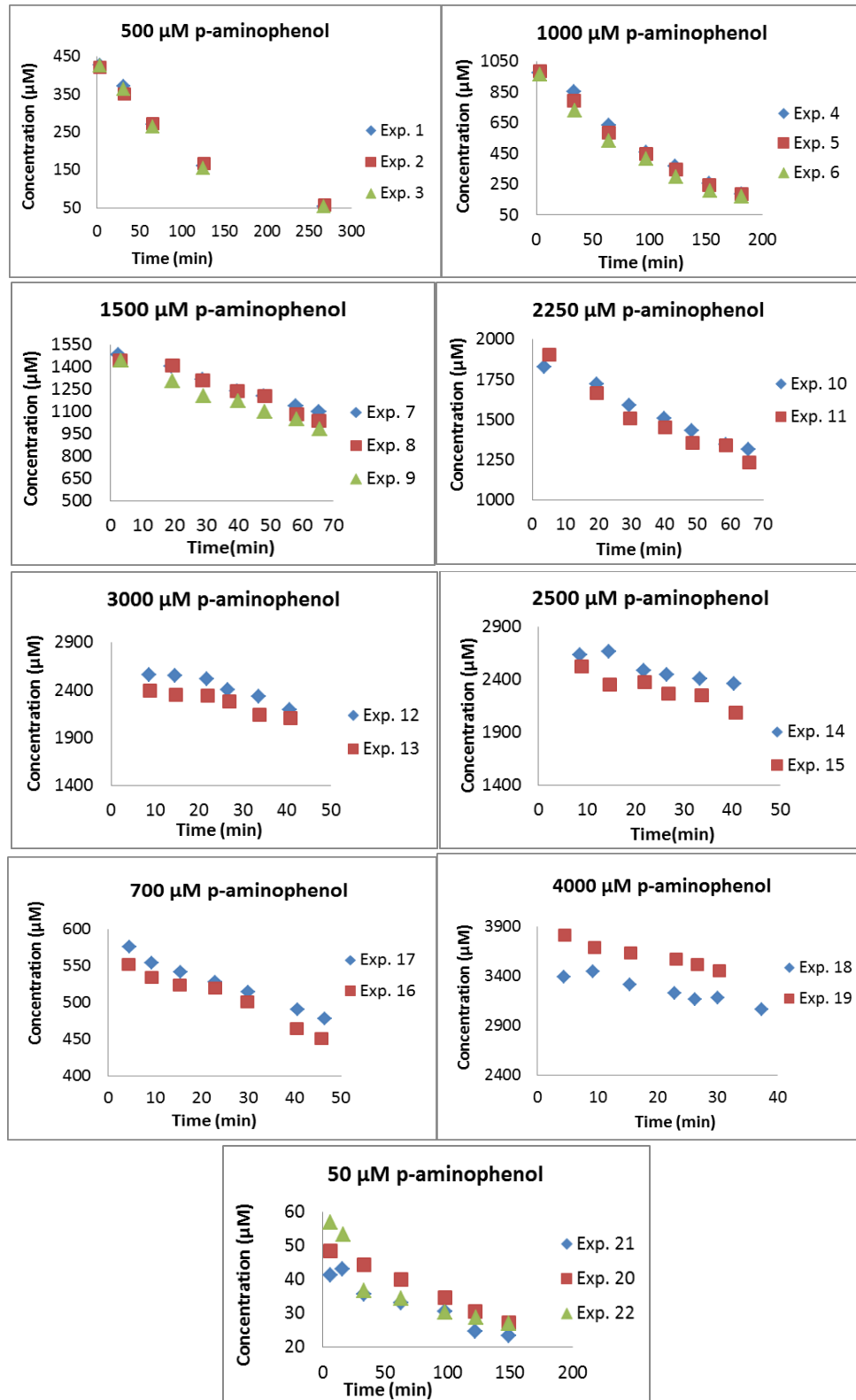
Figure 2.12- Depletion plots of PAP using hepatocyte. Each "Exp." represents a single study. Points correspond to observed concentrations

Table 2.19- Estimation of initial rate of substrate loss
(slope) for aniline by linear regression

Exp. #	Concentration (μM)	v_0 (slope)	SE of Slope	R^2
1	8.926	0.069	0.0092	0.97
2	8.405	0.062	0.0023	1.00
3	9.846	0.064	0.0029	1.00
4	21.23	0.097	0.0050	0.99
5	22.43	0.098	0.0077	0.98
6	23.25	0.099	0.0036	1.00
7	38.45	0.192	0.0316	0.95
8	34.03	0.185	0.0186	0.98
9	43.97	0.217	0.0051	1.00
10	97.51	0.394	0.0488	0.96
11	104.5	0.411	0.0417	0.97
12	104.2	0.414	0.0389	0.97
13	149.4	0.624	0.0734	0.96
14	143.6	0.522	0.0683	0.95
15	1094	1.003	0.0558	0.98
16	1084	1.144	0.0676	0.98

Table 2.20- Estimation of initial rate of substrate loss (slope)
for p-chloroaniline by linear regression

Exp. #	Concentration (μM)	v_0 (slope)	SE of Slope	R^2
1	1.090	0.018	0.000	1.00
2	0.976	0.020	0.006	0.92
3	1.026	0.013	0.000	1.00
4	103.3	0.333	0.020	0.99
5	91.83	0.275	0.025	0.98
6	109.1	0.320	0.016	0.99
7	977.5	1.849	0.288	0.89
8	997.1	1.736	0.150	0.98
9	887.6	1.502	0.062	0.99
10	583.7	1.016	0.016	1.00
11	572.6	1.173	0.091	0.97
12	558.7	1.226	0.212	0.97
13	1415	2.020	0.079	0.99
14	1414	1.926	0.204	0.96
15	1593	2.002	0.177	0.97
16	2188	2.099	0.127	0.98
17	1954	2.087	0.138	0.98
18	2109	2.154	0.142	0.98
19	49.74	0.225	0.017	0.98
20	46.40	0.188	0.013	0.98
21	45.81	0.183	0.016	0.98

Table 2.21- Estimation of initial rate of substrate loss
(slope) for 2,6-dimethylaniline by linear regression

Exp. #	Concentration (μM)	ν_0 (slope)	SE of Slope	R^2
1	8.524	0.052	0.012	0.95
2	8.424	0.056	0.004	0.99
3	8.574	0.036	0.001	1.00
4	47.65	0.246	0.007	1.00
5	47.74	0.283	0.003	1.00
6	45.11	0.293	0.014	0.99
7	97.79	0.386	0.019	0.99
8	101.4	0.519	0.011	1.00
9	100.1	0.430	0.013	1.00
10	279.0	0.878	0.046	0.99
11	241.8	0.822	0.036	1.00
12	282.3	0.898	0.044	1.00
13	467.8	1.256	0.076	0.99
14	424.7	1.091	0.092	0.98
15	487.8	1.134	0.043	0.99
16	887.4	1.545	0.177	0.95
17	945.7	1.525	0.192	0.94
18	924.4	1.507	0.138	0.97

Table 2.22- Estimation of initial rate of substrate loss
(slope) for o-toluidine by linear regression

Exp. #	Concentration (μM)	v_0 (slope)	SE of Slope	R^2
1	2.612	0.024	0.007	0.91
2	3.950	0.029	0.008	0.93
3	3.911	0.027	0.001	1.00
4	21.37	0.095	0.011	0.97
5	34.75	0.138	0.034	0.94
6	32.05	0.123	0.028	0.91
7	640.8	1.234	0.183	0.94
8	653.4	1.470	0.298	0.89
9	593.5	1.159	0.105	0.96
10	101.1	0.258	0.013	0.99
11	101.0	0.313	0.015	1.00
12	96.30	0.321	0.032	0.98
13	1246	1.408	0.427	0.69
14	1182	1.722	0.285	0.90
15	1247	1.973	0.443	0.80
16	299.3	0.755	0.113	0.96
17	288.3	0.718	0.248	0.81
18	298.8	0.544	0.074	0.95

Table 2.23- Estimation of initial rate of substrate loss (slope) for p-aminophenol by linear regression

Exp. #	Concentration (µM)	v_0 (slope)	SE of Slope	R^2
1	429.7	2.393	0.042	1.00
2	442.7	2.544	0.283	0.99
3	438.2	2.610	0.225	0.99
4	1004	5.610	0.375	0.99
5	991.0	5.835	0.397	0.99
6	953.4	5.923	0.649	0.98
7	1507	6.521	0.700	0.98
8	1504	6.824	0.590	0.96
9	1459	7.730	0.993	0.97
10	1869	9.084	0.596	0.99
11	1839	10.00	1.450	0.96
12	2713	11.65	1.705	0.92
13	2504	9.503	1.428	0.92
14	2758	11.04	2.411	0.87
15	2593	11.58	2.029	0.89
16	562.1	2.607	0.594	0.95
17	587.9	3.112	0.663	0.96
18	3535	12.85	1.385	0.96
19	3841	12.44	1.121	0.97
20	49.31	0.151	0.002	1.00
21	44.45	0.246	0.168	0.68
22	57.75	0.421	0.139	0.82

<u>Estimation of V_{max} and K_m by nonlinear regression</u>

Optimal V_{max} and K_m values of model compounds were estimated by fitting the Michaelis-Menten equation to the slopes versus initial concentrations relationship via nonlinear regression. Actual data points and Michaelis-Menten model fitted curves are displayed in Figure 2.13 and results are shown in Table 2.23. The observed velocities were well described by the Michaelis-Menten model. V_{max} values ranged from 2.48 nmol/min/mg protein (aniline) to 22.83 nmol/min/10^6 hepatocyte (PAP). K_m values covered from 187.50 µM (aniline) to 2971 µM (PAP). Aniline has the lowest values of V_{max} and K_m, and is expected to follow nonlinear kinetics at concentration ≥ 1 mM.

Table 2.24- Summary for V_{max} and K_m values predicted from nonlinear regression. (Values shown as means of V_{max} [nmol/min/mg protein] and K_m [μM]) with S.E.)

Parameter	Aniline	PCA	2,6-DMA	o-TOL	PAP*
V_{max}	2.48 ± 0.031	6.19 ± 0.095	3.98 ± 0.049	4.48 ± 0.150	22.83 ± 1.37
K_m	187.5 ± 10.93	901.1 ± 65.43	318.8 ± 18.55	486.3 ± 71.86	2971 ± 304.7

* Unit for PAP: V_{max}: nmol/min/10^6 hepatocytes; K_m: [μM]
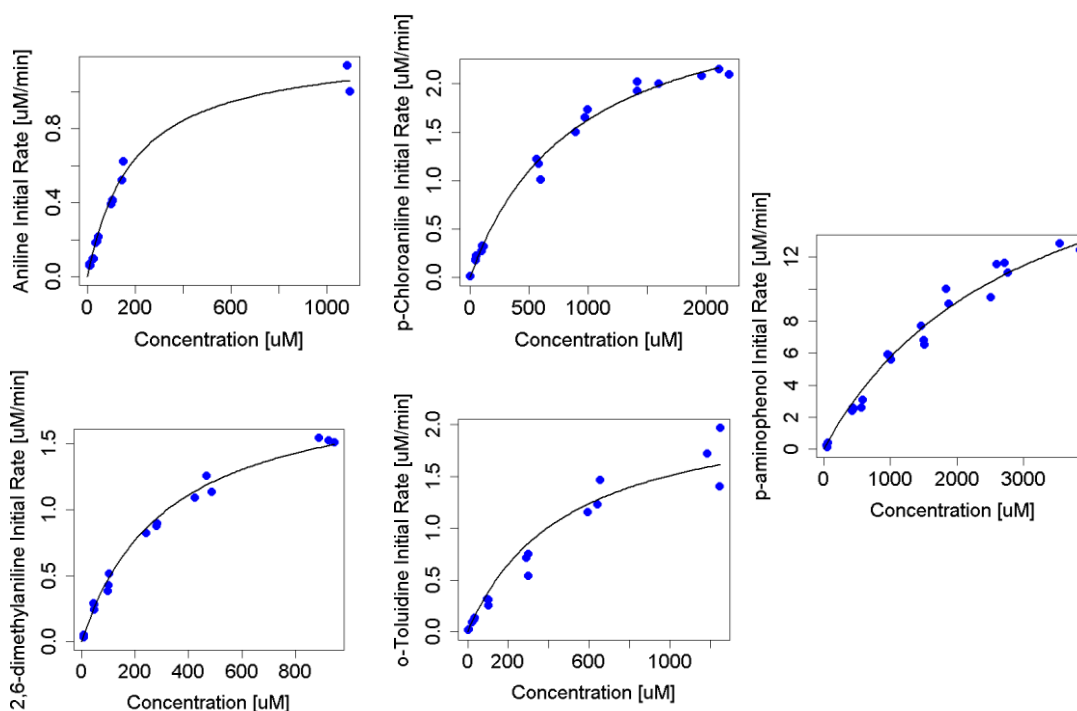
Figure 2.13- Initial metabolic rates versus substrate concentrations. Actual data points obtained from linear regression of substrate depletion profiles and Michaelis-Menten model fitted curves using non-linear regression are displayed.

Estimation of V_{max} and K_m via MCMC sampling by Bayesian approach

Nonlinear least square estimates of K_m and V_{max} for each substance were used as initial values for the MCMC sampling in the Bayesian approach to obtain the posterior probability of corresponding metabolic parameters. The MCMC simulation using the Metropolis-Hastings algorithm was carried out to obtain probability distributions for each parameter (V_{max} and K_m) that describe the likely values and associated uncertainty. This

87

information was incorporated in a stochastic PBPK model to help evaluate risk. The MCMC input requirements include:

- The kinetic model is Michaelis-Menten. Unknown parameters are V_{max}, K_m, initial substrate concentrations and parameters of variance model

- Observed data from each depletion profile for each model compound

- Prior distributions for V_{max} and K_m are conventional noninformative priors

- Nonlinear least square estimates of V_{max} and K_m were used as starting points for the Markov chain.

- Likelihood functions as described below.

Observed concentrations of model compounds are assumed to be normally distributed with mean μ and variance σ_i^2:

$$y_i \sim N(\mu, \sigma_i^2) \text{ and } \varepsilon_i \sim N(0, \sigma_i^2)$$

$$y_i = f_i(x, \theta) + \varepsilon_i$$

$$E\{y_i\} = \mu = f_i(x, \theta) \quad ; \quad Var\{y_i\} = Var\{\mu + \varepsilon_i\} = \sigma_i^2$$

Where, y_i is observed concentration, f_i is predicted concentration using Michaelis - Menten model and unknown parameters (θ) of V_{max}, K_m.

Based on the plots between standard errors of the slopes versus initial substrate concentrations (Figure 2.14), the error model was heteroscedastic (multiplicative error model), which refers to non-constant error for all observations.

$$\sigma_i^2 = \omega f_i{}^{\gamma}$$

Where, ω and γ are unknown parameters of the variance model which describe a power law with an additive offset for the experimental error. The likelihood function of observed data from each depletion profile is expressed in equation:

$$L(y_i|f_i, \sigma_i^2) = \prod_{i=1}^{n} \frac{1}{\sigma_i\sqrt{2\pi}} \exp\left(-\frac{(y_i - f_i)^2}{2\sigma_i^2}\right)$$
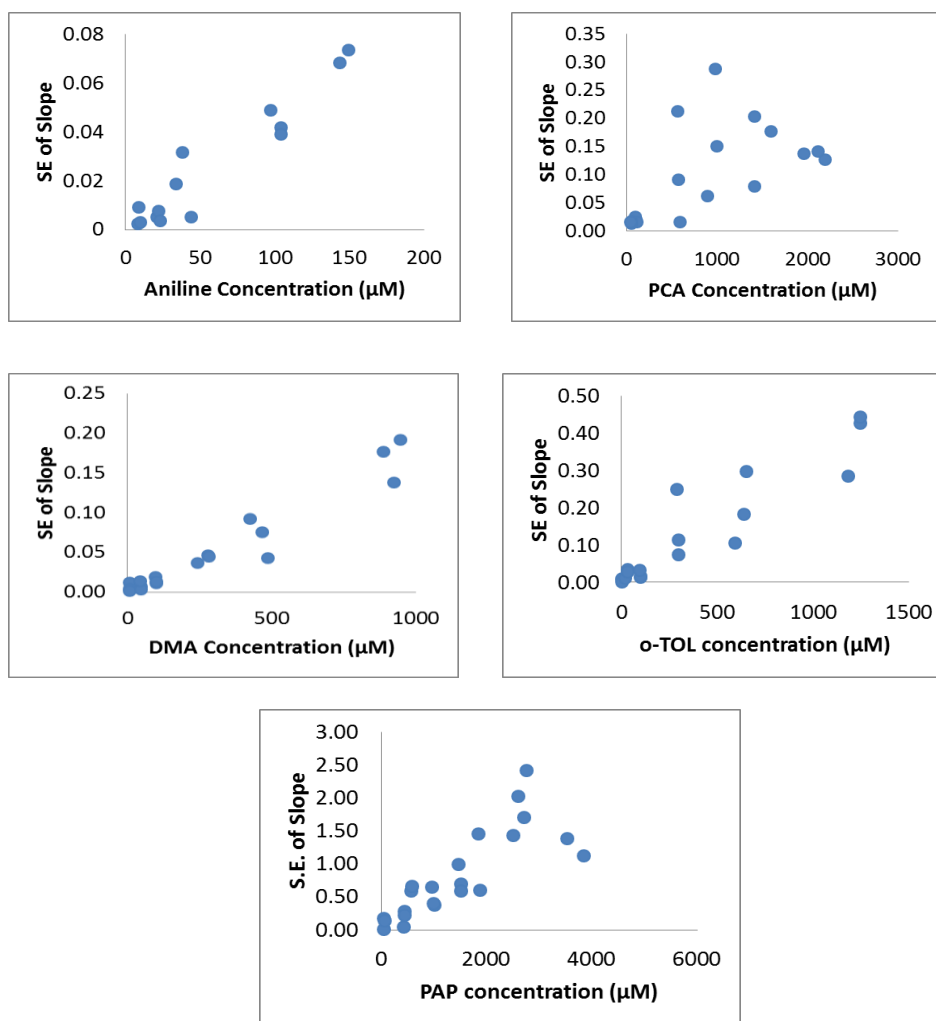
Figure 2.14- Standard errors of the slopes versus initial substrate concentrations. The standard error values were approximately proportional to initial substrate concentrations; this suggests that a simple constant error model is inappropriate.

The MCMC sampler converged after 100,000 iterations. The convergence of Markov chain was assessed by the history plot of MCMC chain. The results for aniline are shown in Figure 2.15 as an example of MCMC convergence, where the traces of MCMC chain over model parameters were essentially random over the sampling chain and displayed no apparent trends.
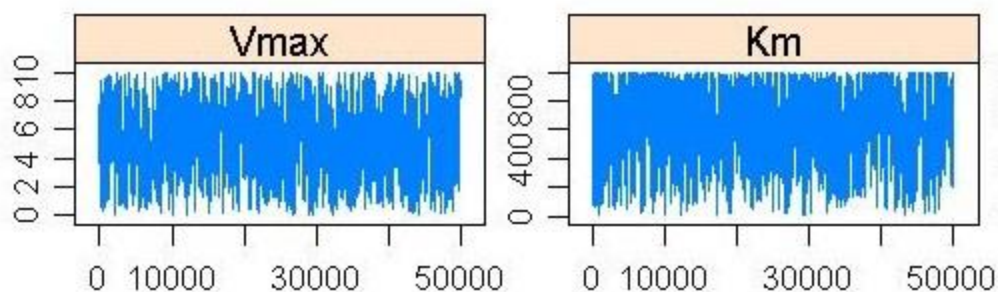
Figure 2.15- The history plots of MCMC chain for V_{max}, K_m of aniline indicates the convergence by no apparent trends.

In the MCMC results, 50,000 initial iterations were discarded and the remaining sampler output was used for inference. The Table 2.24 summaries the results of MCMC simulations for metabolic parameters for the five model compounds.

Table 2.25- Metabolic constants of model compounds obtained from fitting Michaelis-Menten equation to all depletion curves via MCMC sampling.

(V_{max}: nmol/min/mg protein], and K_m: [μM]. For PAP, V_{max}: nmol/min/10^6 hepatocytes)

Substrate	Parameter	Mean ± S.D	95% Confidence Interval (lower)	95% Confidence Interval (upper)
Aniline	V_{max}	2.6 ± 0.24	2.14	3.08
	K_m	195 ± 26.5	147	252
p-Chloroaniline	V_{max}	5.94 ± 0.48	4.98	6.88
	K_m	761 ± 105	572	971
2,6-Dimethylaniline	V_{max}	4.2 ± 0.35	3.54	4.92
	K_m	347 ± 42.4	270	439
o-Toluidine	V_{max}	4.2 ± 0.51	2.42	6.4
	K_m	457 ± 168	209.5	874
p-Aminophenol	V_{max}	28.6 ± 7.60	13.62	43.22
	K_m	3064 ± 717	1416	3975

The estimated maximal velocity and Michaelis constants for aniline were 2.6 nmol/min/mg protein and 195 μM respectively. Compared to other compounds, aniline

has the lowest value of K_m which corresponds to higher substrate affinity for metabolic enzymes. The mean K_m and V_{max} estimates for p-aminophenol were 3064 μM and 28.61 nmol/min/10^6 hepatocytes, respectively. The standard deviations corresponded to coefficients of variance ranging from 9% to 36%. From Table 2.24, the apparent *in vitro* intrinsic clearance values (V_{max}/K_m) for aniline, PCA, 2,6-DMA and o-TOL were found to be similar (0.01) which suggested that cytochrome P450 has similar catalytic activity towards these four compounds.

Posterior distributions of enzyme kinetic parameters

The posterior distributions were generated for V_{max} and K_m of each model compound to reflect associated uncertainty. The results are displayed in Figure 2.16. The pair plots between V_{max} and K_m parameters reveal that high correlation exists between these two paramters. The correlation covariances between V_{max} and K_m parameters were incorporated into PBPK model via MC sampling to investigate model parameter uncertainty and variability.

Model prediction

The initial metabolic rates of aniline, PCA, 2,6-DMA, o-TOL and PAP were predicted as function of concentration using values of V_{max}, K_m sampled from their posterior distributions (Figure 2.17). The range of predicted initial rates covers most of the observed values, which demonstrates that the model predictions were consistent with the observed data.

Figures 2.18- 2.26 showing the fit of model with the actual depletion profiles and 95% confidence interval simulated via the MCMC sampling.
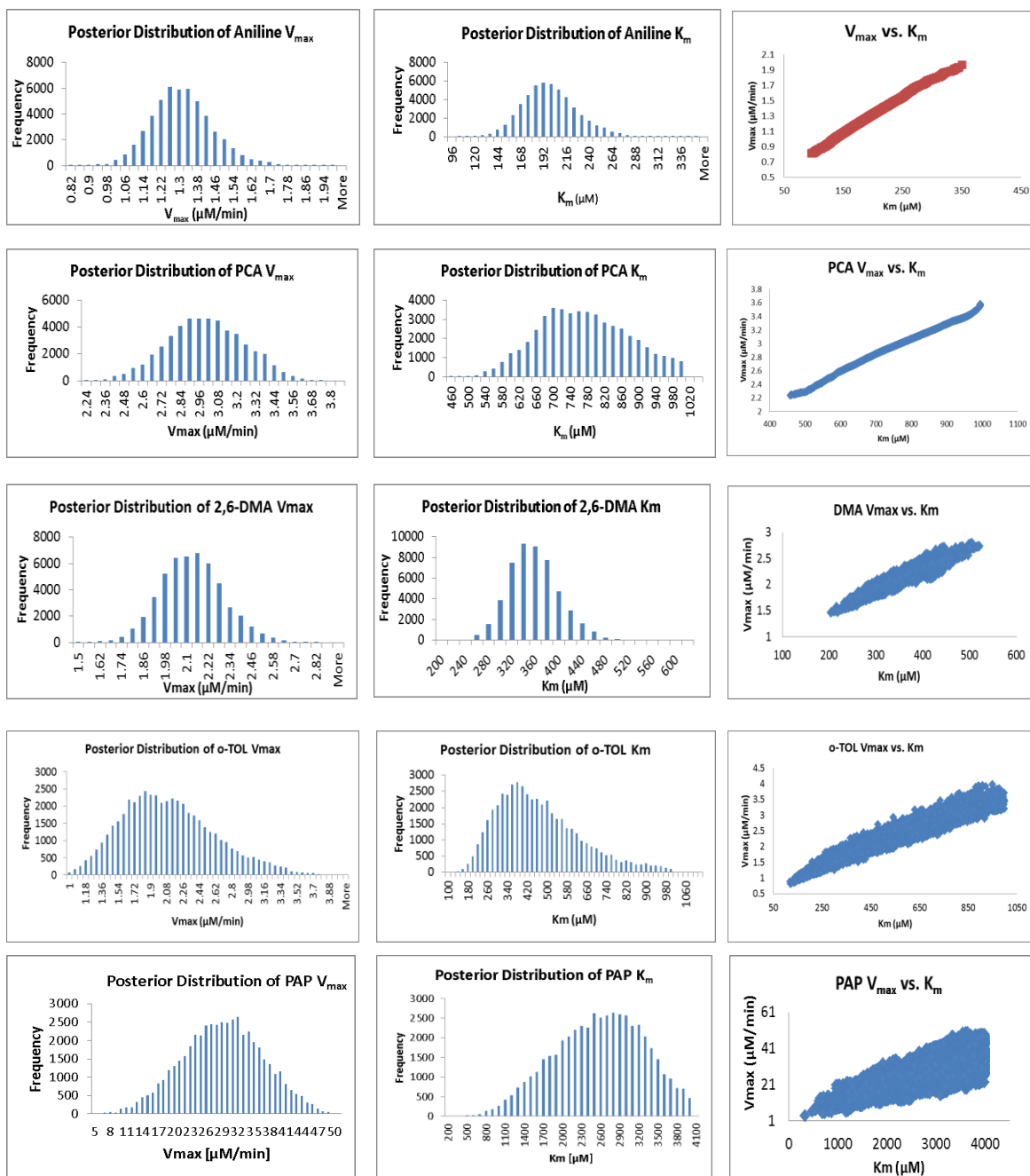
Figure 2.16- V_{max} and K_m posterior distributions and their pair plots for aniline, PCA, 2,6-DMA, o-TOL and PAP, respectively.
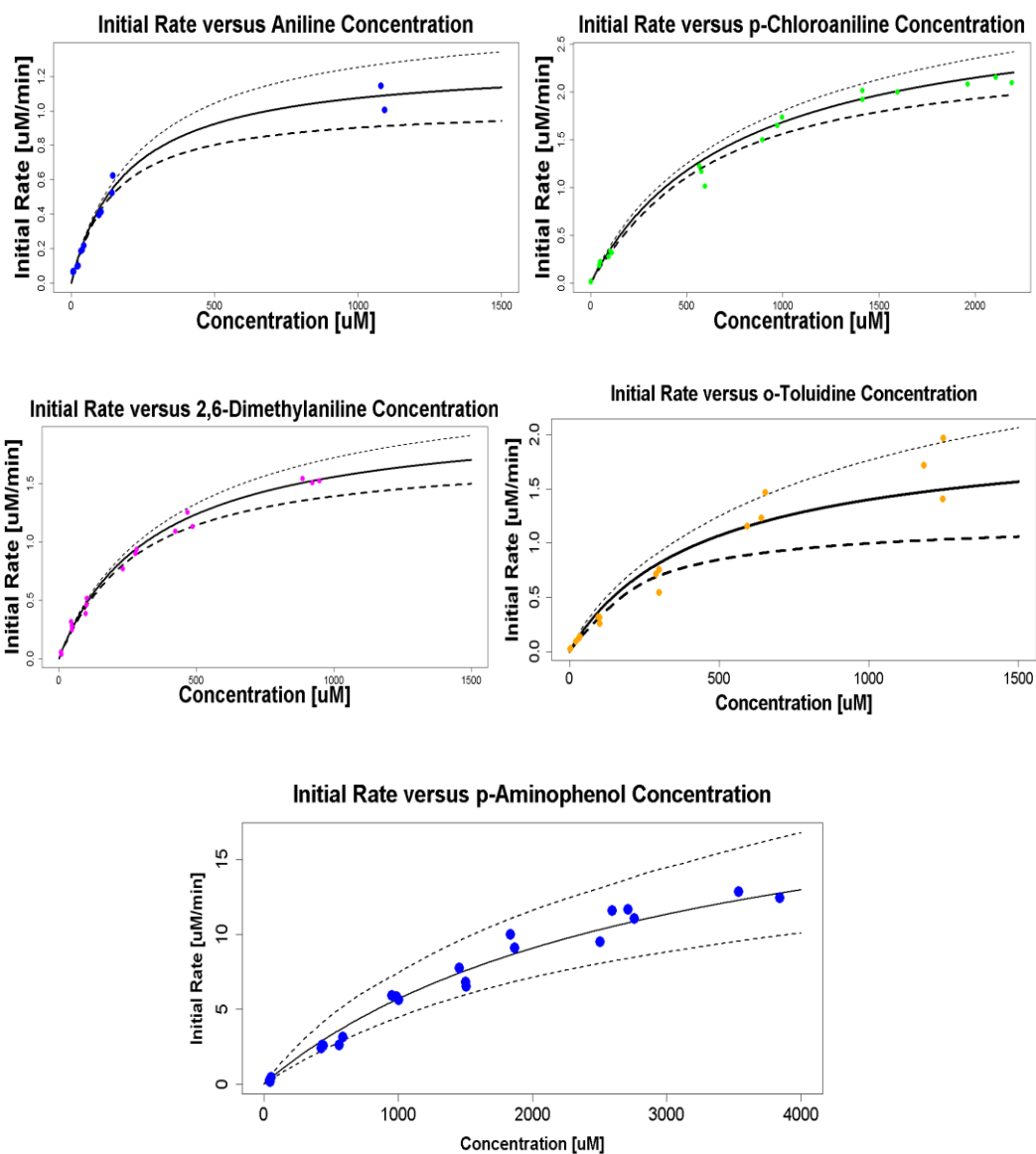
Figure 2.17- Distribution of initial metabolic reaction rates of aniline, PCA; 2,6-DMA, o-TOL and PAP. Points present initial rates estimated from observed depletion profile. The solid and dash curves represent the mean, 95% upper bound and 95% lower bound of initial rates predicted by MCMC sampling, respectively.

Figure 2.18- Aniline depletion data from rat liver microsome studies (points) and 95% confidence interval of model predicted curves simulated by the MCMC sampling using V_{max} and K_m values obtained from their posterior distributions.
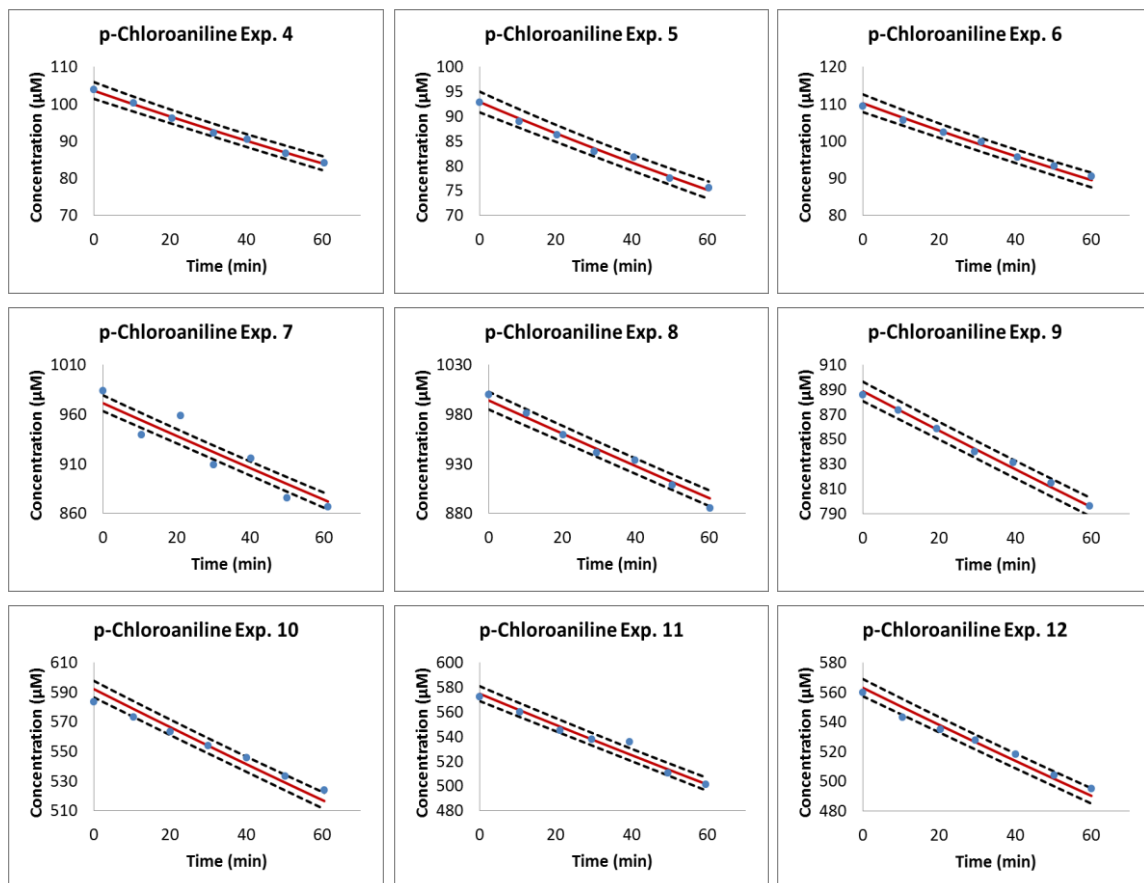
Figure 2.19- p-Chloroaniline depletion data from rat liver microsome studies (points) and 95% confidence interval of model predicted curves simulated by the MCMC sampling using V_{max} and K_m values obtained from their posterior distributions.
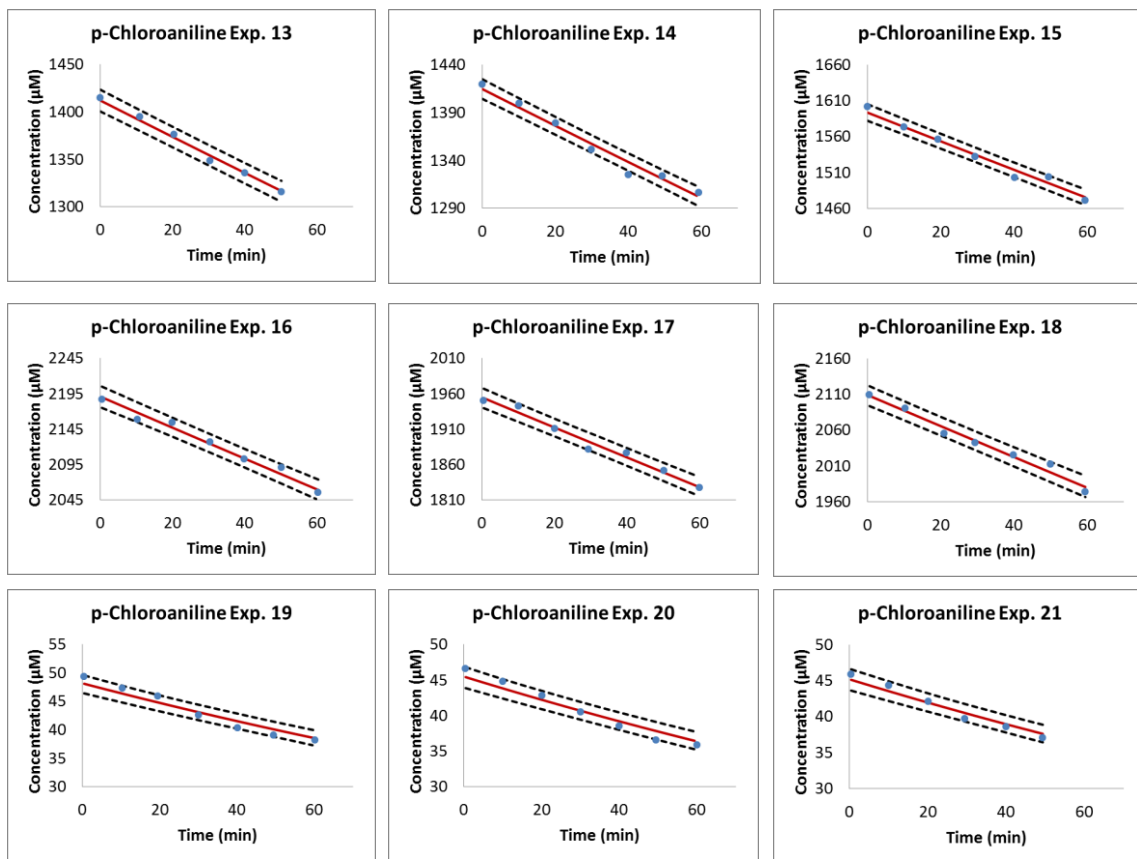
Figure 2.20- p-Chloroaniline depletion data from rat liver microsome studies (points) and 95% confidence interval of model predicted curves simulated by the MCMC sampling using V_{max} and K_m values obtained from their posterior distributions) - continued
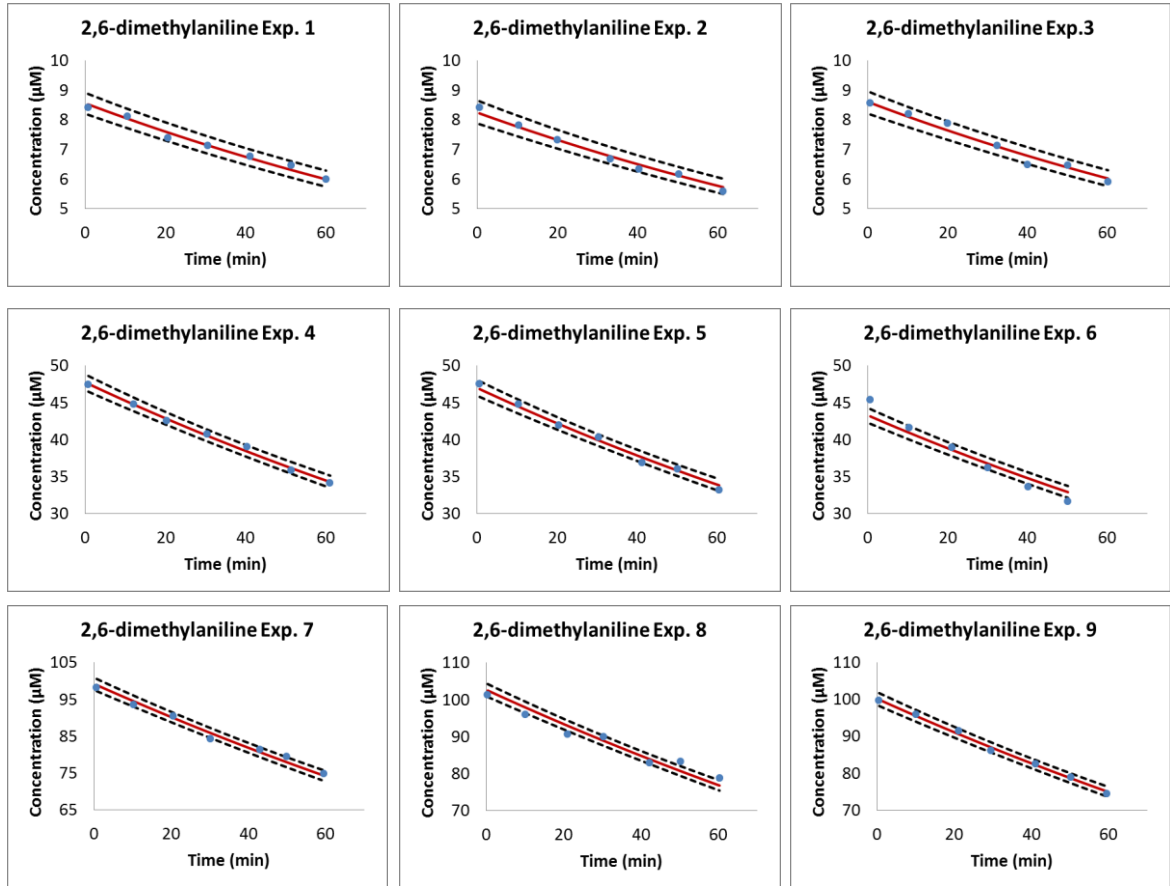
Figure 2.21- 2,6-Dimethylaniline depletion data from rat liver microsome studies (points) and 95% confidence interval of model predicted curves simulated by the MCMC sampling using V_{max} and K_m values obtained from their posterior distributions.
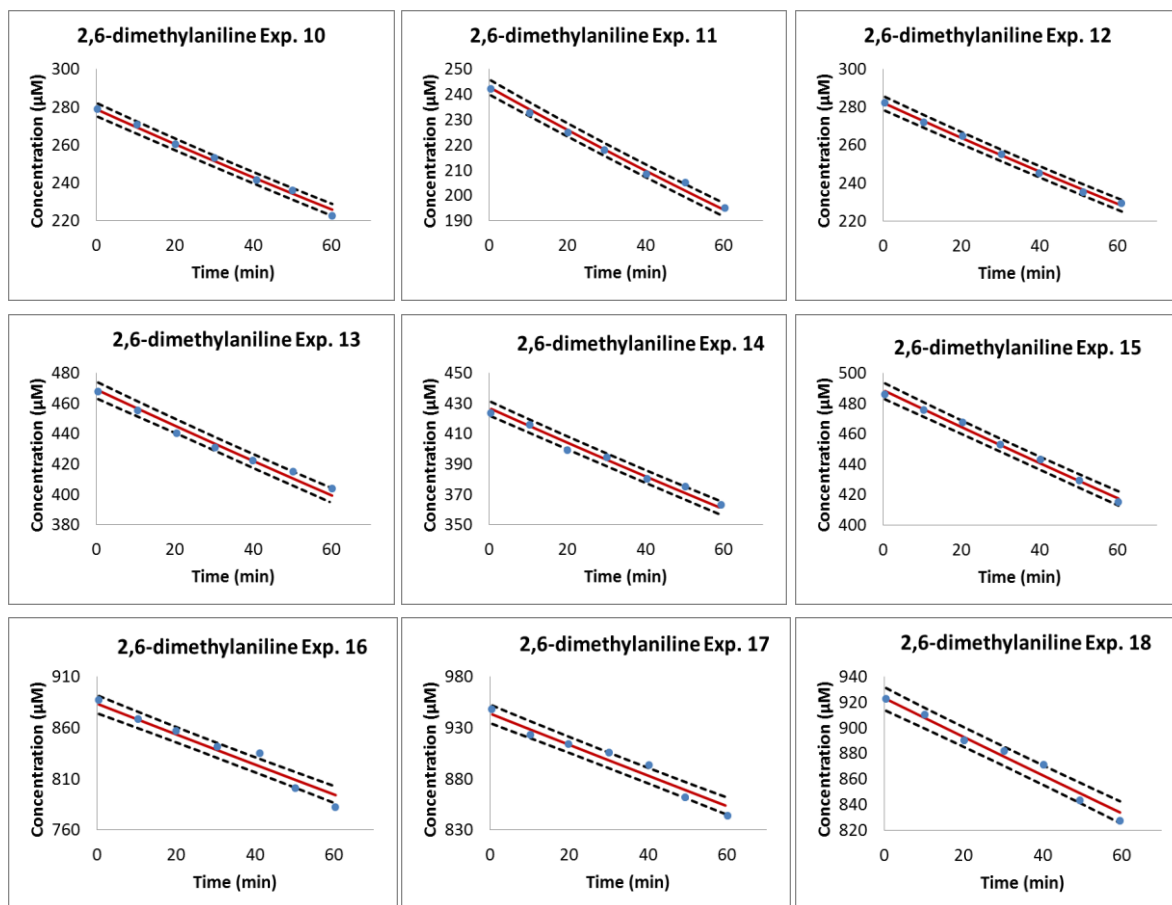
Figure 2.22- 2,6-Dimethylaniline depletion data from rat liver microsome studies (points) and 95% confidence interval of model predicted curves simulated by the MCMC sampling using V_{max} and K_m values obtained from their posterior distributions - continued
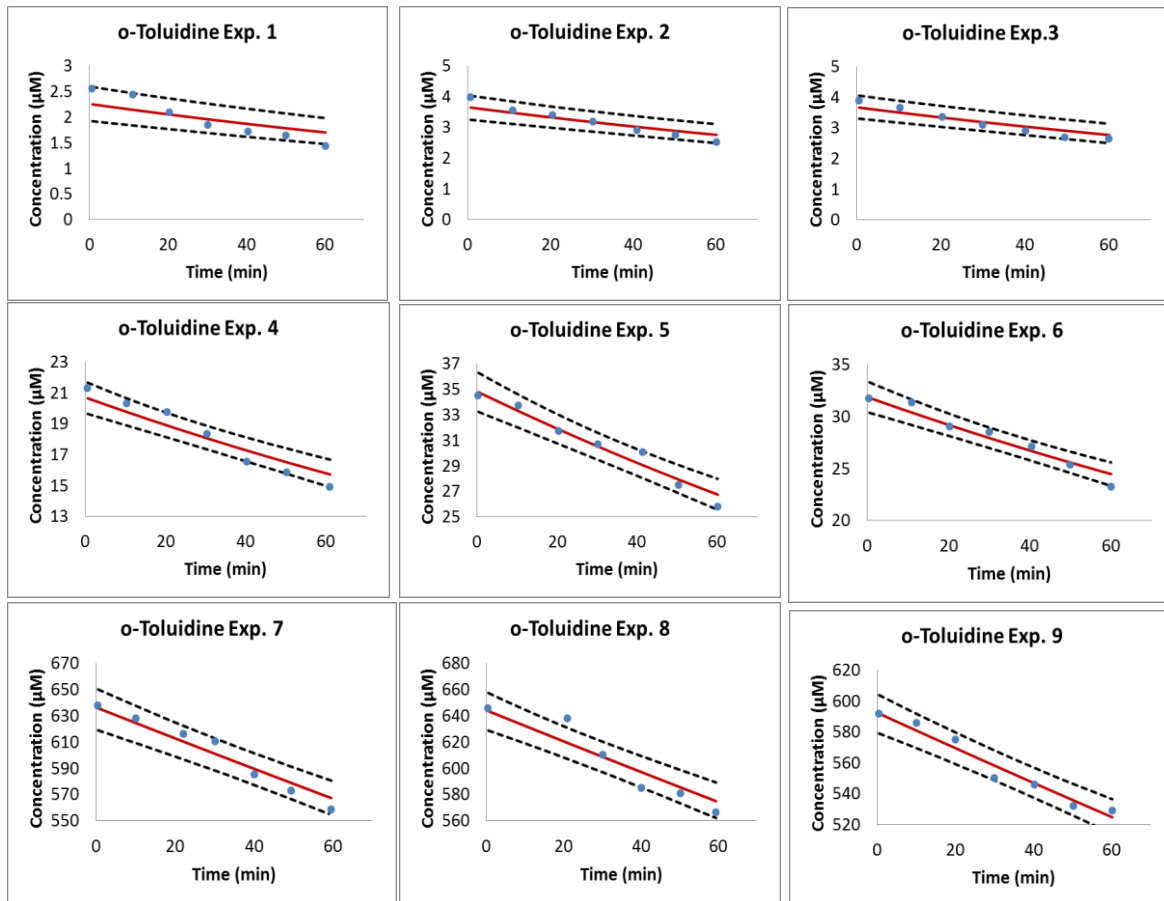
Figure 2.23- o-Toluidine depletion data from rat liver microsome studies (points) and 95% confidence interval of model predicted curves simulated by the MCMC sampling using V_{max} and K_m values obtained from their posterior distributions.
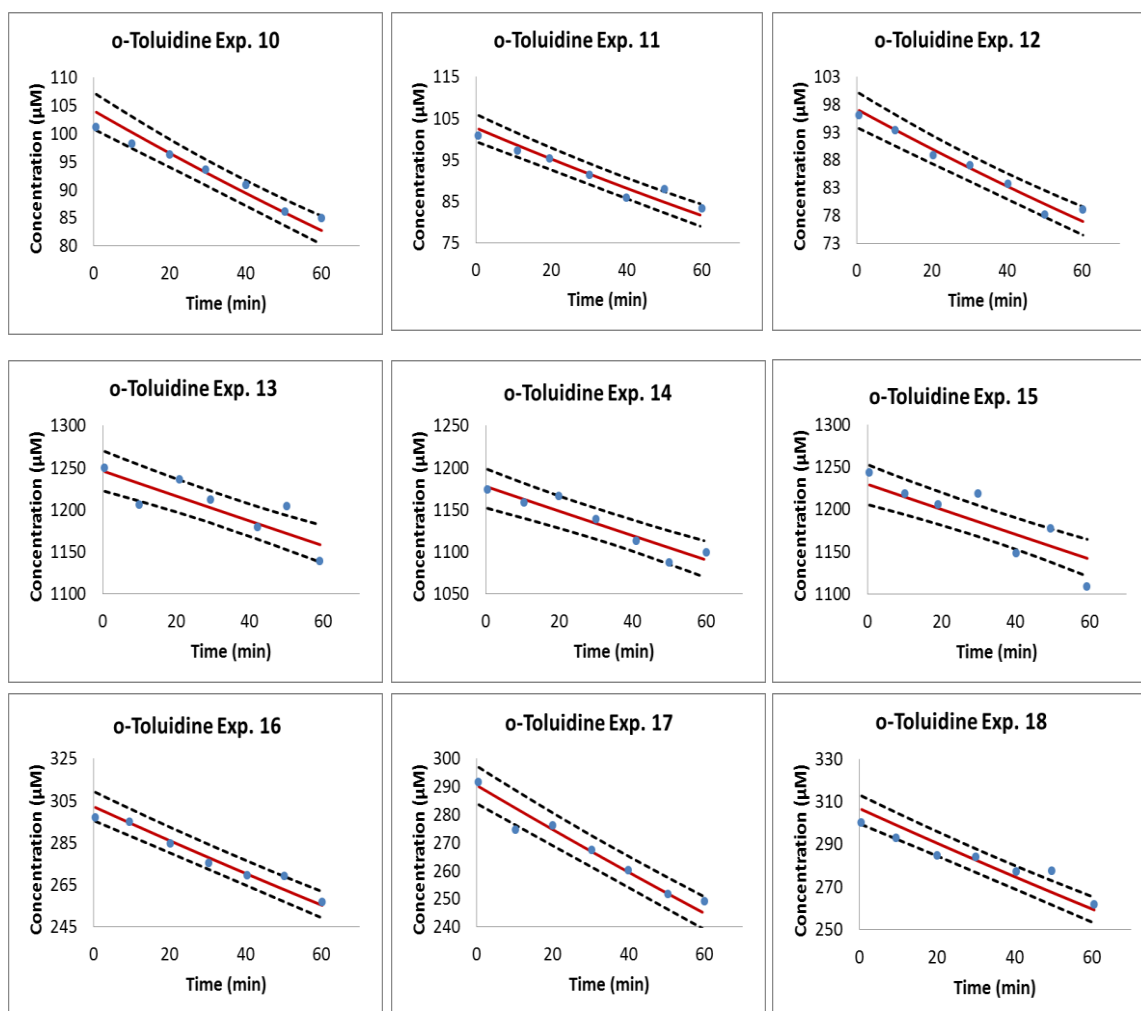
Figure 2.24- o-Toluidine depletion data from rat liver microsome studies (points) and 95% confidence interval of model predicted curves simulated by the MCMC sampling using V_{max} and K_m values obtained from their posterior distributions – continued.
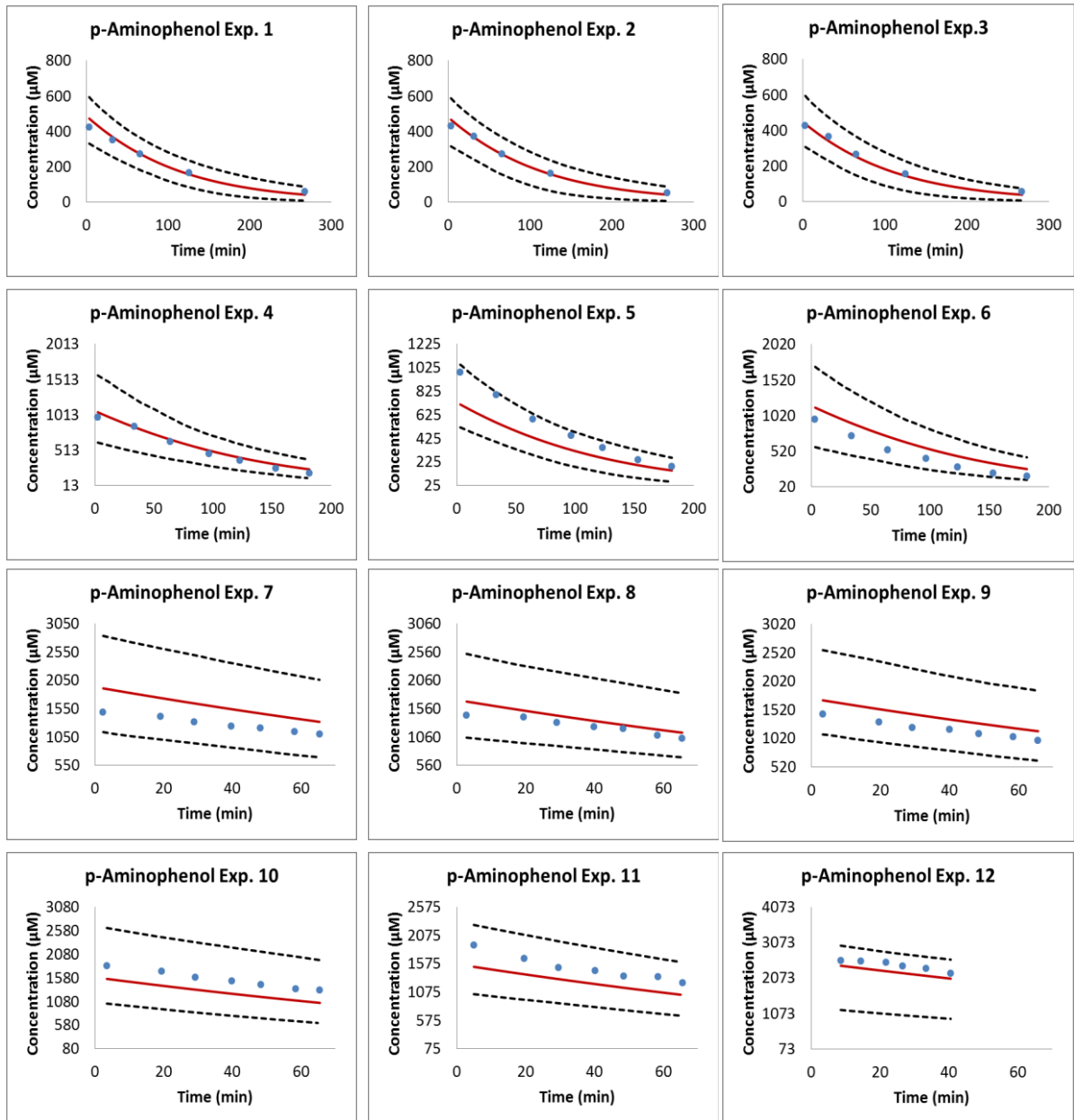
Figure 2.25- p-Aminophenol depletion data from rat liver microsome studies (points) and 95% confidence interval of model predicted curves simulated by the MCMC sampling using V_{max} and K_m values obtained from their posterior distributions.
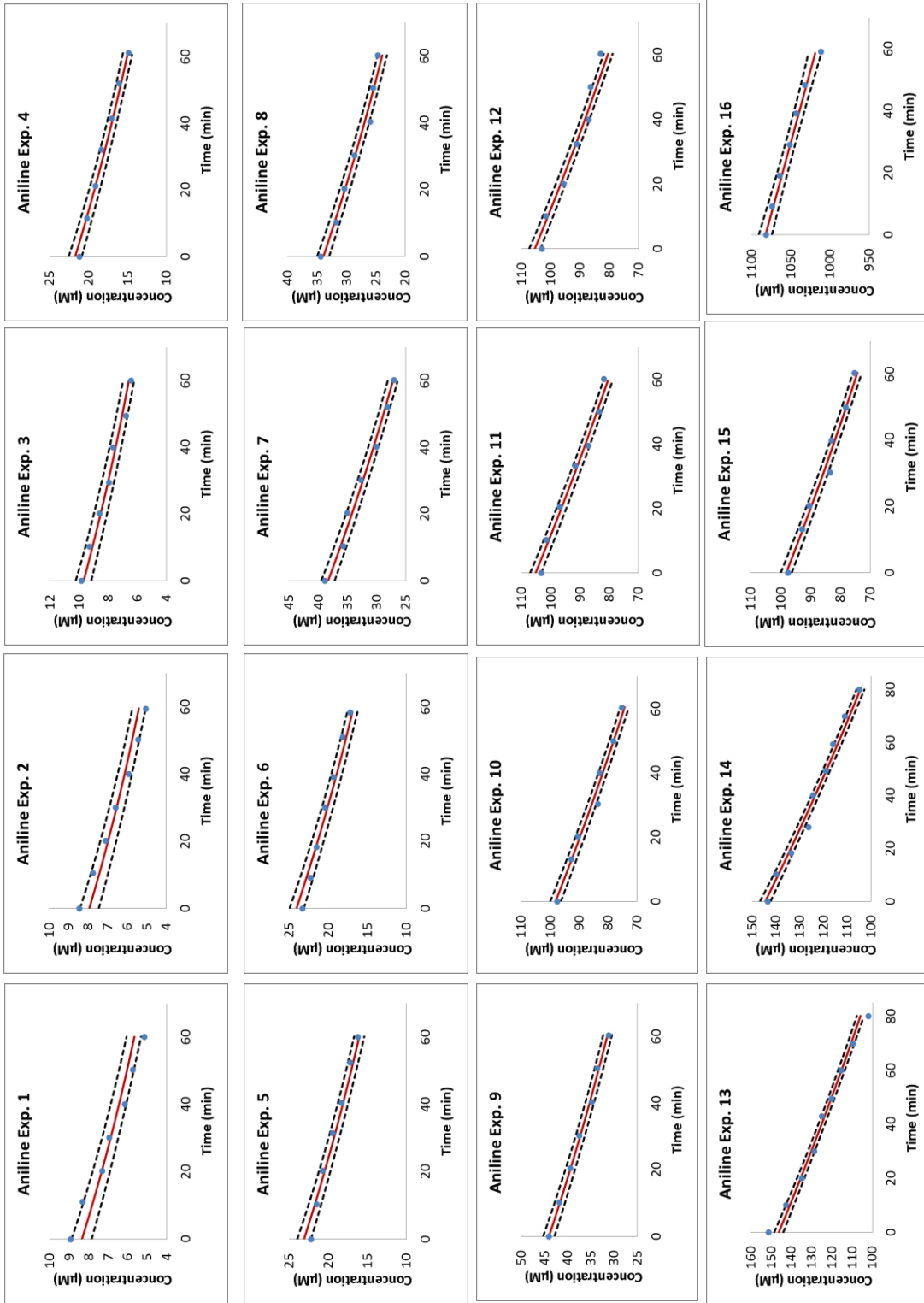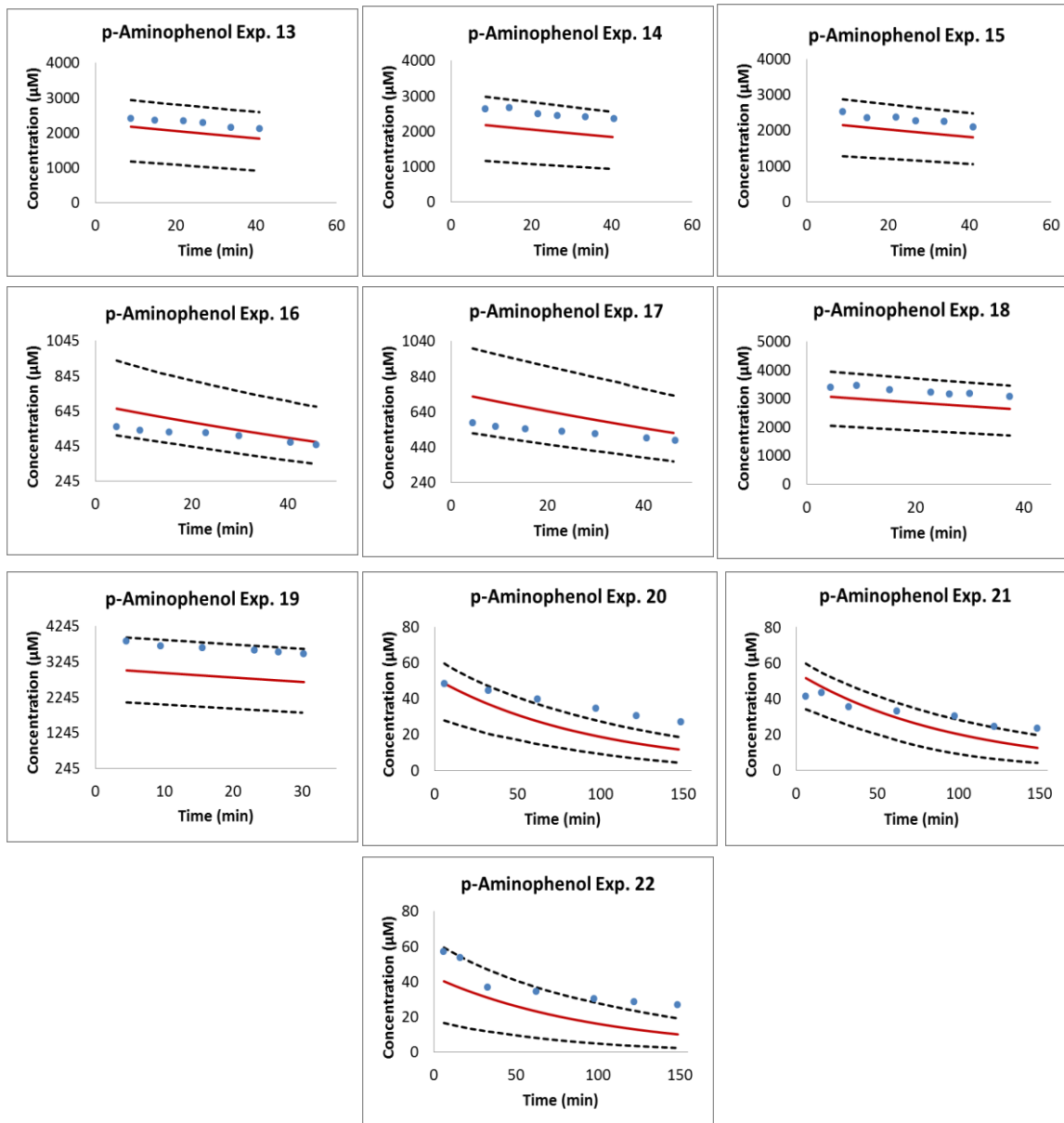
Figure 2.26- p-Aminophenol depletion data from rat liver microsome studies (points) and 95% confidence interval of model predicted curves simulated by the MCMC sampling using V_{max} and K_m values obtained from their posterior distributions – continued.

2.3.3. Plasma and microsomal protein binding

The mean and standard deviation (n=3) for the fraction unbound in microsomes and plasma of five model compounds at different concentrations are tabulated in the Tables 2.25 – 2.29. The average unbound fractions in microsomes and plasma over all concentrations of aniline were 0.90 and 0.67, respectively. For PCA, unbound fractions in microsomes and plasma were 0.77 and 0.22, respectively. 2,6-DMA has average of 0.67 fraction unbound in microsomes and 0.34 fraction unbound in plasma. o-TOL unbound fractions in microsomes and plasma were 0.81 and 0.60, respectively. PAP unbound fractions in microsomes and plasma were 1.02 and 0.74, respectively. In general, binding to microsomal protein is less than plasma protein for these model compounds.

Table 2.26- Protein unbound fraction of aniline in microsomes and plasma measured using ultrafiltration

Plasma		Microsomes	
Concentration (μM)	fu_p (mean $\pm$ SD)	Concentration (μM)	fu_{mic} (mean $\pm$ SD)
2	0.73	2	0.87
10	0.68 $\pm$ 0.003	50	0.86 $\pm$ 0.061
20	0.69 $\pm$ 0.023	100	0.93 $\pm$ 0.012
100	0.70 $\pm$ 0.001	500	0.91 $\pm$ 0.013
1000	0.61 $\pm$ 0.05	1000	0.91 $\pm$ 0.004
fu_{device}: 0.94 $\pm$ 0.02			

Table 2.27- Protein unbound fraction of p-chloroaniline in microsomes and plasma measured using ultrafiltration

Plasma		Microsomes	
Concentration (μM)	fu_p (mean $\pm$ SD)	Concentration (μM)	fu_{mic} (mean $\pm$ SD)
2	0.21 $\pm$ 0.03	10	0.80 $\pm$ 0.01
10	0.26 $\pm$ 0.02	100	0.73 $\pm$ 0.02
100	0.21 $\pm$ 0.01	1000	0.66 $\pm$ 0.06
1000	0.23 $\pm$ 0.03	2000	0.88 $\pm$ 0.02
2000	0.25 $\pm$ 0.03		
fu_{device}: 0.97 $\pm$ 0.06			

Table 2.28- Protein unbound fraction of 2,6-dimethylaniline in
microsomes and plasma measured using ultrafiltration

Plasma		Microsomes	
Concentration (μM)	fu_p (mean ± SD)	Concentration (μM)	fu_{mic} (mean ± SD)
20	0.36 ± 0.02	20	0.66 ± 0.03
100	0.34 ± 0.04	100	0.68 ± 0.04
1000	0.30 ± 0.06	1000	0.68 ± 0.05
fu_{device}: 0.87 ± 0.02			

Table 2.29- Protein fraction unbound of o-toluidine in microsomes
and plasma measured using ultrafiltration

Plasma		Microsomes	
Concentration (μM)	fu_p (mean ± SD)	Concentration (μM)	fu_{mic} (mean ± SD)
20	0.69 ± 0.04	20	0.90 ± 0.01
50	0.61 ± 0.05	200	0.79 ± 0.06
1000	0.51 ± 0.01	500	0.78 ± 0.03
		1000	0.69 ± 0.05
fu_{device}: 0.89 ± 0.02			

Table 2.30-Protein unbound fraction of p-aminophenol in
microsomes and plasma measured using ultrafiltration

Plasma		Microsomes	
Concentration (μM)	fu_p (mean ± SD)	Concentration (μM)	fu_{mic} (mean ± SD)
10	0.81 ± 0.4	50	1.03 ± 0.26
20	0.71 ± 0.03	100	1.02 ± 0.063
100	0.73 ± 0.11	1000	0.97 ± 0.025
1000	0.70 ± 0.014	3000	1.08 ± 0.04
fu_{device}: 0.95 ± 0.01			

2.3.4. Effective intestinal permeability

Correlation of Caco-2 permeation with molecular properties

The multiple linear regression of the training data set (n = 17) using 14 descriptors resulted in a subset model (8 predictors) with the smallest BIC value. Parameter estimates were listed in the Table 2.30. High value of adjusted correlation coefficient (R^2_{adj} = 0.970) suggests that Caco-2 permeabilities and 8 molecular descriptors are highly correlated. The plot of observed $logP_{app}$ and predicted $logP_{app}$ shows that the predicted and observed values are close and the model selected fits the data set with small variability (Figure 2.27).

Table 2.31- Parameter estimates of the selected
model for Caco-2 cell permeability prediction

Variable	Estimate	Adjusted R^2	BIC
Intercept	-3.09		
a_acc	1.79		
a_don	-0.99		
E_tor	-0.055		
E_vdw	-0.145	0.97	-49.98
logP	0.59		
SMR	5.77		
VSA	-0.069		
Weight	-0.088		
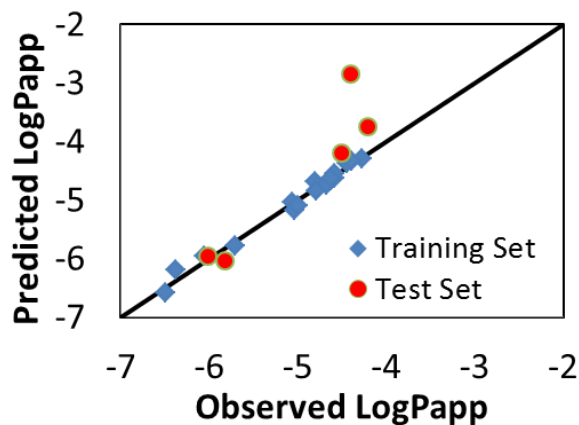
Figure 2.27- Pair plot between predicted apparent
permeability ($logP_{app}$) from model selected and
experimental values obtained from Hou et al (20).

105

The prediction power of the model was validated by a test set of 5 compounds which are ethionamide, acebutolol, guanabenz, epinephrine and lidocaine. The predicted and observed Caco-2 permeabilities of the test set were shown in Table 2.31. Besides ethionamide, the difference between predicted and observed values is less than 0.5. The good predictions for the tested compounds confirm the reliability and reproducibility of the selected molecular descriptors and the model based on them.

This model was used to predict unknown Caco-2 permeabilities of drug degradation products as PBPK model parameters. Molecular descriptors and predicted $logP_{app}$ for the model drug degradants are tabulated in Table 2.32 and 2.33.

Table 2.32- Observed Caco-2 permeabilities from Hou et al (20) and predicted values of 5 test compounds using model selected.

Test compound	Predicted $logP_{app}$	Observed $log\ P_{app}$
ethionamide	-2.85	-4.40
acebutolol	-6.04	-5.83
guanabenz	-4.19	-4.50
epinephrine	-5.95	-6.02
lidocaine	-3.75	-4.21

Table 2.33- Molecular descriptors for drug degradants obtained from MOE software

Compound	b_rotR	rgyr	a_acc	a_don	E_sol	E_tor	E_vdw	VSA	TPSA
p-chloroaniline	0	2.19	0	1	-6.43	7.54	13.90	142.97	26.02
2,6-dimethylaniline	0	2.07	0	1	-5.68	-4.53	16.73	169.52	26.02
o-toluidine	0	1.90	0	1	-7.56	7.44	16.21	144.27	26.02
p-aminophenol	0	1.99	1	2	-12.79	7.55	14.49	135.47	46.25
aniline	0	1.75	0	1	-7.69	-7.54	13.22	126.98	26.02

Table 2.34- Physical properties from MOE and predicted Caco-2 values using selected model for drug degradants

Compound	apol	SMR	logS	$\log P_{(o/w)}$	MW	Predicted $\log P_{app}$
p-chloroaniline	17.8408	3.5864	-1.84	1.826	127.574	-5.048
2,6-dimethylaniline	23.8483	3.9808	-0.4905	1.288	123.199	-5.618
o-toluidine	19.4211	3.5591	-1.2662	1.53	107.156	-4.013
p-aminophenol	17.1296	3.2519	-0.7438	0.926	109.128	-4.666
aniline	16.3276	3.0854	-1.1058	1.234	93.129	-4.881

Conversion of apparent Caco-2 permeability to *in vivo* permeability

The apparent Caco-2 permeability from *in vitro* experiments was converted to *in vivo* permeability using relevant correlation. The *in vitro/in vivo* permeability correlation (Figure 2.28) was reproduced from data of Alsenz's study using 28 compounds with reported *in vivo* intestinal permeabilities (P_{eff} ($\times 10^{-4}$ cm/s)) determined in healthy human subjects and *in vitro* Caco-2 cell permeabilities (P_{app} ($\times 10^{-6}$ cm/s)) obtained from Alsenz's laboratory at pH 7.4 (72). Below is summary of the correlation (Table 2.34).
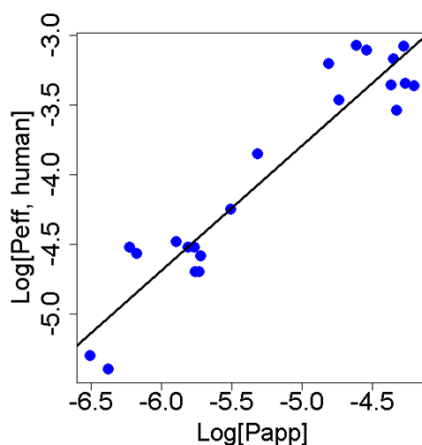
Figure 2.28- Correlation of Caco-2 permeability and *in vivo* human permeability using data from Alsenz (67)

Table 2.35- *In vitro / in vivo* permeability correlation

Coefficient	Estimate	SE
Intercept	0.899	0.056
$logP_{app}$	0.707	0.076
$logP_{eff} = 0.899 \times logP_{app} + 0.707$		
$R^2 = 0.90$		

The Caco-2 permeabilities of drug degradants were converted to effective human permeabilities using the correlation obtained above (Table 2.35). Using the correlation below between human and rat intestinal permeability from Fagerholm et al (73), the *in vivo* permeability in rats were calculated for model compounds:

$$P_{eff,\ human} = 3.6 \times P_{eff,\ rat} + 0.03 \times 10^{-4}$$

The results were shown in Table 3.35.

Table 2.36-Conversion of *in vitro* permeabilities to *in vivo* human and rat permeabilities of model degradants using correlation below between human and rat intestinal permeability from Fagerholm et al (73)

Compound	$logP_{app}$	$logP_{eff,human}$	$logP_{eff,rat}$
Aniline	-4.88	-3.68	-4.24
p-Chloroaniline	-5.05	-3.83	-4.40
2,6-Dimethylaniline	-5.62	-4.35	-4.94
o-Toluidine	-4.01	-2.90	-3.46
p-Aminophenol	-4.67	-3.49	-4.05

2.4. Discussion

2.4.1. Tissue to plasma partition coefficients

The mechanistic Kpu equation (Eq. 2.7) has been used to predict tissue to plasma partition coefficients of selected drug degradants for both rats and humans. These coefficients were used in conjunction with species-specific plasma and tissue volumes to determine unbound volume of distribution at steady state ($Vd_{u,ss}$) by Equation 2.10. Traditionally, V_{ss} is mainly determined as the product of clearance (Dose/AUC_{plasma}) and mean residence time (MRT) in the body. V_{ss} can be estimated by using plasma concentration- time profiles obtained after a single intravenous dose in laboratory animals and human. Due to the potential toxicity of model drug degradants, there are limited disposition data available in humans. Therefore, the prediction accuracy of the mechanistic Kpu model for degradation compounds was assessed by comparing the predicted values of $Vd_{u,ss}$ with the *in vivo* $Vd_{u,ss}$ of parent or similar-structure compounds. Acetaminophen, parent drug of PAP, has experimental rat and human $Vd_{u,ss}$ in the range of 0.61 − 0.91 L/kg and 0.85 − 1.42 L/kg, respectively (64). Lidocaine and prilocaine are the parent drugs of 2,6-DMA and o-TOL. The *in vivo* human $Vd_{u,ss}$ for lidocaine and prilocaine are 2.96 L/kg and 6.09 L/kg, respectively (38). Aromatic amines with similar structure, such as procainamide and clonidine have human $Vd_{u,ss}$ values of 2.27 L/kg (38) and 2.63 L/kg (74). Overall, the predicted values of $Vd_{u,ss}$ of model drug degradants were in the range of values published in literature for the parent compounds. The predicted $Vd_{u,ss}$ for o-TOL differ from its parent value by a factor of 5. This result may be due to the change of aromatic amine pKa from parent to degradant. Prilocaine is a relatively strong base (pKa of 7.9) than o-TOL (pKa of 4.45). Thus, tissue to plasma partition coefficients of model compounds were reasonably predicted with tissue-composition based equations. The uncertainty associated with tissue composition data, as well as compound specific parameter such as lipophilicity and ionization constant, which were

obtained from various literature resources were evaluated in subsequent PBPK model development.

2.4.2. Metabolic rate constants

The primary kinetic parameters V_{max} and K_m for the model compounds were determined for PBPK model parameterization using substrate depletion method. The Michaelis-Menten equation was fitted to all substrate disappearance profiles by means of Markov Chain Monte Carlo simulations. The objective of this experimental study was to estimate overall enzyme kinetics, thus the substrate depletion rate are more useful than metabolite appearance rate measurement to obtain metabolic parameters. The estimated parameters for aniline were compared with available values in literature. McCarthy et al. (75) conducted microsomal enzyme assays from Fischer 344 rats and reported the kinetic parameters for aniline, V_{max} of 0.82 nmol/min/mg protein and K_m of 1.47 mM for p-hydroxylation pathway. For N-hydroxylation pathway, V_{max} was estimated to be 0.46 nmol/min/mg protein and K_m was estimated to be 4.12 mM. The discrepancy between the values obtained from our study and McCarthy (75) or other resources (76, 77) can be explained by the difference in experimental conditions. For example, microsomes in our study were obtained from different strain rat (Sprague-Dawley), concentration of microsomes used in McCarthy study was higher (1.25 mg protein/ml). Bidlack and coworker (78) investigated the effect of acetone on the p-hydroxylation of aniline using microsomes prepared from Sprague-Dawley rats. The kinetic values of V_{max} and K_m were determined by measuring the formation of metabolite p-aminophenol and reported as 1.8 nmol/min/mg protein and 140 μM, respectively. Our estimated parameters differ from these corresponding values by a factor of 1.4, however, the ratio of V_{max}/K_m is similar between those two.

One of the benefits of using MCMC method to obtain Bayesian inference is to update prior information from observed data. Due to the limited available resources of

metabolism study for our model compounds, the non-informative prior was used. When the data are more informative than the prior distribution, the posterior distribution is almost entirely determined by the likelihood, and the prior distribution produces little influence. Therefore, the results of parameters estimated from nonlinear regression are close to the estimates obtained from MCMC sampling. If substantial prior information exists, the Bayesian inference for enzyme kinetic parameters could be more robust.

2.4.3. Microsomal and plasma protein binding

Plasma and microsomal protein unbound fractions of model compounds were determined using ultrafiltration method. The values obtained were compared with literature. Protein plasma unbound of aniline was reported to be 0.75 (63) and 0.63 (79), which are in good agreement with our finding of 0.67. Similarly, acetaminophen (parent drug of p-aminophenol) was reported to have plasma protein unbound fraction of 0.88 (64), whereas fu_p of p-aminophenol is 0.74 based on our measurements. Lidocaine (parent drug of 2,6-dimethylaniline) was estimated to have a plasma protein unbound of 0.38 in rat and 0.35 in human (40); and its degradant mean fu_p value of 0.34 in our study.

The results suggest that ultrafiltration technique provided reliable measurements of protein binding for model compounds. One of the limitations of ultrafiltration method is the nonspecific binding of substrates to the filter membrane (80). However, the extent of non-specific binding to ultrafiltration units for the model compounds was relatively low (less than 10%). Besides, the selected substrates have small molecular weight (MW < 150), hence, potential molecular sieving effects as reported for drug molecules with high molecular weights (81) were not present.

2.4.4. Intestinal permeability

A QSAR model for predicting Caco-2 cell permeability ($logP_{app}$) was derived from $logP_{app}$ values measured in Caco-2 cell of 22 aromatic amines in literature. All computed descriptor combinations were evaluated to find the one that gave the best

predictors based on BIC criteria. From the table of parameter estimates (Table 2.30), permeability decreases with increasing van der Waals surface area, high number of hydrogen bond donors, or large MW. On the other hand, permeability was positively influenced by molar refractivity and high $logP_{o/w}$. The similar trends in the effect of physical properties and molecular descriptors on permeability are described in the model of Sherer et al. (82). Solubility did not play a role in the selected model, which is reasonable for this group of small compounds of weakly-base substituted-anilines with pKa 4 – 5.

The predicted values of Caco-2 permeability suggest that 5 model compounds are highly permeable. Since Caco-2 permeability has not been made for the model compounds, the agreement between predicted and observed values is not be able to evaluate. However, for this group of small compounds with reported rapid absorption, the model developed for Caco-2 permeability prediction was deemed to be adequate.

2.5. Conclusion

All necessary parameters for the selected compounds for the rat and human PBPK model were estimated. Physiological parameters (e.g. blood flow, tissue volume and composition) for rats and humans were compiled from the literature. Some of biophysical and pharmacokinetic parameters were available in the literature, such as lipophilicity (logP), blood to plasma ratio while others required *in vitro* experimentation and *in silico* prediction based on established procedures. Tissue to plasma partition coefficients of model compounds were reasonably predicted with tissue-composition based equations from Rodgers and Rowland model. Metabolic parameter distributions and their correlation were predicted from MCMC simulations. Microsomal and plasma protein unbound fractions of model compounds were determined by ultrafiltration and in good agreement with literature data. Effective intestinal permeability was estimated by

QSAR model. These obtained model parameters were applied in the systems of PBPK differential equations to describe the fate of substrate in the body.

For human PBPK development, the physiological and anatomical parameters of rats will be replaced with those corresponding to adult population. Selected pharmacokinetic parameters were interspecies scaled. For example, the metabolic rate constant V_{max} was adjusted by the amount of protein in human intact liver taken from literature. These steps will be described in details in Chapter 3.

CHAPTER 2 LITERATURE CITED

1. Valentin J. 2002. Basic anatomical and physiological data for use in radiological protection: Reference values: ICRP publication 89. *Annals of the ICRP.* 32 : 1-277

2. Brown RP, Delp MD, Lindstedt SL, Rhomberg LR, Beliles RP. 1997. Physiological parameter values for physiologically based pharmacokinetic models. *Toxicology and Industrial Health.* 13 : 407-84

3. Davies B, Morris T. 1993. Physiological parameters in laboratory animals and humans. *Pharmaceutical Research.* 10 : 1093-5

4. Price PS, Conolly RB, Chaisson CF, Gross EA, Young JS. 2003. Modeling interindividual variation in physiological factors used in PBPK models of humans. *Critical Reviews in Toxicology.* 33 : 469-503

5. Gentry PR, Haber LT, McDonald TB, Zhao Q, Covington T, Nance P, Clewell HJ, III, Lipscomb JC, Barton HA. Data for physiologically based pharmacokinetic modeling in neonatal animals: Physiological parameters in mice and sprague-dawley rats. *Journal of Children's Health.* 363-411

6. Thompson CM, Johns DO, Sonawane B, Barton HA, Hattis D. 2009. Database for physiologically based pharmacokinetic (PBPK) modeling: Physiological data for healthy and health-impaired elderly. *Journal of Toxicology & Environmental Health: Part B.* 12 : 1-24

7. Poulin P, Theil F. 2000. A priori prediction of tissue:Plasma partition coefficients of drugs to facilitate the use of physiologically-based pharmacokinetic models in drug discovery. *Journal of Pharmaceutical Sciences.* 89 : 16-35

8. Rodgers T, Leahy D, Rowland M. 2005. Physiologically based pharmacokinetic modeling 1: Predicting the tissue distribution of moderate-to-strong bases. *Journal of Pharmaceutical Sciences.* 94 : 1259-76

9.   Rodgers T, Rowland M. 2006. Physiologically based pharmacokinetic modelling 2: Predicting the tissue distribution of acids, very weak bases, neutrals and zwitterions. *Journal of Pharmaceutical Sciences.* 95 : 1238-57

10.   Poulin P, Schoenlein K, Theil F. 2001. Prediction of adipose tissue: plasma partition coefficients for structurally unrelated drugs. *Journal of Pharmaceutical Sciences.* 90 : 436-47

11.   Iwatsubo T, Hirota N, Ooie T, Suzuki H, Shimada N. 1997. Prediction of in vivo drug metabolism in the human liver from in vitro metabolism data. *Pharmacology & Therapeutics.* 73 : 147-71

12.   Sjögren E, Lennernäs H, Andersson TB, Gråsjö J, Bredberg U. 2009. The multiple depletion curves method provides accurate estimates of intrinsic clearance (CLint), maximum velocity of the metabolic reaction (Vmax), and Michaelis constant (Km): Accuracy and robustness evaluated through experimental data and monte carlo simulations. *Drug Metabolism and Disposition.* 37 : 47-58

13.   Obach RS, Reed-Hagen AE. 2002. Measurement of michaelis constants for cytochrome P450-mediated biotransformation reactions using a substrate depletion approach. *Drug Metabolism and Disposition.* 30 : 831-7

14.   Jones HM, Houston JB. 2004. Substrate depletion approach for determining in vitro metabolic clearance: Time dependencies in hepatocyte and microsomal incubations. *Drug Metabolism and Disposition.* 32 : 973-82

15.   Kerns EH, Li Di. 2008. Drug-like properties: Concepts, structure design and methods from ADME to toxicity optimization, Elsevier. 552pp

16.   Austin RP, Barton P, Cockroft SL, Wenlock MC, Riley RJ. 2002. The influence of nonspecific microsomal binding on apparent intrinsic clearance, and its prediction from physicochemical properties. *Drug Metabolism and Disposition.* 30 : 1497-503

17.   Dow N. 2006. Determination of compound binding to plasma proteins. *Current protocols in Pharmacology.* 34 : 1-15

18.   van De Waterbeemd H, Camenisch G, Folkers G, Raevsky OA. 1996. Estimation of Caco-2 cell permeability using calculated molecular descriptors. *Quantitative Structure-Activity Relationships.* 15 : 480-90

19.   Palm K, Luthman K, Ungell A, Strandlund G, Artursson P. 1996. Correlation of drug absorption with molecular surface properties. *Journal of Pharmaceutical Sciences.* 85 : 32-9

20.   Hou TJ, Zhang W, Xia K, Qiao XB, Xu XJ. 2004. ADME evaluation in drug discovery. 5. correlation of Caco-2 permeation with simple molecular properties. *Journal of Chemical Information and Computer Sciences.* 44 : 1585-600

21.   Nordqvist A, Nilsson J, Lindmark T, Eriksson A, Garberg P, Kihlén M. 2004. A general model for prediction of Caco-2 cell permeability. *QSAR & Combinatorial Science.* 23 : 303-10

22.   Norinder U, Österberg T, Artursson P. 1997. Theoretical calculation and prediction of caco-2 cell permeability using MolSurf parametrization and PLS statistics. *Pharmaceutical Research.* 14 : 1786-91

23.   Österberg T, Norinder U. 2000. Prediction of polar surface area and drug transport processes using simple parameters and PLS statistics. *Journal of Chemical Information and Computer Sciences.* 40 : 1408-11

24.   Fujiwara S, Yamashita F, Hashida M. 2002. Prediction of Caco-2 cell permeability using a combination of MO-calculation and neural network. *International Journal of Pharmaceutics.* 237 : 95-105

25.   Schwarz G. 1978. Estimating the dimension of a model. *The annals of statistics.* 6 : 461-4

26.   O'Hagan A. 2008. The Bayesian approach to statistics. In *Handbook of Probability: Theory and Applications,* ed. Tamas Rudas, 85-100. SAGE Publications

27. Gelman A, Carlin JB, Stern HS, Rubin DB. 2004. *Bayesian data analysis,* CRC press. 2nd ed.

28. R Core Team. 2012. R: A language and environment for statistical computing.

29. Soetaert K, Petzoldt t, Setzer W. 2010. Solving differential equations in R: Package deSolve. *Journal of Statistical Software.* 33 : 1-25

30. Soetaert K, Petzoldt t. 2010. Inverse modelling, sensitivity and monte carlo analysis in R using package FME. *Journal of Statistical Software.* 33 : 1-28

31. Delp MD, Manning RO, Bruckner JV, Armstrong RB. 1991. Distribution of cardiac output during diurnal changes of activity in rats. *American Journal of Physiology - Heart and Circulatory Physiology.* 261 : H1487-93

32. MacPherson J, Tothill P. 1978. Bone blood flow and age in the rat. *Clinical Science and Molecular Medicine.* 54 : 111-3

33. Bernareggi A, Rowland M. 1991. Physiologic modeling of cyclosporin kinetics in rat and man. *Journal of Pharmacokinetics and Pharmacodynamics.* 19 : 21-50

34. Idvall J, Aronsen K, Stenberg P. 1980. Tissue perfusion and distribution of cardiac output during ketamine anesthesia in normovolemic rats. *Acta Anaesthesiologica Scandinavica.* 24 : 257-63

35. Sasaki Y, Wagner HN,Jr. 1971. Measurement of the distribution of cardiac output in unanesthetized rats. *Journal of Applied Physiology.* 30 : 879-84

36. de la Grandmaison GL, Clairand I, Durigon M. 2001. Organ weight in 684 adult autopsies: New tables for a caucasoid population. *Forensic Science International.* 119 : 149-54

37. Kawai R, Lemaire M, Steimer J, Bruelisauer A, Niederberger W, Rowland M. 1994. Physiologically based pharmacokinetic study on a

cyclosporin derivative, SDZ IMM 125. *Journal of Pharmacokinetics and Pharmacodynamics.* 22 : 327-65

38. Rodgers T, Rowland M. 2007. Mechanistic approaches to volume of distribution predictions: Understanding the processes. *Pharmaceutical Research.* 24 : 918-33

39. Peters SA. 2008. Evaluation of a generic physiologically based pharmacokinetic model for lineshape analysis. *Clinical Pharmacokinetics.* 47 : 261-75

40. Rodgers T, Rowland M. 2007. Mechanistic approaches to volume of distribution predictions: Understanding the processes. *Pharmaceutical Research.* 24 : 918-33

41. Peters SA. 2012. *Physiologically-based pharmacokinetic (PBPK) modeling and simulations: Principles, methods, and applications in the pharmaceutical industry,* America: John Wiley & Sons

42. Bolton P, Hall F. 1967. Thermodynamic functions of ionization of the anilinum and toluidinium ions. *Australian Journal of Chemistry.* 20 : 1797-804

43. Bunting JW, Stefanidis D. 1990. A systematic entropy relationship for the general-base catalysis of the deprotonation of a carbon acid. A quantitative probe of transition-state solvation. *Journal of the American Chemical Society.* 112 : 779-86

44. Pytela O, Otyepka M, Kulhánek J, Otyepková E, Nevečná T. 2003. Correlation of dissociation constants of 2-and 2, 6-substituted anilines in water by methods based on the similarity principle and quantum-chemistry calculations. *The Journal of Physical Chemistry A.* 107 : 11489-96

45. Sheppard WA. 1965. The electronic properties of fluoroalkyl groups. fluorine p-π interaction1. *Journal of the American Chemical Society.* 87 : 2410-20

46.   Broderius SJ, Kahl MD, Hoglund MD. 1995. Use of joint toxic response to define the primary mode of toxic action for diverse industrial organic chemicals. *Environmental Toxicology and Chemistry*. 14 : 1591-605

47.   Albert A, Serjeant EP. 1962. *Ionization constants of acids and bases: A laboratory manual,* Methuen London

48.   Biggs A, Robinson R. 1961. The ionisation constants of some substituted anilines and phenols: A test of the hammett relation. *Journal of the Chemical Society (Resumed)*. 388-93

49.   Van de Graaf B, Hoefnagel A, Wepster B. 1981. Substituent effects. 7. microscopic dissociation constants of 4-amino-and 4-(dimethylamino) benzoic acid. *The Journal of Organic Chemistry*. 46 : 653-7

50.   Bacarella A, Grunwald E, Marshall H, Purlee EL. 1955. The potentiometric measurement of acid dissociation constants and pH in the system methanol-water. pKa values for carboxylic acids and anilinium ions. *The Journal of Organic Chemistry*. 20 : 747-62

51.   Gervasini A, Auroux A. 1993. Thermodynamics of adsorbed molecules for a new acid-base topochemistry of alumina. *The Journal of Physical Chemistry*. 97 : 2628-39

52.   Susten AS, Niemeier RW, Simon SD. 1990. In vivo percutaneous absorption studies of volatile organic solvents in hairless mice II. toluene, ethylbenzene and aniline. *Journal of Applied Toxicology*. 10 : 217-25

53.   De Bruijn J, Busser F, Seinen W, Hermens J. 1989. Determination of octanol/water partition coefficients for hydrophobic organic chemicals with the "slow-stirring" method. *Environmental Toxicology and Chemistry*. 8 : 499-512

54.   Leo A, Hansch C, Elkins D. 1971. Partition coefficients and their uses. *Chemical Reviews*. 71 : 525-615

55.   Fujita T, Iwasa J, Hansch C. 1964. A new substituent constant, π, derived from partition coefficient. *Journal of the American Chemical Society.* 86 : 5175-80

56.   Vandenbelt J, Henrich C, Vanden Berg S. 1954. Comparison of pKa values determined by electrometric titration and ultraviolet absorption methods. *Analytical Chemistry.* 26 : 726-7

57.   Araki K, Murakami H, Ohseto F, Shinkai S. 1992. Acid dissociation and activation parameters for ring inversion of diaminocalix [4] arene. *Chemistry Letters.* 539-42

58.   Hall NF, Sprinkle MR. 1932. Relations between the structure and strength of certain organic bases in aqueous solution. *Journal of the American Chemical Society.* 54 : 3469-85

59.   Perrin DD. 1972. *Dissociation constants of organic bases in aqueous solution: Supplement 1972,* Butterworths

60.   Serjeant EP, Dempsey B. 1979. *Ionisation constants of organic acids in aqueous solution,* Vol. 23. Pergamon

61.   Schanker LS, Tocco DJ, Brodie BB, Hogben CAM. 158. Absorption of drugs from the rat small intestine. *Journal of Pharmacology and Experimental Therapeutics.* 123 : 81-8

62.   Harrison JH, Jollow DJ. 1986. Role of aniline metabolites in aniline-induced hemolytic anemia. *Journal of Pharmacology and Experimental Therapeutics.* 238 : 1045-54

63.   Shore PA, Brodie BB, Hogben CAM. 1957. The gastric secretion of drugs: A pH partition hypothesis. *Journal of Pharmacology and Experimental Therapeutics.* 119 : 361-9

64.   Poulin P, Theil F. 2002. Prediction of pharmacokinetics prior to in vivo studies. 1. Mechanism-based prediction of volume of distribution. *Journal of Pharmaceutical Sciences.* 91 : 129-56

65.   Kao J, Faulkner J, Bridges JW. 1978. Metabolism of aniline in rats, pigs and sheep. *Drug Metabolism and Disposition.* 6 : 549-55

66.   Nohynek GJ, Duche D, Garrigues A, Meunier P, Toutain H, Leclaire J. 2005. Under the skin: Biotransformation of para-aminophenol and para-phenylenediamine in reconstructed human epidermis and human hepatocytes. *Toxicology Letters.* 158 : 196-212

67.   Strober W. 2001. Trypan blue exclusion test of cell viability. *Current protocols in immunology.* A. 3B. 1,A. 3B. 2

68.   Chemical Computing Group Inc. 2014. *Molecular operating environment (MOE)*, 2013.08.

69.   Laitinen L, Kangas H, Kaukonen A, Hakala K, Kotiaho T, et al. 2003. N-in-one permeability studies of heterogeneous sets of compounds across caco-2 cell monolayers. *Pharmaceutical Research.* 20 : 187-97

70.   Pade V, Stavchansky S. 1997. Estimation of the relative contribution of the transcellular and paracellular pathway to the transport of passively absorbed drugs in the Ccaco-2 cell culture model. *Pharmaceutical Research.* 14 : 1210-5

71.   Nakao K, Fujikawa M, Shimizu R, Akamatsu M. 2009. QSAR application for the prediction of compound permeability with in silico descriptors in practical use. *Journal of Computer-Aided Molecular Design.* 23 : 309-19

72.   Alsenz J, Haenel E. 2003. Development of a 7-day, 96-well caco-2 permeability assay with high-throughput direct UV compound analysis. *Pharmaceutical Research.* 20 : 1961-9

73.   Fagerholm U, Johansson M, Lennernäs H. 1996. Comparison between permeability coefficients in rat and human jejunum. *Pharmaceutical Research.* 13 : 1336-42

74.   Lombardo F, Obach RS, Shalaeva MY, Gao F. 2002. Prediction of volume of distribution values in humans for neutral and basic drugs using physicochemical measurements and plasma protein binding data. *Journal of Medicinal Chemistry.* 45 : 2867-76

75.   McCarthy DJ, Waud WR, Struck RF, Hill DL. 1985. Disposition and metabolism of aniline in fischer 344 rats and C57BL/6 $\times$ C3H F1 mice. *Cancer Research.* 45 : 174-80

76.   Gram TE, Rogers LA, Fouts JR. 1967. Further studies on the metabolism of drugs by subfractions of hepatic microsomes. *Journal of Pharmacology and Experimental Therapeutics.* 155 : 479-93

77.   Eling TE. 1970. Kinetic changes in microsomal drug metabolism with age and diphenylhydantoin treatment. *European Journal of Pharmacology.* 11 : 101-8

78.   Bidlack WR, Lowery GL. 1982. Multiple drug metabolism: P-nitroanisole reversal of acetone enhanced aniline hydroxylation. *Biochemical Pharmacology.* 31 : 311-7

79.   Cheng Y, Ho E, Subramanyam B, Tseng J. 2004. Measurements of drug–protein binding by using immobilized human serum albumin liquid chromatography–mass spectrometry. *Journal of Chromatography B.* 809 : 67-73

80.   Tasker RA, Nakatsu K. 1982. Factors affecting ultrafiltration-assessed values for drug binding. *Clinical Chemistry.* 28 : 1244-6

81.   Kurz H, Trunk H, Weitz B. 1977. Evaluation of methods to determine protein-binding of drugs. equilibrium dialysis, ultrafiltration, ultracentrifugation, gel filtration. *Arzneimittelforschung.* 27 : 1373-80

82.   Sherer EC, Verras A, Madeira M, Hagmann WK, Sheridan RP, et al. 2012. QSAR prediction of passive permeability in the LLC-PK1 cell line: Trends in molecular properties and cross-prediction of caco-2 permeabilities. *Molecular Informatics.* 31 : 231-45

CHAPTER 3.   VELOPMENT OF RAT AND HUMAN PBPK MODELS AND PARAMETER SENSITIVITY ANALYSIS

3.1.Introduction

The PBPK modeling can be used to predict the exposure of a toxic substance in a target tissue. In the previous chapter, the methodology for PBPK model construction was described. The ability of a PBPK model to account for uncertainty and population variability was also discussed. In this chapter, an oral input model is added to the disposition model described in Chapter II and the results for oral exposure are presented. Sensitivity and uncertainty analyses were used to evaluate the impact of model input parameters on model predictions.   In addition, by incorporating population variability of physiological parameters, the overall variability in the concentration time profile was estimated.

3.1.1. Absorption modeling

Yu and coworkers developed a compartmental absorption and transit (CAT) model to simulate the rate and extent of drug absorption for passively transported drugs. The gastrointestinal (GI) tract is divided into three segments: stomach, small intestine, and colon. The model describes simultaneous transit flow in stomach, small intestine and colon, and is used to estimate total absorption in the GI tract. The transit flow in the small intestine was described by seven single compartments, which have the same residence time but different volumes and flow rates. Drug flows through each segment by linear transfer kinetics and is absorbed passively across the small intestinal membrane. Absorption from the stomach and colon is assumed to be negligible compared with that from the small intestine. The absorption rate constant is proportional to the effective permeability. The drug is non-degradable and formulated in an immediate release dosage form. The CAT model was used to predict the fraction of dose absorbed for ten compounds and compare with their observed values from the literature. The estimated

fractions of dose absorbed based on the CAT model were found to provide good agreement with observed data.

Compared to the original CAT model, the advanced CAT (ACAT) model (1) incorporates characteristics of drug formulation (dissolution and precipitation), permeability and degradation, metabolism and transport in each segment. The rate of drug concentration change in each small intestinal compartment is described by a set of differential equations, including release of drug from formulation, dissolution of drug particles, transit of drug into and out of a compartment, luminal degradation of the drug, and absorption of the drug into the systemic circulation. For example, in the ith segment (i = 1…8), differential equations used to describe the rate of change of dissolved drug concentration are the following:

$$\frac{dC_{dissolved}^i}{dt} = \frac{1}{V_i}\left(k_t M_{dissolve}^{i-1} - k_t M_{dissolve}^i + k_d C_{undissolved}^i \left(S_i - C_{dissolved}^i\right) V_i - \right.$$
$$\left. \frac{dC_{absorbed}^i}{dt} - \frac{dC_{degraded}^i}{dt}\right) \qquad \text{(Eq. 3.1)}$$

Drug absorption: $\quad \frac{dC_{absorbed}^i}{dt} = k_a^i M_{dissolve}^i \qquad \text{(Eq. 3.2)}$

Drug degradation: $\frac{dC_{degraded}^i}{dt} = k_{deg}^i M_{dissolve}^i \qquad \text{(Eq. 3.3)}$

$M_{dissolved}^i$, $C_{dissolved}^i$, $C_{undissolved}^i$ are the lumen dissolved amount, dissolved and undissolved concentration of drug for the ith compartment, respectively. V_i is volume of luminal compartment i^{th}; k_t is the rate constant of the small intestine transit; k_d, k_a, k_{deg} are the drug dissolution, absorption and degradation rate constants, and S_i is aqueous drug solubility.

The ACAT model consists of 9 compartments including stomach, 7 segments of small intestine and colon and a series of enterocyte compartments corresponding to each luminal compartment. Drug is absorbed from the GI tract, through the apical membrane

of the enterocyte. Inside the enterocyte, the drug may across the basolateral membrane into the blood stream.

3.1.2. Source of model parameter uncertainty and human variability

In population based-risk assessment, one of the challenges is to address the uncertainty and the variability associated with model parameters. For example, inter-individual differences in biotransformation among human populations with diverse genetics and lifestyles can result in considerable variability in the metabolism of xenobiotics, and hence significantly impact its ADME. The overall inter-individual variability in exposure profiles can be simulated by incorporating variability associated with key PBPK parameters (2). In order to identify which parameters are key in tissue dosimetry, sensitivity analysis can be used.

Absorption

The physiological characteristics of the GI tract and the physicochemical characteristics of the administered compound can affect bioavailability. For example, the surface area of the GI tract, blood flow rate, gastrointestinal pH, intestinal transit time and gastric emptying rate can markedly influence the rate of absorption (3). The size and distribution of the villi and folds vary from one segment of the GI tract resulting in absorption surface differences. The surface area of the small intestine decreases sharply from proximal to distal intestine, thus the proximal part of the small intestine has the greatest capacity for absorption of most drugs (4). In addition, the longer the time a compound is in contact with an area of a particular segment surface, the more extensive the absorption process in that segment. The regional pH in the GI tract can alter drug solubility and hence the dissolution of solid dosage forms. Gastrointestinal pH may also affect drug permeability by influencing the ratio of ionized and non-ionized moieties of a substance (5). The intestinal mucosa also can influence the rate and amount of absorption due to metabolic activities. According to Levine (3), for drugs given in small doses or for

125

those slowly absorbed or slowly released from pharmaceutical preparations, the effect of intestinal biotransformation may be of major significance. For drugs that are subjected to active transport via membrane, the expression of various transporters in the membranes of intestinal epithelial cells can markedly affect the intestinal absorption of drugs administered orally (5). In addition to the effect of these physiological properties, drug absorption also depends on the physicochemical properties of the administered compound.

<u>Distribution</u>

The distribution of a substance throughout the body is influenced by physiological properties of the species as well as physicochemical and biochemical properties of the substance. The rate of drug distribution can be perfusion-rate limited or permeation-rate limited, in which blood flow or membrane is controlling factor. The extent to which a chemical distributes throughout the body is typically described as the volume of distribution (Vd) or volume of distribution at steady state (Vd_{ss}). The binding of a drug to plasma and tissue proteins contributes to the apparent distribution volume of drug. Drugs with low tissue-to-plasma partition coefficients may have high plasma concentration, and vice versus. The partitioning of drugs between plasma and tissue is governed by various physiological properties including body composition (tissue and organ volume/weight), tissue composition, blood flow, hematocrit, concentrations of plasma binding proteins, expressed levels of transporters and fluid pH (5, 6). Volumes of some tissues differ between genders. For example, in women, volume of adipose tissues increases rapidly during puberty, after which women maintain body fat levels approximately 2-fold higher than men. Body fat increases in women from an average of approximately 33% at age 20 to approximately 48% on average in women over 70 years of age (6). Brown and coworker (7) reported values for the volume (or weight) fraction of organs and tissues for mice, rats, dogs, and humans, as well as the standard deviation associated with these

mean values. The ICRP report (8) also provided the human reference values of tissues and organs and their ranges due to differences in age, gender, race or other factors. This report presents detailed information on age- and gender-related differences in the anatomical and physiological characteristics of reference individuals. Tissue composition is used in PBPK modelling to predict tissue-to-plasma partition coefficients (9, 10). However, the available resources in literature are not sufficient to evaluate inter-individual variability associated with those data. Drug properties determining the distribution behavior of a drug include its ionization, permeability, bind to plasma proteins, partition into red blood cells and its affinity to influx or efflux transporter proteins (5).

<u>Metabolism</u>

Although drug metabolism can take place in many organs (e.g. gut, liver, lung, blood), the major site of metabolism for most drugs is the liver. The physiologic variables that can influence drug hepatic clearance include hepatic blood flow, protein binding in plasma and intrinsic hepatocellular activity. For drugs with high extraction ratio, the hepatic clearance is perfusion-rate limited and more sensitive to blood flow than changes in binding or cellular processes. On the other hand, the metabolic clearance of low extraction ratio drugs is affected by variation in blood or plasma binding and/or changes in cellular eliminating processes. The intrinsic clearance of drug, concentration of microsomal proteins, number of hepatocytes and unbound fraction in blood and microsomes are the key parameters causing inter-individual variability in drug metabolism. In addition to hepatic clearance, metabolic enzymes also express in the gut with lower levels than those for the liver, causing the drug first-pass metabolism in the enterocytes (11). Gut intrinsic clearance, drug permeability through the enterocyte membrane, and blood flow are significant parameters associated with elimination variation.

127

<u>Excretion</u>

The major site of drug excretion is the kidney. The net renal drug excretion is the result of three processes – glomerular filtration, tubular secretion and tubular reabsorption. The primary determinants of renal excretion include renal blood flow, plasma protein binding, urine flow, urine pH, and activity of renal transporters (5).

3.2.Methods

3.2.1. Construct PBPK model in rats

PBPK modeling involves in the development of mathematical descriptions of the uptake and disposition of drugs in an integrated and biologically plausible manner. Constructing a PBPK model consists of several steps, including: (1) defining structure of a PBPK model and representing the model in mathematical terms; (2) obtaining model parameter values; (3) solving differential equations and performing simulations; (4) evaluating and refining the model.

<u>Defining model structure</u>

The structure of PBPK model in rats was determined according to the exposure conditions, the pharmacokinetic characteristics and toxicology studies of model compounds. It consists of two major sub-models which describe disposition input.

Disposition model: In the disposition model, the relevant organs or tissues were selected. Since aniline and similarly structural compounds (PCA, 2,6-DMA, o-TOL and PAP) are lipophilic and mainly metabolized in the liver, compartments representing the adipose and liver are included in the model structure. To account for the target organ of toxicity, compartments for the spleen and kidney were also included. Skin, muscle and bone expected to contribute significantly to mass balance of substrate are also incorporated. A disposition model in rats was constructed representing 14 compartments, including those for lungs, adipose, heart, brain, muscle, spleen, pancreas, stomach, gut,

kidney, bone, skin and thymus and 2 blood compartments (arterial and venous blood). The anatomical arrangement and interconnection of tissues was based on circulatory blood flow as illustrated in Figure 3.1. Model compounds were reported to be rapidly absorbed and passively permeate tissue and cellular membranes with no known transporter. Therefore, each tissue was assumed to be perfusion-rate limited.
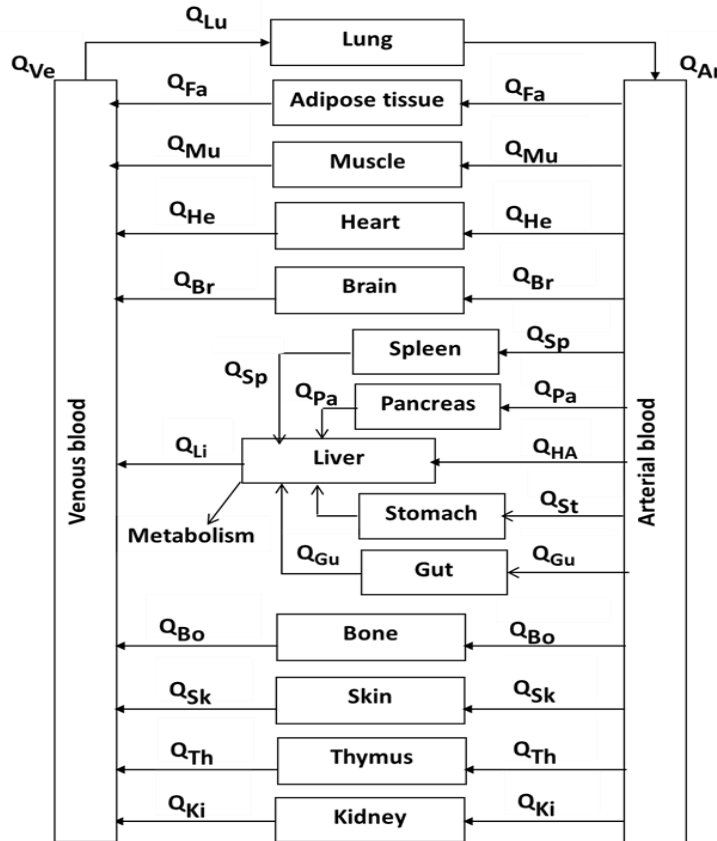

Figure 3.1- Conceptual representation of a Whole Body PBPK Model. Blood flow rates associated with the 14 compartments are represented by Q. Elimination is depicted as occurring only from liver.

Input model: The input unit of the rat PBPK model was based on the advance compartmental absorption and transit model (ACAT) that originally developed by Yu et al. (1, 12). It consisted of 9 compartments, including stomach, large intestine, 7 segments of small intestine and corresponding enterocyte or GI wall compartments. The input

129

model assumed that absorption from the stomach is insignificant compared with that from the small intestine; transport across the small intestinal membrane is passive, and the absorption rate is proportional to effective permeability. Although pH-dependent solubility is included in the ACAT, it played no role in the absorption of the model weakly base compounds with pKa $\geq$ 4.0. The model is based on fasted state physiological parameters. The diagram of ACAT model can be described in Figure 3.2.
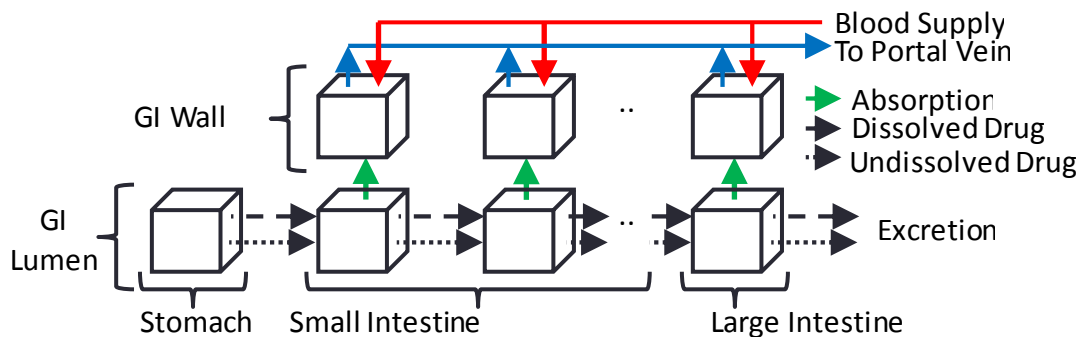

Figure 3.2- The schematic diagram of the gastrointestinal input model

Mathematical representation: The PBPK model is a system of ordinary differential equations (ODEs) that are integrated for a specified amount of time according to study of Harrison et al. The system of ordinary differential equations derived from a perfusion-limited assumption for tissue uptake is given in Appendix A and B.

Model parameters

The estimation of model parameters is described in Chapter 2. These include physiological parameters AND compound physicochemical and biochemical parameters, which obtained from literature, *in silico* calculation or by *in vitro* experimentation.

In vitro to in vivo extrapolation of metabolic parameters: The enzyme metabolic parameters determined from *in vitro* experiments were scaled to *in vivo* using the equations 3.4 and 3.5 as below:

$$V_{max, in\ vivo}(mmol/hr) = V_{max, in\ vitro} \times MPPGL \times W_{Liver} \qquad (Eq.\ 3.4)$$

$$K_{m, \text{in vivo}}(\text{mM}) = K_{m,\text{in vitro}} \times fu_{\text{mic}} \qquad \text{(Eq. 3.5)}$$

For PAP, the maximal velocity in vivo was determined by using Equation 3.6
$$V_{\text{max, in vivo}}(\text{mmol/hr}) = V_{\text{max, in vitro}} \times \text{HPGL} \times W_{\text{Liver}} \qquad \text{(Eq. 3.6)}$$

$V_{\text{max, in vitro}}$ (mmol/hr/mg protein or mmol/hr/# cells) and $K_{m, \text{in vitro}}$ (mM) are metabolic parameters determined from in vitro experiment using rat liver microsomes or hepatocytes. The units for MPPGL and HPGL are mg protein per gram liver and number of hepatocytes per gram liver. Table 3.1 summarizes literature values for microsomal protein recovery, and cell number which were used for *in vitro* to *in vivo* extrapolation of metabolic parameters from microsomal and hepatocytes studies, respectively.

Table 3.1- Physiological parameters for scaling *in vitro* drug metabolism data

Physiological parameters	Parameter value	
	Rat[1,2]	Human[3]
Microsomal protein yield (MPPGL) (mg protein/g liver)	45	32
Hepatocyte number (HPGL) (cells/g liver)	120×10^6	99×10^6

[1] Value of microsomal protein in rats taken from Houston et al (16) as literature average
[2] Value of hepatocyte number taken from Pang et al. (17)
[3] Value from Barter and coworkers (18)

Accounting for acetylation pathway of metabolism: Aniline was reported to be metabolized in liver by acetylation and hydroxylation pathways (13). The microsomal metabolic system does not include Phase 2 enzymes, such as N-acetyltransferase (NAT) to metabolize aniline. Therefore, the overall clearance of aniline and other model compounds were adjusted to account for acetylation pathway using literature data. Grossman et al. (14) studied the relative contribution of the two pathways of aniline metabolism by measuring the overall formation of hydroxyacetanilide. Acetylation was found to contribute route contributes to 60%, and para-hydroxylation with subsequent acetylation of the p-aminophenol contributed 40% to the clearance of a hemotoxic dose of aniline. Using this information, the measured metabolic rate from liver microsomes

(which only account for hydroxylation pathway) was multiplied by a factor of 2.5 to estimate the overall aniline clearance.

<u>Solving differential equations and performing simulations</u>

The model implementation was written in R and the deSolve and FME packages were used to solve the ODEs.

<u>Evaluating the model</u>

The PBPK model in rats was evaluated for its usefulness by comparing the predicted concentration time profile of aniline after oral dose simulation with the experimental data from Harrison et al.(15). Because only aniline animal PK data available, exposure profile of aniline at different doses were simulated to evaluate the model.

3.2.2. Extrapolation from rat to human PBPK model

The scale up to human model was accomplished by adjusting the physiological parameters to human levels for healthy adult population. In particular, body weight (BW) was set at 70 kg for male individuals and 60 kg for females. Other physiological parameters, such as tissue volumes and blood flows were adjusted for males and females using corresponding reference values represented in Chapter 2. Tissue to plasma partition coefficients, protein fraction unbound, blood to plasma ratio and effective permeability were assumed to be identical to those parameters in rat model, regardless of gender. Metabolic parameters were scaled from *in vitro* measurements using scaling factors for human population.

3.2.3. Characterization of model parameter uncertainty and variability

The uncertainty and variability of rat and human PBPK model parameters were characterized using the sensitivity analysis. The physiological parameters chosen to investigate their variability included tissue/organ volumes, blood flows, hematocrit, amount of microsomal protein per gram liver (MPPGL) and hepatocyte number (HPGL).

The compound – specific parameters investigated were tissue (adipose, liver and muscle) to plasma partition coefficients, metabolic parameters, unbound fraction, logP, pKa, and effective permeability. The coefficients of variation (CV) were determined from experimental data or estimated from data in literature.

3.2.4. Prediction of population pharmacokinetic variability and global sensitivity analysis

The impact of the uncertainties and variability in parameter values on model predictions were analysis by using the Monte Carlo method. Primary parameter values were randomly drawn from their normal distributions by 10,000 sampling points for each parameter. Parameter distributions were defined as normal distributions with the means, variances calculated from the CV values. Parameter values were bounded below and above 2 to 3 standard deviations. The correlation between V_{max} and K_m was incorporated in Monte Carlo sampling for model prediction. The model was simulated at each of parameter combination. This process is repeated many times until the probability distribution for the desired model output (e.g. concentration profiles and AUC at target tissue) was generated. Global sensitivity analysis was also conducted to identify which model parameters most strongly affected model output variability.

3.3. Results

3.3.1. Predicted exposure of model compounds in rats

<u>Simulation of blood concentrations</u>

Blood time-concentration profiles of five model compounds were predicted for an oral solution dose using the rat PBPK model. Different doses of aniline were simulated and compared with data reported by Harrison and Jollow (15) to evaluate the usefulness of the rat model. The model prediction of aniline after a 0.15 mmol/kg oral dose is presented in Figure 3.3. The mean values of measured blood concentrations of aniline after intraperitoneal (i.p.) administration of 0.15 mmol/kg aniline in saline were

compared to model simulations. Based on reported rapid absorption and high percent absorbed of aniline (19), the exposures after oral and intraperitoneal doses are expected to be comparable. The shape and magnitude of predicted blood concentration-time course are in agreement with observed data. Due to its rapid absorption, peak concentration of aniline after i.p. administration to the rat was not measured. However, according to Harrison et al., peak levels of aniline metabolites, such as phenylhydroxylamine and nitrozobenzene, were achieved within 10 minutes after aniline administration. These observations suggest that the t_{max} of aniline is less than 10 minutes. Similarly, the model-estimated t_{max} was 4 minutes. The model accurately simulated the rapid elimination of aniline from the blood at this dose. Aniline elimination after low doses was reported to approximate first order kinetics with a half-life of approximately 16 minutes at the 0.15 mmol/kg dose level (15). The model predicted the half-life of aniline after 0.15 mmol/kg p.o. dose is 13.4 minutes, which is consistent with the observed data. The area under the curve and volume of distribution at steady state were predicted to be 8.01 (mg*hr/L) and 0.14 L, respectively.
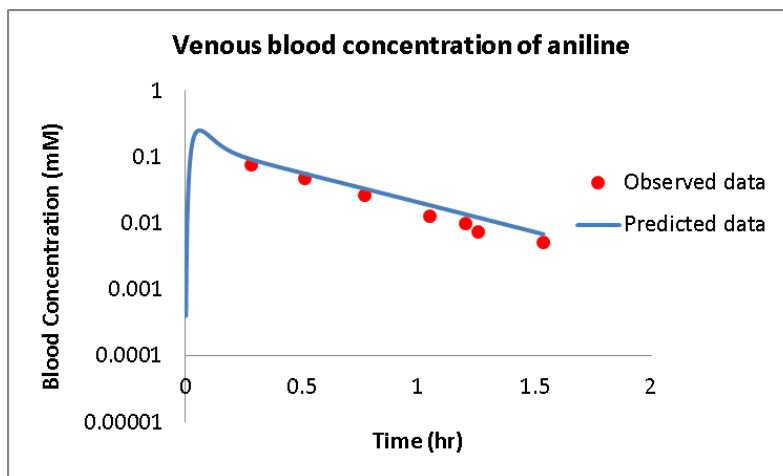

Figure 3.3- Model predictions and time course data of blood concentration of aniline after an oral dose of 0.15 mmol/kg. Continuous line represents the predictions of the rat PBPK model. Points represent the mean values after an i.p. dose (0.15 mmol/kg) of aniline in rats (n = 4).

Similarly, blood concentration-time profiles of aniline after a 0.375 mmol/kg i.p. dose were predicted. Figure 3.4 depicts model simulations compared to the average blood concentration of aniline after a dose of 0.375 mmol/kg i.p. Simulation of blood concentrations following p.o. exposures by the present model resulted in good agreement with the reported data.
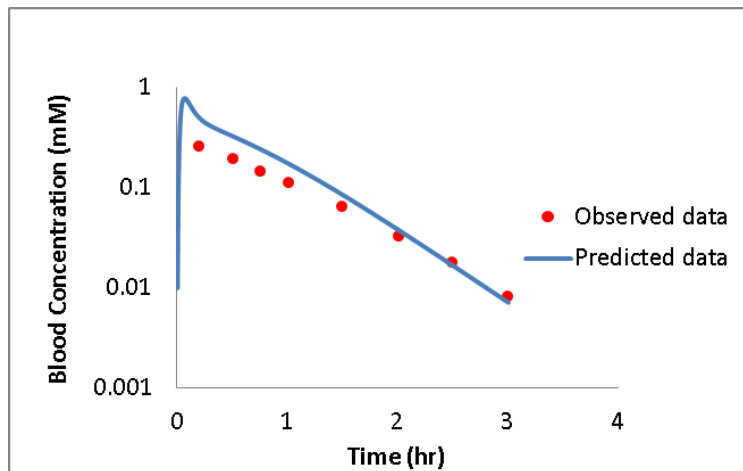

Figure 3.4- Model predictions and time course data of blood concentration of aniline after an oral dose of 0.375 mmol/kg. Continuous line represents the predictions of the rat PBPK model. Points represent the mean values after an i.p. dose (0.375 mmol/kg) of aniline in rats (n = 4).

As the i.p. dose was increased, the observed kinetics of aniline elimination appear to be more complicated than at lower doses. The plasma time courses of aniline at the higher doses (0.75 – 2.25 mmol/kg) were predicted by the model with apparent capacity-limited phase of clearance occurring between 1 and 6 hours after aniline administration (Figure 3.5).

Simulation of target tissue exposure in rats:

In contrast to traditional PK, PBPK modeling allows the prediction of the disposition profiles at individual tissue or organs of interest. For the group of model drug degradation products, target organ was selected as spleen, for aniline, PCA, DMA and o-TOL. The target organ was the kidney for PAP. The concentration time courses in target

135

tissues were simulated for these compounds after oral administration of 0.15 mmol/kg doses (Figure 3.6).
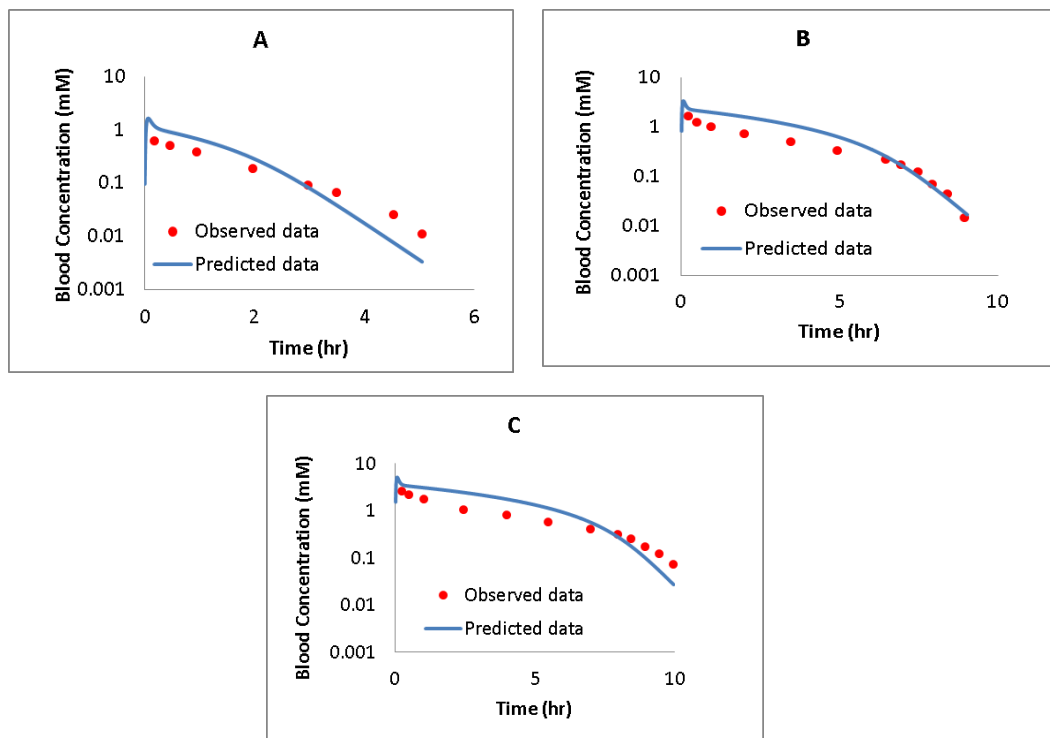

Figure 3.5- Model predictions and time course data of blood concentration of aniline after an oral dose of 0.75 mmol/kg (A), 1.5 mmol/kg (B) and 2.25 mmol/kg (C), respectively. Continuous line represents the predictions of the rat PBPK model. Points represent the mean values after i.p. doses of aniline in rats (n = 4).
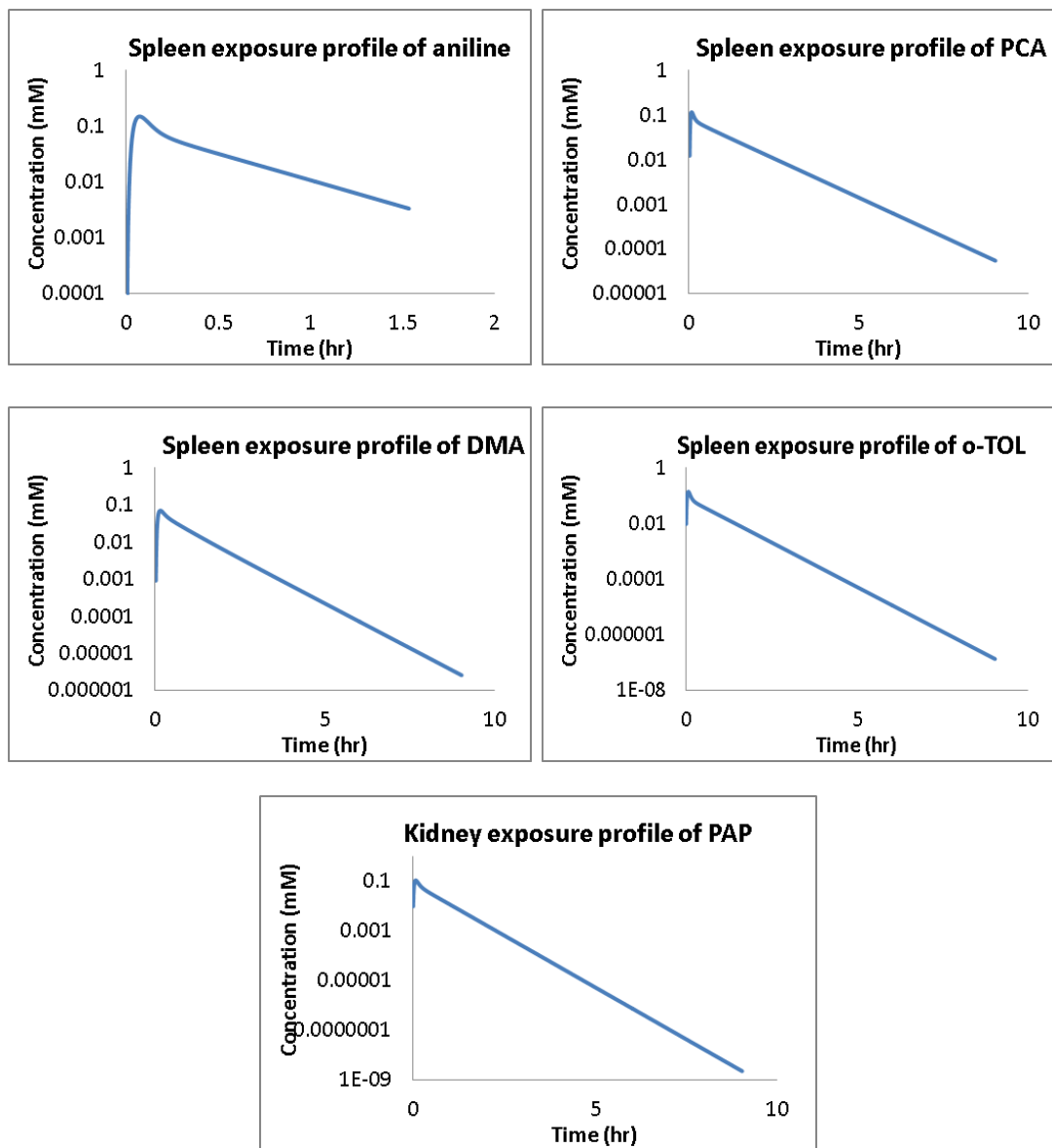
Figure 3.6- The rat PBPK simulations of spleen tissue exposure profiles for aniline, PCA, DMA, o-TOL and kidney exposure profile for PAP after oral dose of 0.15 mmol/kg

3.3.2. Predicted target tissue dispositions of model compounds in humans

After adjusting the parameters from rats to humans, the PBPK model was used to simulate the target tissue exposure for model compounds in males (Figure 3.7) and females (Figure 3.8).
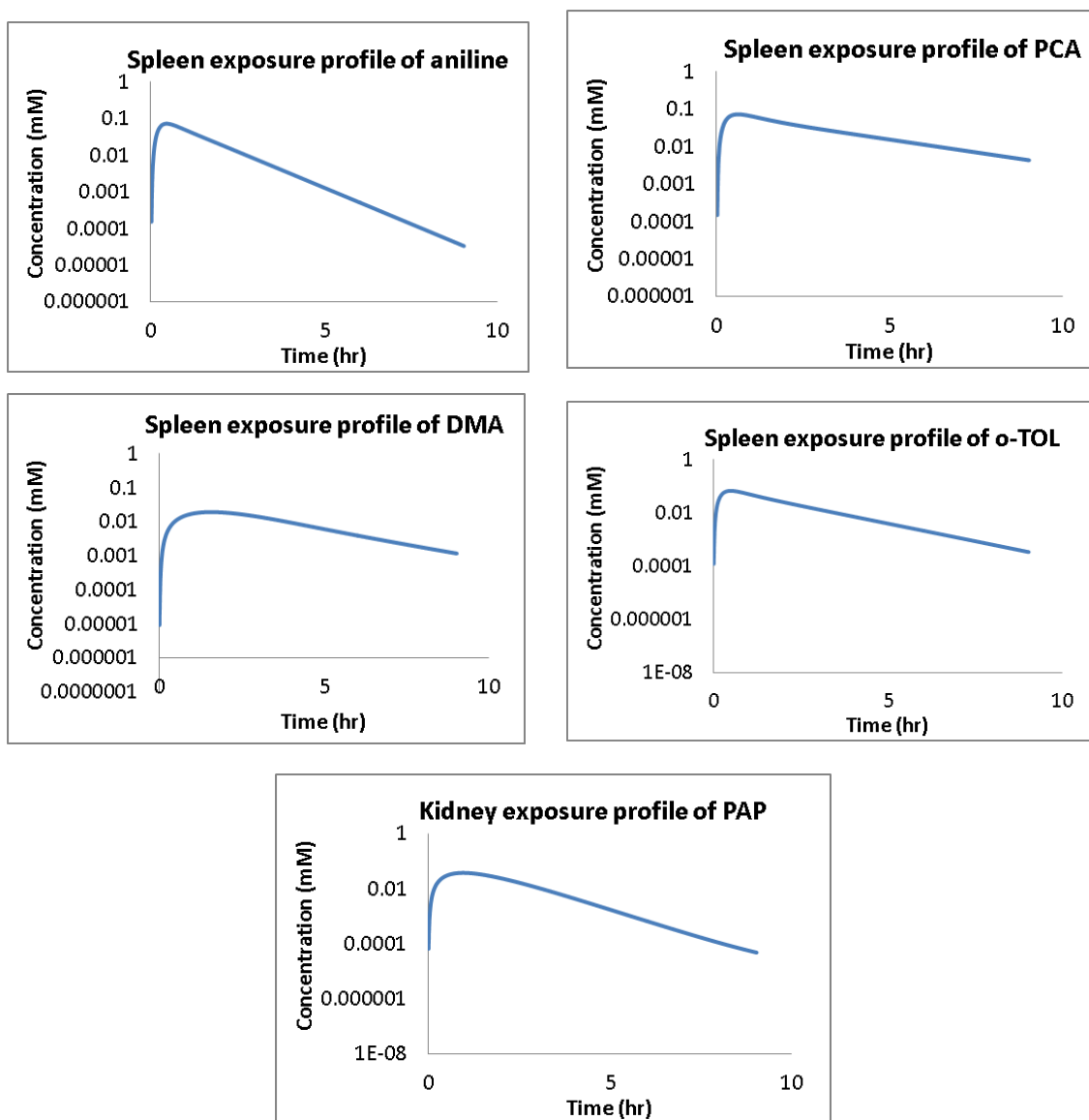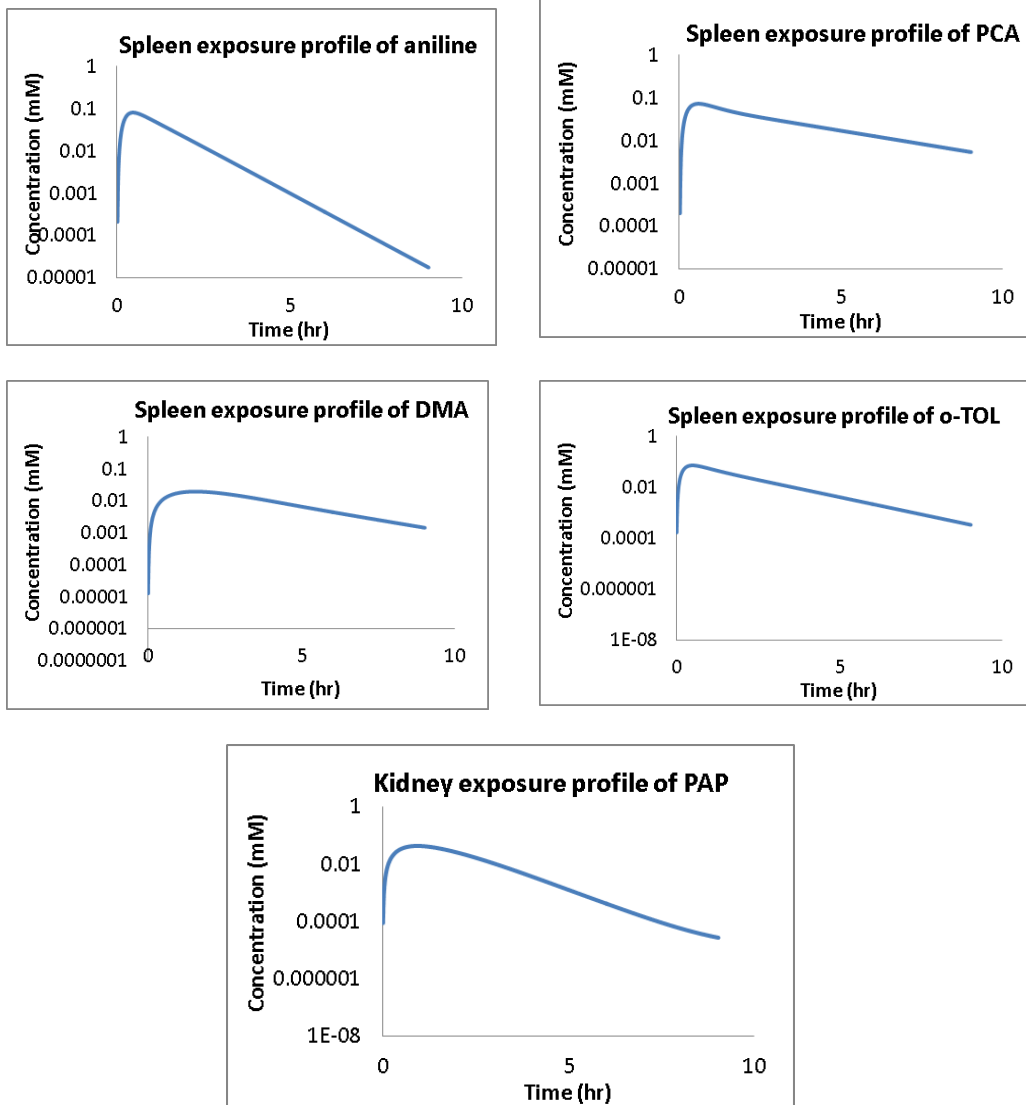

Figure 3.7- The human PBPK simulations of spleen tissue exposure profiles for aniline, PCA, DMA, o-TOL and kidney exposure profile for PAP after oral dose of 0.15 mmol/kg in males

Figure 3.8- The human PBPK simulations of spleen tissue exposure profiles for aniline, PCA, DMA, o-TOL and kidney exposure profile for PAP after oral dose of 0.15 mmol/kg in females

3.3.3. Characterization of primary parameter variation

In order to investigate the effect of parameter variation on model output and to simulate inter-individual variability, coefficients of variation (CV) of primary parameter values were estimated from experimental data or from literature resources or when no information was available, a large CV value was used as described below.

Coefficients of variation determined from experimental data

The uncertainty of measured parameters (e.g. metabolic constants, unbound fraction in plasma and microsomes) was obtained from the standard deviation of the reported mean values (Table 3.2).

Table 3.2- Coefficients of variation of measured parameters

Parameter	% CV				
	Aniline	PCA	2,6-DMA	o-TOL	PAP
V_{max}	9.2	8.1	8.3	12.1	26.6
K_m	13.6	13.8	12.2	36.8	34.7
fu_p	3.3	4.8	5.6	8.2	15.1
fu_{mic}	7.1	9.1	4.5	7.2	5.9

Coefficients of variation estimated from published data

The CV values of organ weights and blood flows in rats and humans were calculated from standard deviations and mean values reported in Table 2.1 of Chapter 2 (Table 3.3). The CV of the physicochemical parameters such as pKa, $logP_{o/w}$; human effective permeability, hematocrit, amount of microsomal protein per gram liver (MPPGL) and hepatocyte number (HPGL) were estimated from available literature (Table 3.4).

Table 3.3- Coefficients of variation of physiological parameters
in rats and humans

Organ	% CV		
	Rat		Human
	Organ weight	Blood Flow	Organ weight / Blood Flow
Adipose	3	19	30[a]
Bone	4	9	30[a]
Brain	25	15	30[a]
Stomach	13	28	29
Gut	17	15	20
Heart	12	2	19
Kidneys	15	13	25
Liver	18	30[a]	23
Lungs	18	19	30a
Muscle	18	10	30a
Pancreas	22	63	29
Skin	14	11	30
Spleen	25	60	57
Thyroid	40	30a	50
Artery	30a	30a	30a
Vein	30a	30a	30a

[a] When data was not available, a value of 30 was used to represent moderate level of variation based on reference of Clewell et al. (21). Coefficients of variation for human organ weights and blood flows were assumed to be identical.

Table 3.4- Coefficients of variation of physicochemical and other
selected parameters

Parameter	% CV	Reference
pKa	0.4	Pankratov et al. (22)
logP	0.6	De Bruijn et al. (23)
Human effective permeability	80	Winiwarter et al. (24)
Hematocrit	3	Thirup et al. (25)
MPPGL	34	Barter et al.(18)
HPGL	58	Barter et al. (18)

<u>Coefficients of variation assumed as reasonable estimates</u>

The tissue-to-plasma partition coefficient (Kpu) is a key parameter which determines the extent of that compound distribution. The Kpu values were predicted using the Rodger and Rowland mechanistic equation and assumed to be the same across species. In this model, tissue composition (lipid, water and protein content) and compound physicochemical properties were used as inputs for these Kpu predictions. Due to the lack of available information for human tissue composition and the reliability of the mechanistic equation (20), the CV for Kpu of primary organs (e.g. adipose tissue, muscle and liver) was assumed to be 30%.

3.3.4. Model predictions accounting for parameter uncertainty and population variability

By using the Monte Carlo method, the model predictions for blood concentration-time profiles of aniline in rats after oral doses of 0.15 mmol/kg (Figure 3.9, A), 0.375 (Figure 3.9, B), 0.75 (Figure 3.9, C), 1.5 (Figure 3.9,D), and 2.25 mmol/kg (Figure 3.9, E) were obtained. The continuous curve represents the mean concentration time values. The dashed lines are the 95% confidence interval of the concentration time after 10,000 iterations. The model predictions were compared with observed data which are displayed as the points on Figure 3.9.

In addition to the prediction of disposition profile accounting for uncertainty and variability, the model output, such as AUC of target organ was predicted as a statistical distribution rather than point estimates. Probability distribution for each of the model parameters was randomly sampled, and the model was run using the chosen set of parameter values. This process was repeated many times until the probability distribution for the desired model output was generated. Figure 3.10 illustrates the prediction of AUC in kidney rat after oral dose of NOAEL of PAP accounting for model parameter variability via MC sampling.
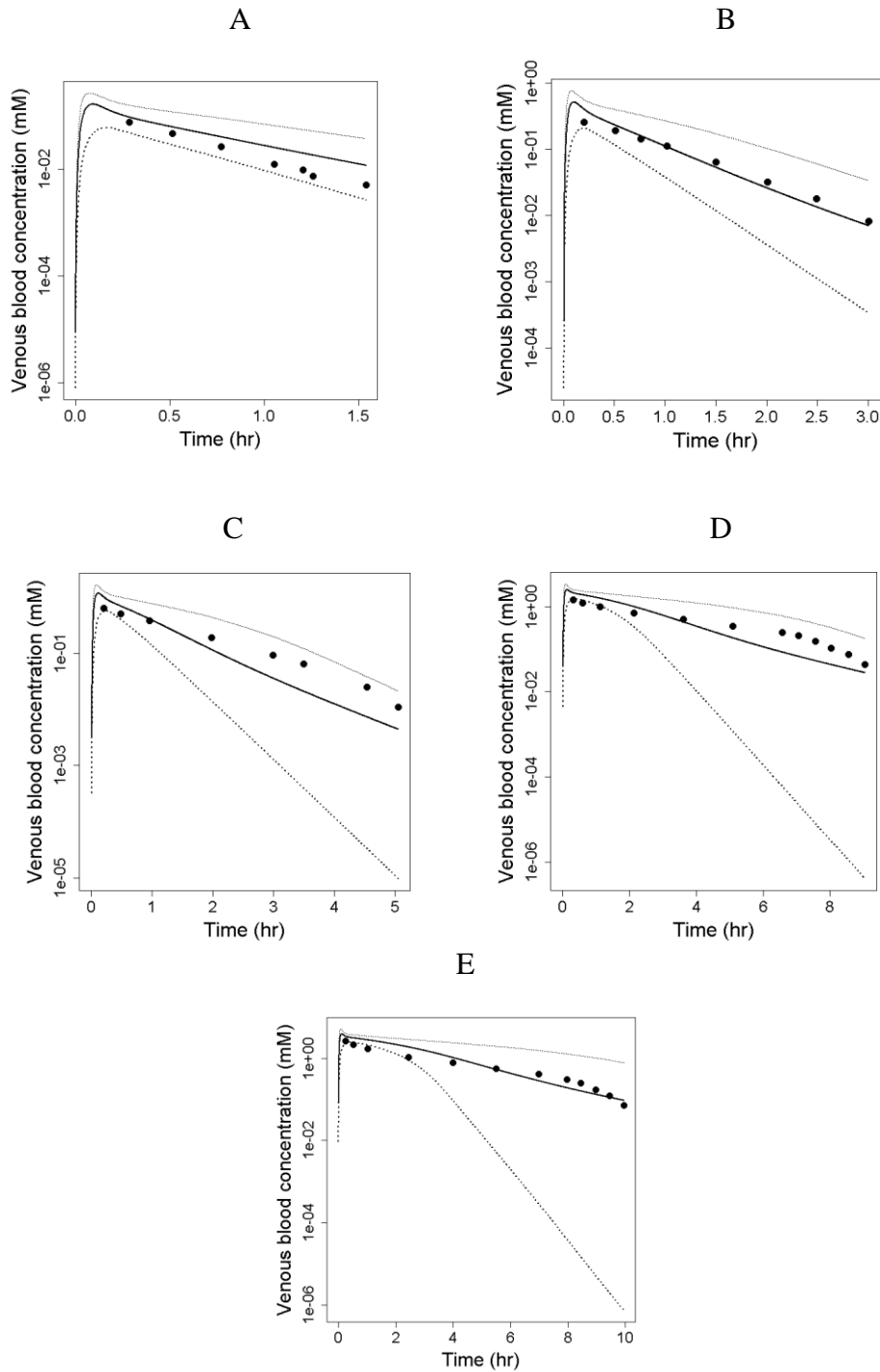
Figure 3.9- Predicted (curves) and experimental (points) blood
concentrations of aniline for oral exposure of rats to 0.15 mmol/kg (A),
0.375 mmol/kg (B), 0.75 mmol/kg (C), 1.5 mmol/kg (D) and 2.25 mmol/kg
(E) doses. The continuous and dash lines are corresponding to the mean and
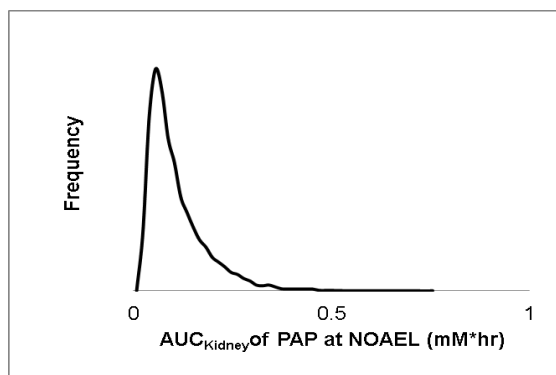95% confidence interval of concentrations predicted via the MC sampling.

143

Figure 3.10- Toxicity target tissue exposure
profile (AUC for kidney concentration time
profiles in rat) after oral dose at the
NOAEL for PAP based on MC sampling of
model parameter variability

3.3.5. Sensitivity analysis of model output to primary parameters

Monte Carlo method was used to determine the effect on model outcome as a function of an appropriate parameter probability density function. Monte Carlo sampling was conducted to identify which model parameters most strongly affected model output accuracy. All selected parameters were varied together in their corresponding distributions. The effect of each parameter variation on model output (AUC of target tissue) was estimated via pair plots between AUC and each parameter. The observation of a trend between output and specific parameter suggests that the output is sensitive to parameter variation. If the pair plot contains randomly scattered points, the weak or no correlation exists between model output and the parameter. In other words, the variation of parameter does not affect the model output value. Pair plots for AUC in spleen rat versus parameter investigated after simulation of 0.375 mmol/kg oral dose are illustrated in Figure 3.11. The apparent relationship between the AUC in spleen and V_{max} indicates that the measured V_{max} is the most sensitive parameter on the model output of aniline. Other parameters, including physiological parameters such as blood flows, organ

volumes, and compound specific parameters, such as $logP_{o/w}$, permeability, tissue to plasma partition coefficients were not as impactful as V_{max} due to the lack of a trend with the AUC in spleen. Similarly, V_{max} is the most important parameter for PCA, DMA, o-TOL and PAP model output (Figure 3.12). The model outputs for PCA, DMA, o-TOL and PAP were not sensitive to other parameters.
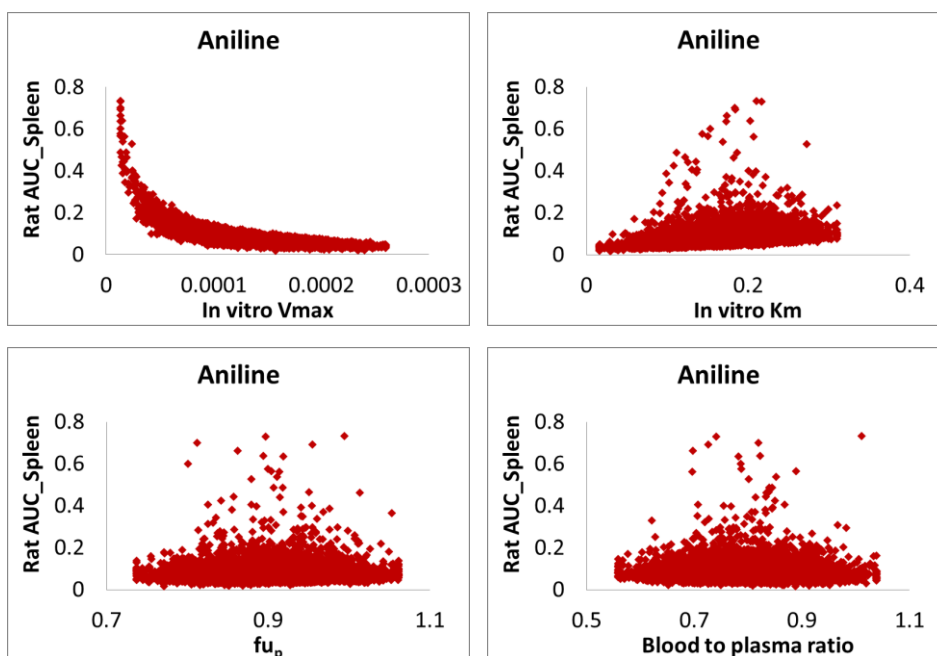

Figure 3.11- Global sensitivity; the model output – AUC in spleen as a function of the parameter values; parameters were generated according to truncated normal distribution.
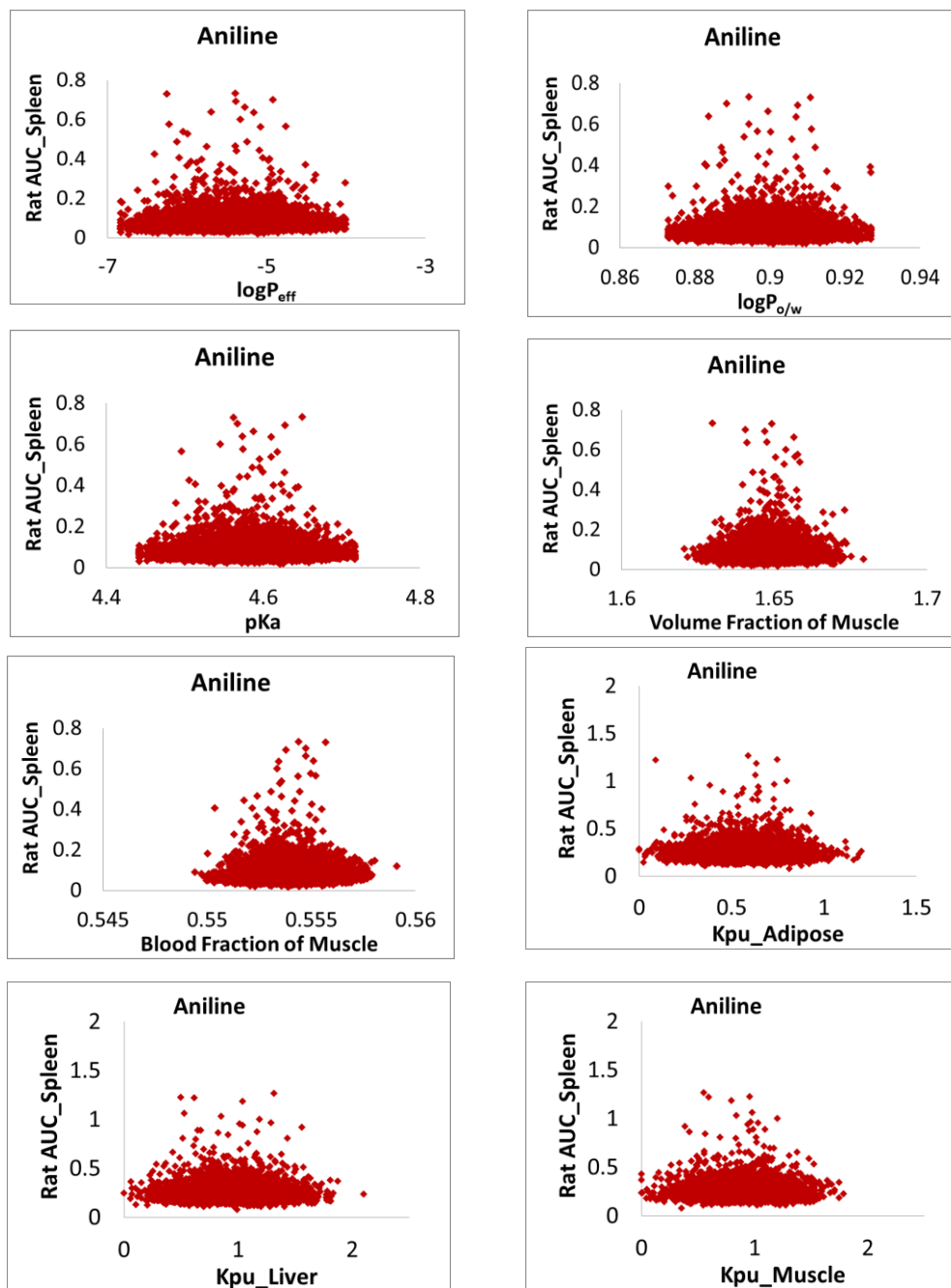
Figure 3.12- Global sensitivity; the model output – AUC in spleen as a function of the parameter values; parameters were generated according to truncated normal distribution - continued
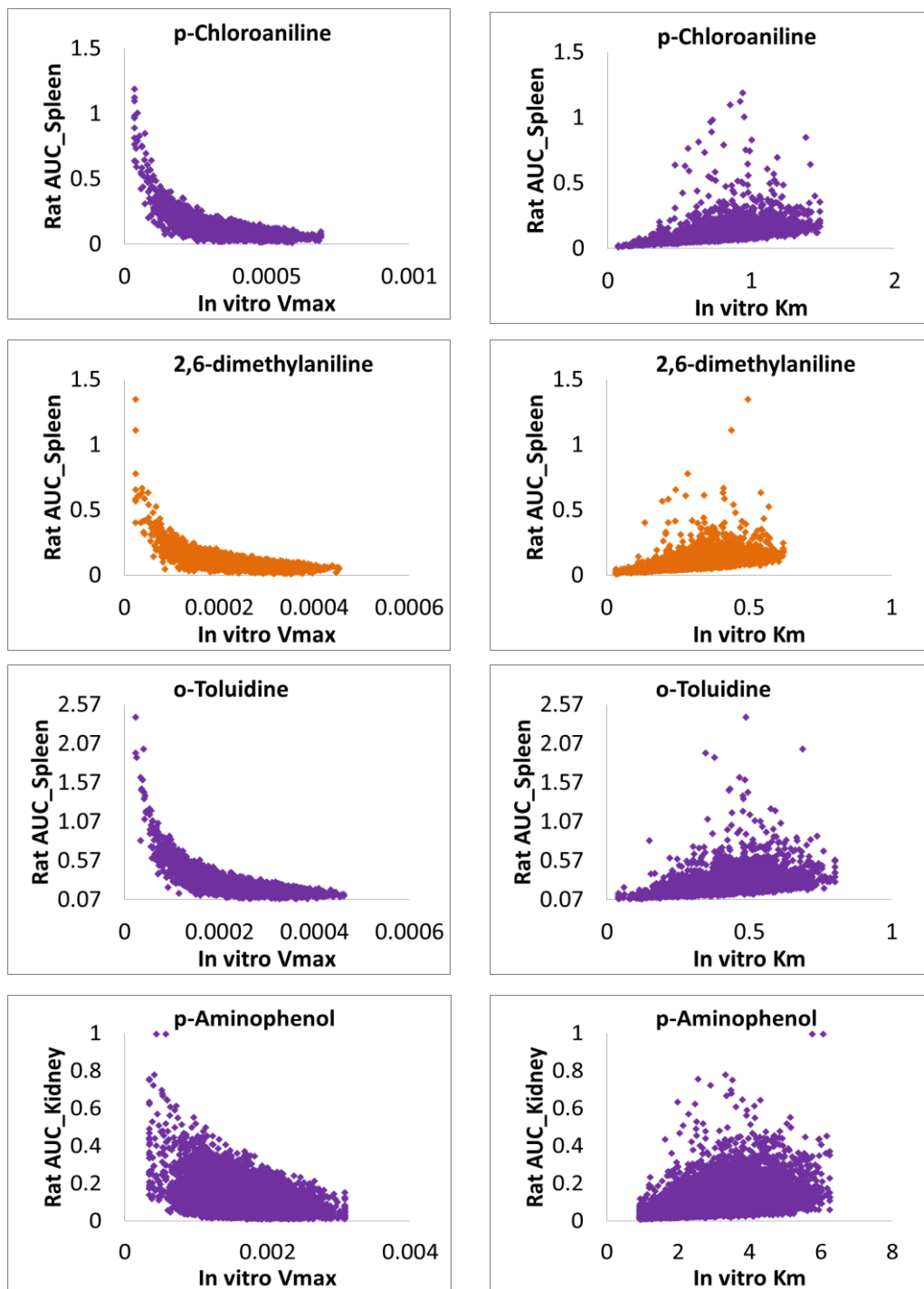
Figure 3.13- Sensitivity analysis of metabolic constants for PCA, DMA, o-TOL and PAP on AUC in spleen and kidney, respectively

3.4. Discussion

3.4.1. Simulation of blood concentration time profile in rats

Internal dose (target tissue exposure) is a relevant indicator of toxicity and risk. The use of PBPK modeling facilitates prediction of prediction of toxicant pharmacokinetics and target tissue exposure when human data cannot be safely obtained.

A PBPK model was developed to characterize the disposition of aniline and 4 other model compounds in rats. *In vitro* metabolic constants and protein binding were measured. Tissue-to-plasma partition coefficients were predicted using the tissue-composition method. Effective permeability was calculated based on the multiple-linear regression between Caco-2 permeability and molecular descriptors. The pharmacokinetic study performed in Sprague Dawley rats of Harrison et al. was used to evaluate the usefulness of the model (15, 26). For model evaluation, a simple comparison of the forward prediction of the model at the initial estimates of the parameters to experimental data was conducted. No parameter optimization (i.e. "fitting") was involved. The model appeared to be in reasonable agreement with literature data. At lower aniline dose (0.15 mmol/kg), the model predictions of blood concentrations closely matched the observed data and displayed a linear disposition. When the doses were increased, non-linear kinetics predictions were consistent with experimental data. The complexity of disposition kinetics in the distribution phase as well as the shape of the blood-level profiles was reasonably predicted.

3.4.2. Global sensitivity analysis

Issues of uncertainty and variability are of significant importance to health risk assessment. The Monte Carlo simulations were conducted to identify the potential impact of model parameters on the variability of model output. When coupled with Monte Carlo simulations, the PBPK model provided quantitative characterization of model compound pharmacokinetics, accounting for the uncertainty and variability in some key parameters.

Metabolic constants were identified as the most important parameters. Other parameters including physiological parameters of species, compound physicochemical and biochemical properties did not strongly impact the model predictions. This finding seems reasonable for this group of small lipophilic compounds.

3.5.Conclusion

It is well known that the same administration dose can lead to very different target tissue exposures and effects depending on the species, timing, or individual. In addition, an internal dose is not necessarily proportional to external dose, which can complicates dose-response relationships. PBPK models are able to predict target tissue exposure and can therefore explain dose-response relationship complication and improve the risk assessment. Overall, after being evaluated, the model developed for group of model drug degradation products was considered to be adequate to predict the target tissue exposure of those compounds in rats and humans. The global sensitivity analysis using the MC method allows for the prediction of population target tissue exposure accounting for the uncertainty and variability, which results in improvements in dose-response characterization for population risk assessment.

CHAPTER 3 LITERATURE CITED

1.   Agoram B, Woltosz WS, Bolger MB. 2001. Predicting the impact of physiological and biochemical processes on oral drug bioavailability. *Advanced Drug Delivery Reviews*. 50 : S41-67

2.   Bois FY, Jamei M, Clewell HJ. 2010. PBPK modelling of inter-individual variability in the pharmacokinetics of environmental chemicals. *Toxicology*. 278 : 256-67

3.   Levine RR. 1970. Factors affecting gastrointestinal absorption of drugs. *The American Journal of Digestive Diseases*. 15 : 171-88

4.   Wilson JP. 1967. Surface area of the small intestine in man. *Gut*. 8 : 618-21

5.   Bois FY, Jamei M, Clewell HJ. 2010. PBPK modelling of inter-individual variability in the pharmacokinetics of environmental chemicals. *Toxicology*. 278 : 256-67

6.   Clewell HJ, Teeguarden J, McDonald T, Sarangapani R, Lawrence G, et al. 2002. Review and evaluation of the potential impact of age- and gender-specific pharmacokinetic differences on tissue dosimetry. *Critical Reviews in Toxicology*. 32 : 329-89

7.   Brown RP, Delp MD, Lindstedt SL, Rhomberg LR, Beliles RP. 1997. Physiological parameter values for physiologically based pharmacokinetic models. *Toxicology and Industrial Health*. 13 : 407-84

8.   Valentin J. 2002. Basic anatomical and physiological data for use in radiological protection: Reference values: ICRP publication 89. *Annals of the ICRP*. 32 : 1-277

9.   Rodgers T, Leahy D, Rowland M. 2005. Physiologically based pharmacokinetic modeling 1: Predicting the tissue distribution of moderate-to-strong bases. *Journal of Pharmaceutical Sciences*. 94 : 1259-76

10.   Rodgers T, Rowland M. 2006. Physiologically based pharmacokinetic modelling 2: Predicting the tissue distribution of acids, very weak bases, neutrals and zwitterions. *Journal of Pharmaceutical Sciences*. 95 : 1238-57

11.   Pang KS. 2003. Modeling of intestinal drug absorption: Roles of transporters and metabolic enzymes (for the gillette review series). *Drug Metabolism and Disposition*. 31 : 1507-19

12.   Yu LX, Amidon GL. 1999. A compartmental absorption and transit model for estimating oral drug absorption. *International Journal of Pharmaceutics.* 186 : 119-25

13.   Kao J, Faulkner J, Bridges JW. 1978. Metabolism of aniline in rats, pigs and sheep. *Drug Metabolism and Disposition.* 6 : 549-55

14.   Grossman SJ, Jollow DJ. 1986. Use of the NIH shift to determine the relative contribution of competing pathways of aniline metabolism in the rat. *Drug Metabolism and Disposition.* 14 : 689-91

15.   Harrison JH,Jr, Jollow DJ. 1987. Contribution of aniline metabolites to aniline-induced methemoglobinemia. *Molecular Pharmacology.* 32 : 423-31

16.   Brian Houston J. 1994. Utility of in vitro drug metabolism data in predicting in vivo metabolic clearance. *Biochemical Pharmacology.* 47 : 1469-79

17.   Pang KS, Kong P, Terrell JA, Billings RE. 1985. Metabolism of acetaminophen and phenacetin by isolated rat hepatocytes. A system in which the spatial organization inherent in the liver is disrupted. *Drug Metabolism and Disposition.* 13 : 42-50

18.   Barter ZE, Bayliss MK. 2007. Scaling factors for the extrapolation of in vivo metabolic drug clearance from in vitro data: Reaching a consensus on values of human microsomal protein and hepatocellularity per gram of liver. *Current Drug Metabolism.* 8 : 33-45

19.   Schanker LS, Tocco DJ, Brodie BB, Hogben CAM. 158. Absorption of drugs from the rat small intestine. *Journal of Pharmacology and Experimental Therapeutics.* 123 : 81-8

20.   Rodgers T, Jones HM, Rowland M. 2012. Tissue lipids and drug distribution: Dog versus rat. *Journal of Pharmaceutical Sciences.* 101 : 4615-26

21.   Clewell RA, Clewell III HJ. 2008. Development and specification of physiologically based pharmacokinetic models for use in risk assessment. *Regulatory Toxicology and Pharmacology.* 50 : 129-43

22.   Pankratov AN, Uchaeva IM, Doronin SY, Chernova RK. 2001. Correlations between the basicity and proton affinity of substituted anilines. *Journal of Structural Chemistry.* 42 : 739-46

23.   De Bruijn J, Busser F, Seinen W, Hermens J. 1989. Determination of octanol/water partition coefficients for hydrophobic organic chemicals with the "slow-stirring" method. *Environmental Toxicology and Chemistry.* 8 : 499-512

24.   Winiwarter S, Bonham NM, Ax F, Hallberg A, Lennernäs H, Karlén A. 1998. Correlation of human jejunal permeability (in vivo) of drugs with experimentally and theoretically derived parameters. A multivariate data analysis approach. *Journal of medicinal chemistry*. 41 : 4939-49

25.   Thirup P. 2003. Haematocrit: Within-subject and seasonal variation. *Sports Medicine*. 33 : 231-43

26.   Harrison JH, Jollow DJ. 1986. Role of aniline metabolites in aniline-induced hemolytic anemia. *Journal of Pharmacology and Experimental Therapeutics*. 238 : 1045-54

CHAPTER 4.   PBPK-BASED METHOD FOR SAFETY ASSESSMENT OF DRUG DEGRADATION PRODUCTS

4.1.Introduction

4.1.1. Use of overlap statistics to assess safety risk

Gender wage-earning equality has been a long-standing social issue that has inspired useful quantitative stochastic metrics. For example, in order to detect the occupational sources of gender wage-earning inequality, Gastwirth (1) proposed a probability measure to compare men and women wages with equal labor market skills. The wages of women and men were assumed to come from two corresponding earnings distributions, $F(x)$ and $G(x)$, respectively. To compare male and female earnings distributions, a measure called PROB was developed which is the probability that a randomly-selected woman from the wage distribution $F(x)$ earns at least as much as a randomly-chosen man from $G(x)$. An example of the visual interpretation of this statistic is illustrated in Figure 4.1-A. In this case, the distribution of female wage-earners does not overlap the male wage-earner distribution, and the former is centered at a lower median wage, therefore the computed PROB value is 0% indicating a 0% probability that a randomly-selected woman earns at least as much as a randomly-chosen man. Wage-earning gender equality is illustrated in Figure 4.1-B wherein the female and male wage-earning distributions are identical and coincident, and the PROB value is 50%.

Thus the PROB statistic provides a meaningful measure of the position of two distributions in stochastic terms. In the context of safety risk assessment, the PROB value provides a quantitative measure of the risk that human exposure to a potential drug degradant toxicant at a specific dose will be greater than the exposure level for a rat at the critical dose (NOAEL) based on the population pharmacokinetic models for a specific degradant. Mathematically, the PROB value can be computed using Equation 4.1 below:

$$\text{PROB} = \int_0^\infty [1 - F(x)] \cdot g(x) dx \quad (\text{Eq. 4.1})$$

Where $F(x)$ is the cumulative probability of human exposure following a specific dose being x, and $g(x)$ is the probability density of the rat exposure following the NOAEL dose being x.

For the current application, the distributions that need to be compared for safety risk assessment are 1) the exposure levels in the target tissues for a specific drug degradation product in rats at the critical dose (NOAEL based on toxicity data) and 2) the exposure levels in target tissue in humans at a specific dose (see Figure 4.2). These distributions are obtained by simulating the rat and human PBPK models at appropriate dose levels and using appropriate levels of critical parameter uncertainty. These two distributions are compared by computing the PROB value (the probability that the human exposure exceeds the rat exposure). Then a new human exposure distribution is generated by PBPK human model simulation at a slightly higher dose, and the PROB value is computed again. This procedure is iterated over a range of human doses resulting in an empirical relationship that describes the increasing PROB value (from 0 to 100% or 0 to 1, fractionally) as a function of increasing human dose. Then the critical human dose is identified by purposefully selecting an appropriate, acceptable level of safety risk expressed in terms of the PROB value (i.e. the probability that the human exposure exceeds the rat exposure). For example, if a 1% probability of drug degradation product toxicity was tolerable for the potential benefit of a specific drug therapy, then the critical human exposure level for that drug degradation product would be the value corresponding to a PROB value of 1% (or 0.01, fractionally expressed). The stability specification for that drug product would be based on this critical human exposure level.

In this final chapter, the use of PBPK modeling and the PROB metric for risk assessment are illustrated for the selected group of model drug degradation products. And the results are compared to the convention methods for estimating critical human exposure level using inter-individual and inter-species uncertainty factors.
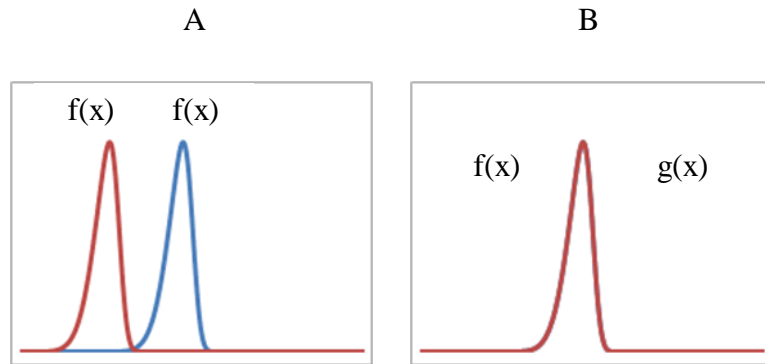
A   B

Figure 4.1- Theoretically female (f(x) - red curve) and male (g(x) - blue curve) earnings distributions. Samples of men and women result in PROB of 0% (A). In ideal situation, samples of men and women result in PROB of 50% (B).
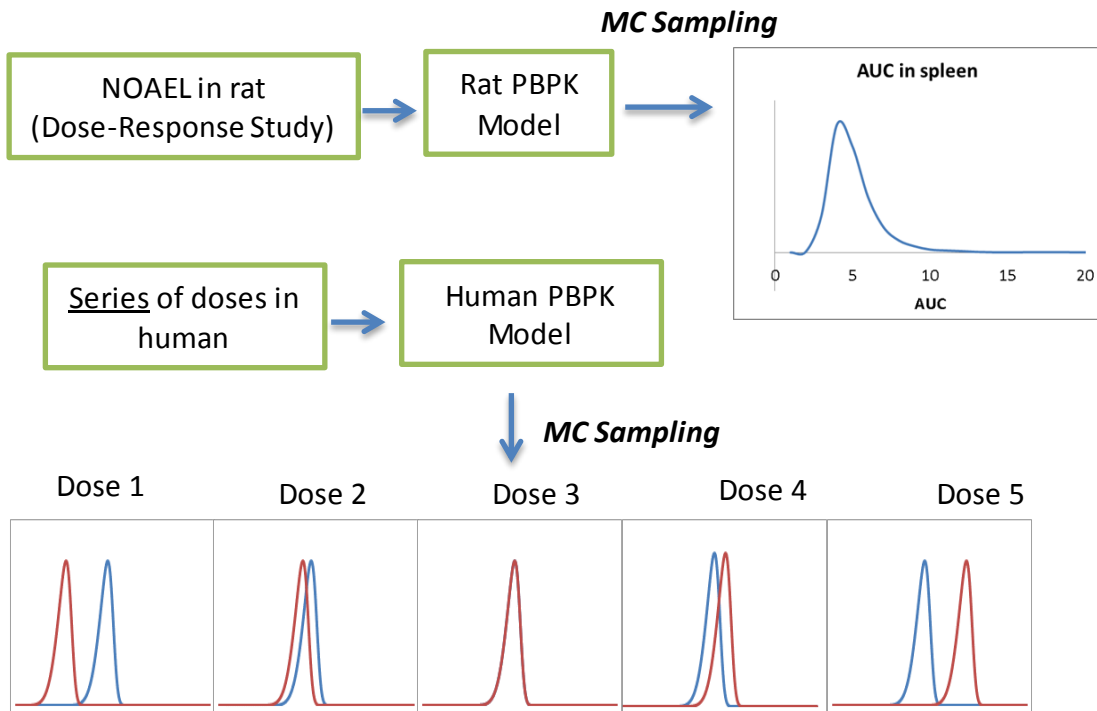
Figure 4.2- Illustration of the use of the overlap statistic, PROB, in drug degradation product safety risk assessment. MC (Monte Carlo) sampling was used to generate rat and human target tissue exposure distributions at each dose.

4.2.Methods

4.2.1. Selection of a measure of target tissue exposure

As suggested by WHO and Clewell et al. (2, 3) for the application of PBPK in risk assessment, an appropriate measure of target tissue exposure metric for model compounds was selected reflecting the active chemical form of substance, its level, duration of exposure, intensity as well as the biological matrix that is consistent with the toxicity mechanism of substance. From Bus et al. (4), aniline and several structurally-related aromatic amines were observed to produce spleen tumors in rats given high doses of compound in 2-year bioassay studies. A critical toxicity mechanism is the specific accumulation of the aromatic amine transported to the spleen via erythrocytes, causing a series of toxic events which contribute to the development of splenic tumors. Based on these findings, the toxicity of aniline and other related compounds (e.g. p-chloroaniline, 2,6-dimethylaniline and o-toluidine) can be estimated by the area under the concentration time curve (AUC) in splenic tissue. Thus, the AUC in spleen of parent compounds (aniline, p-chloroaniline, 2,6-dimethylaniline and o-toluidine) was selected as appropriate measure of target tissue exposure for use in their risk assessment. The AUC in kidney after a single oral dose was chosen as dose metric for p-aminophenol due to its toxic effect on the kidney examined in rats (5).

4.2.2. Prediction of rat exposure distribution at critical dose

The critical dose of model compounds, (NOAEL or LOAEL) was taken from literature and shown in Table 4.1. By varying the key parameters in the rat PBPK model (Chapter 3), selected exposure metric distributions at the critical doses were predicted accounting for model uncertainty and variability via MC sampling. The PBPK model was simulated using 10,000 iterations thereby generating the target tissue AUC probability distributions.

156

Table 4.1- The critical doses for model compounds from literature

Compound	NOAEL (mg/kg)	Reference
Aniline	10	Jenkin et al.(6)
p-Chloroaniline	10	Chhabra et al. (7)
2,6-Dimethylaniline	15[*]	NTP (8)
o-Toluidine	28	Caroline et al. (9)
p-Aminophenol	25	Newton (10)

[*] Lowest observable adverse effect level (LOAEL)

4.2.3. Calculation of PROB values as function of human dose

A series of target tissue exposure distributions for humans were generated as a function of dose by using human PBPK model, critical parameter uncertainty using 10,000 iterations at each dose via MC sampling. The dose range from 0.002 to 0.2 mmol/kg was selected with 0.002 – 0.05 mmol/kg increment from low dose to next higher dose. PROB values were calculated using Eq. 4.2 by comparing the human target tissue exposure distributions at each dose to the rat target tissue exposure distribution at the NOAEL.

Linear spline interpolation at low doses was used to calculate the human safe dose which corresponded to a PROB value of 1%. At this value of PROB, there is a 1% probability that a human exposure level in the target tissue will exceed the critical rat exposure level. The selection of this value is somewhat arbitrary; clearly a lower (or higher) may be arguably more appropriate for a specific drug therapy.

4.2.4. Comparison of human reference dose calculated from PBPK-based and traditional risk assessment approaches

The human reference doses were calculated using the conventional risk assessment approach. Two uncertainty factors with the arbitrary value of 10 were used to account for the animal to human extrapolation and human population variability. Both the

number and value of uncertainty factors were arbitrary but typical. These results were compared to human safe doses obtained from the approach of using PBPK model.

4.3.Results

4.3.1. Distribution of target tissue exposure in rats at critical dose

The probability distribution of AUC in target organ of toxicity at critical dose in rats was predicted for each model compound (Figure 4.3) and described in Table 4.2.
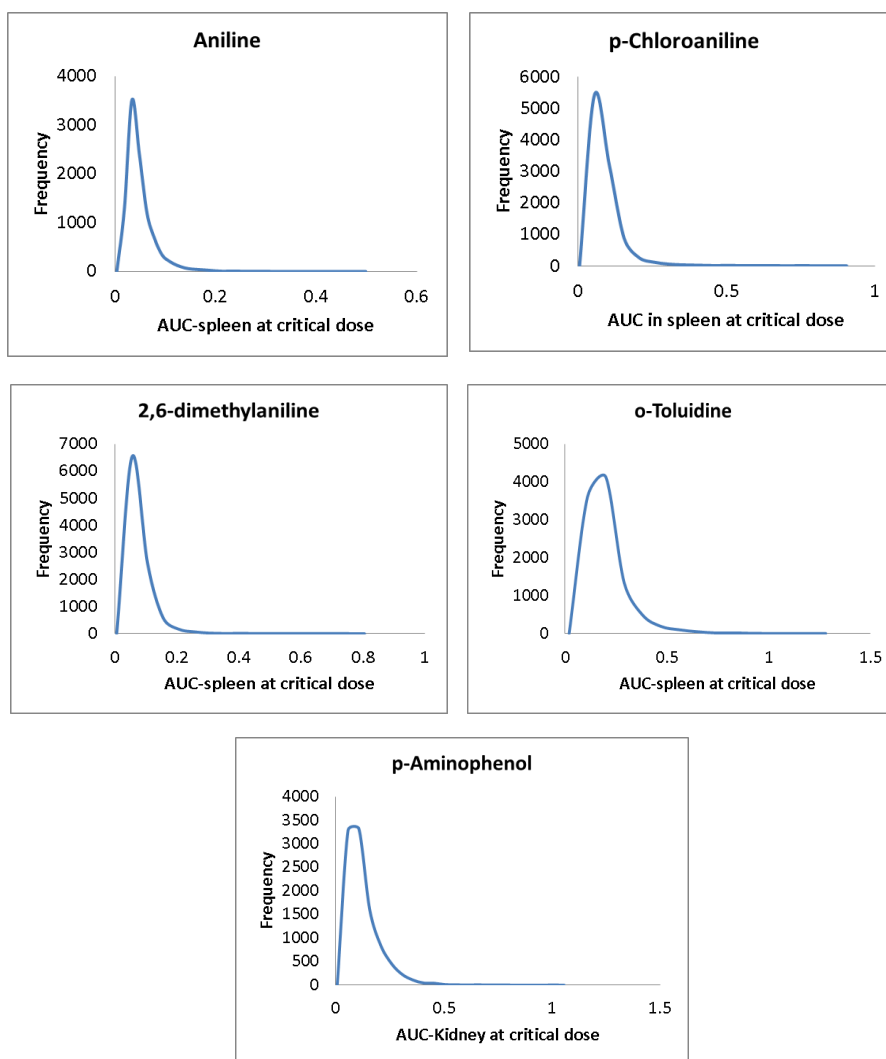

Figure 4.3- Probability distributions of AUC in target organ of toxicity at critical doses

Table 4.2- Probability distribution of AUC
in target organ of toxicity at critical dose

Compound	AUC (mM*hr)	
	Mean	SD
Aniline	0.0427	0.0336
p-Chloroaniline	0.0666	0.0627
2,6-Dimethylaniline	0.0553	0.0506
o-Toluidine	0.1626	0.1200
p-Aminophenol	0.1017	0.0807

4.3.2. Calculation of PROB values based on comparison between human exposure at a specific dose and rat exposure at the critical dose

A series of target tissue exposure distributions were generated by simulating the PBPK human model at dose ranges selected to cover PROB values approximately from 0.1 to 100%. The PROB was calculated by comparing each predicted human exposure with rat exposure at the critical dose. As an example, figure 4.4 was displayed to illustrate the comparison between two exposure distributions between rat at critical dose and human at different selected doses. The estimated PROB values for the five model compounds were shown in Tables 4.3 – 4.7. Calculated PROB values versus males and females population doses are displayed in Figure 4.5 – 4.9.
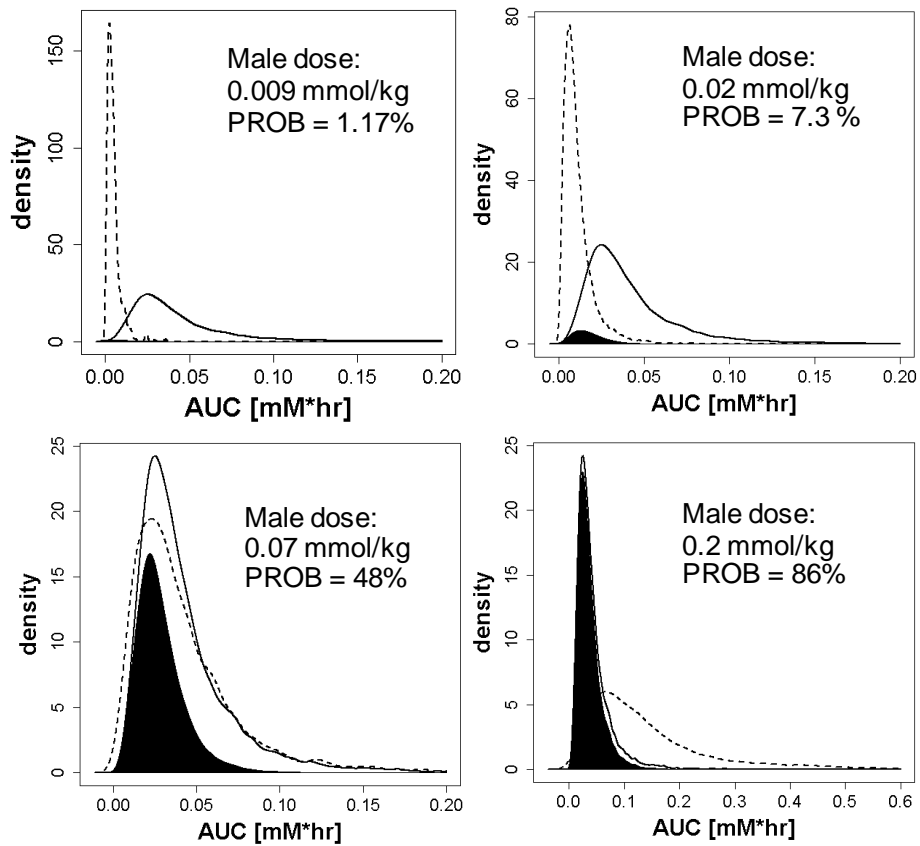
Figure 4.4- Comparison between toxicity target tissue exposure distributions for aniline in the rat model at the NOAEL and predicted toxicity target tissue exposure distributions in human at different doses. The dashed line represents human model simulations and continuous line represents rat simulations. Black areas are the overlap region which pictorially represent the PROB value.

Table 4.3- The values of PROB for male and
female populations after single oral dose of
aniline

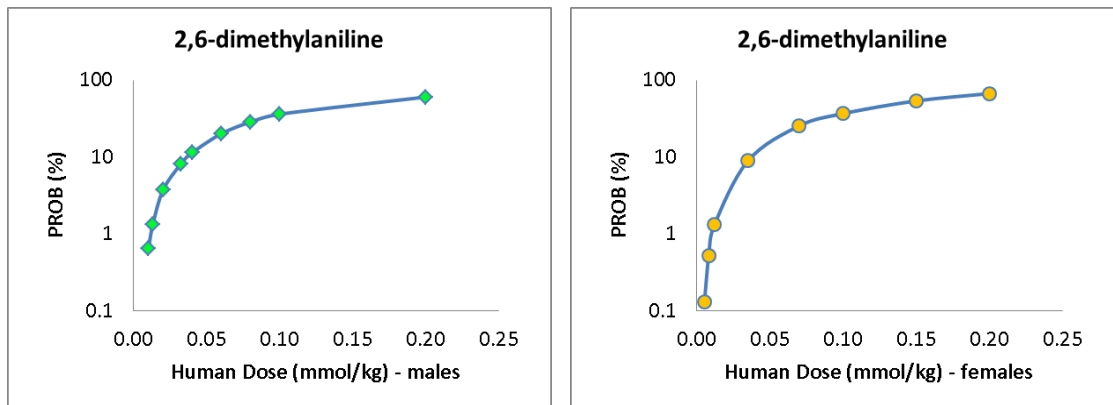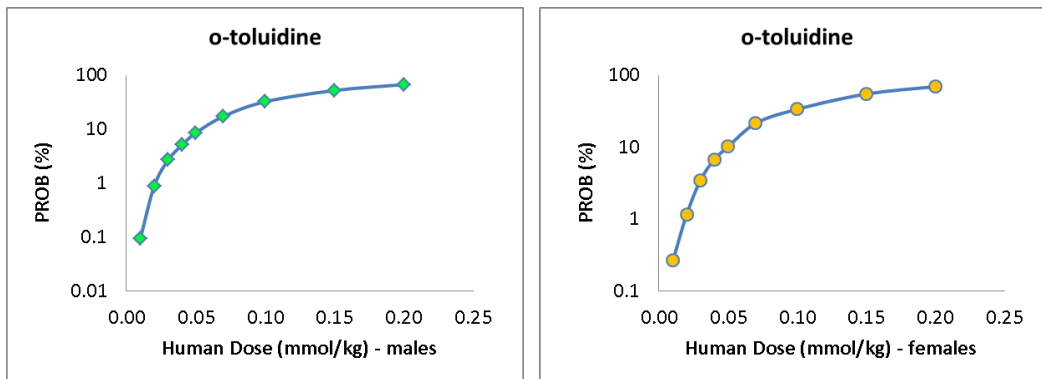| Males		Females	
Dose (mmol/kg)	PROB (%)	Dose (mmol/kg)	PROB (%)
0.002	0.08	0.002	0.054
0.007	0.64	0.005	0.42
0.009	1.17	0.008	1.30
0.016	4.62	0.010	1.94
0.020	7.30	0.015	4.53
0.040	24.42	0.017	6.09
0.070	48.38	0.040	25.6
0.100	62.99	0.070	49.9
0.150	78.14	0.100	64.8
0.200	85.91	0.200	86.9
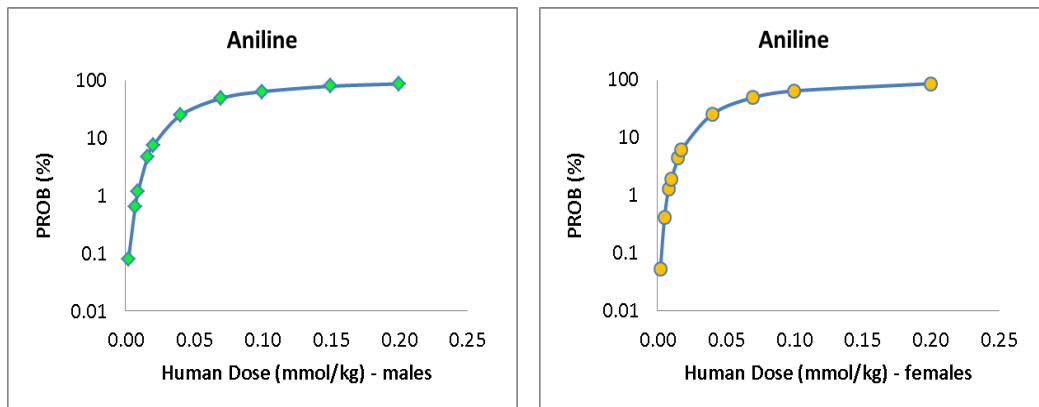
Figure 4.5- Plot of PROBs versus human doses of aniline for male (left) and
female (right) populations.

Table 4.4- The values of PROB for male and female populations after single oral dose of p-chloroaniline

Males		Females	
Dose (mmol/kg)	PROB (%)	Dose (mmol/kg)	PROB (%)
0.002	0.17	0.002	0.21
0.005	0.85	0.004	1.28
0.01	4.42	0.008	4.58
0.012	6.24	0.009	5.71
0.015	9.54	0.01	6.96
0.02	16.2	0.02	20.9
0.04	42.0	0.04	45.0
0.07	64.8	0.06	61.2
0.1	77.9	0.08	71.7
0.2	91.3	0.15	87.1
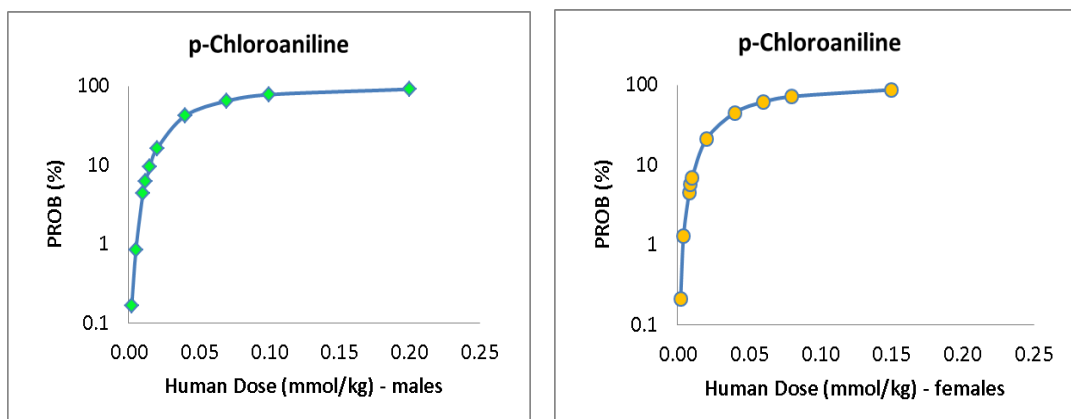
Figure 4.6- Plot of PROBs versus human doses of PCA for male (left) and female (right) populations.

Table 4.5- The values of PROB for male and female populations after single oral dose of 2,6-dimethylaniline

Males		Females	
Dose (mmol/kg)	PROB (%)	Dose (mmol/kg)	PROB (%)
0.002	0.001	0.002	0.00001
0.010	0.65	0.005	0.13
0.013	1.33	0.008	0.53
0.02	3.74	0.012	1.33
0.032	8.04	0.035	9.05
0.04	11.4	0.07	25.5
0.06	20.1	0.1	36.7
0.08	28.5	0.15	53.6
0.1	36.1	0.2	66.8
0.2	60.3		

Figure 4.7- Plot of PROBs versus human doses of 2,6-DMA for male (left) and female (right) populations.

Table 4.6- The values of PROB for male and female populations after single oral dose of o-toluidine

Males		Females	
Dose (mmol/kg)	PROB (%)	Dose (mmol/kg)	PROB (%)
0.005	0.0001	0.005	0.0001
0.01	0.10	0.01	0.27
0.02	0.90	0.02	1.17
0.03	2.71	0.03	3.49
0.04	5.12	0.04	6.79
0.05	8.60	0.05	10.2
0.07	17.4	0.07	21.6
0.10	32.5	0.1	33.8
0.15	52.3	0.15	55.0
0.20	67.4	0.2	69.8

Figure 4.8- Plot of PROBs versus human doses of o-TOL for male (left) and female (right) populations.

Table 4.7- The values of PROB for male and female populations after single oral dose of p-aminophenol

Males		Females	
Dose (mmol/kg)	PROB (%)	Dose (mmol/kg)	PROB (%)
0.002	0.59	0.002	0.61
0.005	0.86	0.005	0.89
0.007	1.09	0.007	1.12
0.02	4.37	0.02	4.52
0.04	11.9	0.04	13.5
0.05	16.7	0.05	19.0
0.07	24.5	0.07	27.8
0.1	37.3	0.1	38.8
0.15	51.2	0.15	50.4
0.2	61.9	0.2	64.7
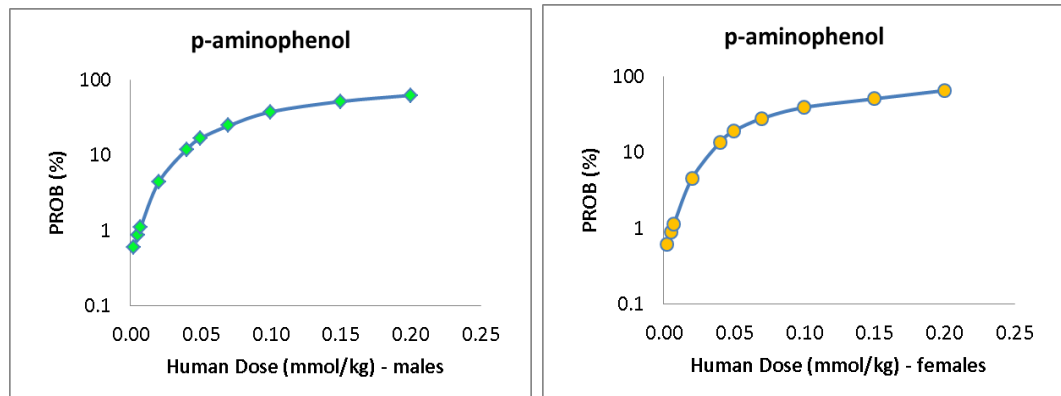
Figure 4.9- Plot of PROBs versus human doses of PAP for male (left) and female (right) populations.

4.3.3. Comparison of human reference dose calculated from PBPK-based and traditional risk assessment approaches

The linear interpolation was used to calculate the human safe doses corresponding to the dose at a PROB value of 1%. As previously noted this "safe" dose corresponds to the human dose at which there is a 1% of probability that a randomly chosen person would have greater target tissue exposure than rat exposed to the critical dose. The results were shown in Table 4.8. The selection of 1% as the critical PROB value is somewhat arbitrary. The selection could be made based on a deliberate consideration of the therapeutic benefit and risk for specific drug therapies.

The conventional risk assessment approach was used for the model compounds to compare with the use of PBPK risk assessment method. Arbitrary (default) uncertainty factor with a value of 10 were used to account for interspecies difference between rats and humans and inter-individual differences in human population. Due to the absence of NOAEL values for 2,6-dimethylaniline, the reported LOAEL was used. The human reference doses were calculated as in Table 4.9. The application of PBPK method resulted in estimated human safe doses that were larger than those obtained by the exemplary application of the conventional method.

Table 4.8- The human safe doses obtained by
the application of PBPK in risk assessment
accounting for uncertainty and variability

Compound	Human RfD by PBPK-based approach (mg/kg)	
	Male	Female
Aniline	0.78	0.65
p-Chloroaniline	0.66	0.44
2,6-Dimethylaniline	1.39	1.25
o-Toluidine	2.20	2.06
p-Aminophenol	0.68	0.65

Table 4.9- Human reference doses of model
compounds calculated by tradition risk
assessment approach

Compound	NOAEL (mg/kg)	Human RfD
Aniline	10	0.10
p-Chloroaniline	10	0.10
2,6-Dimethylaniline	15	0.15
o-Toluidine	28	0.28
p-Aminophenol	25	0.25

4.4.Discussion

Quantitative risk assessment requires the evaluation of two risk components: the severity of potential failure and the probability that failure will occur. For toxicity risk related for drug products, the nature of the toxic response will define its severity, but typically any contribution of degradation product to the safety risk of a drug product is deemed unacceptable. Thus the quantitative estimation of the probability of failure (i.e. a toxic response due to drug degradation exposure) is essential for rational risk assessment of the chemical instability of the drug substance (API). The critical quandary is that the pharmacokinetics of drug degradation products (in contrast to the API) are typically unknown in animals and not appropriate objects for study in human clinical trials. Thus the use of physiologically-based pharmacokinetic models which attempt to leverage all of the available knowledge associated with the physiological, anthropomorphic, biochemical, biophysical and physical chemical characteristics of the human or animal populations and the xenobiotic (e.g. drug degradant) constitutes a rational approach to address this critical issue in drug product risk assessment.

Estimating the failure probability requires identifying sources of uncertainty and assigning those sources a meaningful value to describe their degree of uncertainty. In the

conventional approach, the sources of uncertainty are described in broad categories which are assigned arbitrary values. The estimation of a critical human exposure value is not associated with any risk quantitation; it is simply a point value based on animal toxicity data and a consideration of the possible sources of uncertainty in applying those data to the likely conditions of human exposure. In the proposed PBPK modeling and simulation approach, some of the potential uncertainty sources are evaluated by estimating individual PK parameter uncertainty and using MC methods to generate target tissue exposure distributions for animal and human populations as a function of xenobiotic dose. The approach provides a rational way to account to inter-individual species-specific and inter-species sources of uncertainty.

Moreover, the use of the PROB metric which quantifies the probability that a randomly-chosen human exposure at specific dose is greater than rat exposure at the critical dose provides a way to identify a critical human dose by considering what probability of failure (degradant toxicity) is tolerable for a given drug product. In other word, the benefit-risk decision can be rationally made.

Our PBPK modelling approach accounted for model uncertainty and population variability, the interspecies differences in pharmacokinetics, and inter-individual differences. This approach could obviously be expanded to rationally capture other potentially important sources of uncertainty. For example the following expansions might be appropriate:

1. coupling the PBPK models with pharmacodynamics models for drug degradation toxic responses,

2. expanding the PBPK models to include potentially toxic drug degradant metabolites,

3. inclusion of pharmacogenomics sources of variation (e.g. metabolism or transport) in human PBPK models,

168

4. coupling of PBPK models with drug product stability and dosage regimen models to evaluate time-dependent and therapy-dependent drug degradation product exposure kinetics, and

5. conducting additional animal pharmacokinetic studies to provide greater confidence in the global and local structures of the PBPK models.

4.5.Conclusions

In our study, the PBPK modeling approach resulted in drug degradation product risk specifications that were less stringent than those estimated by conventional risk assessment approach. However, the significance of these results should be tempered by recognizing that this comparison was only an example. In estimating the critical human values using both approaches, we only considered inter-individual and inter-species uncertainty. And for the PBPK approach, we choose an arbitrary critical risk probability value (1%). Nonetheless the PBPK modeling approach provides a rational basis for drug instability risk assessment by focusing on target tissue exposure (i.e. more closely related to tissue response); leveraging physiological, anthropomorphic, biochemical, biophysical and physical chemical knowledge; and providing a quantitative metric for the probability of failure upon which the risk-benefit judgment can be made.

CHAPTER 4 LITERATURE CITED

1. Gastwirth JL. 1975. Statistical measures of earnings differentials. *The American Statistician.* 29 : 32-5

2. WHO. 2010. *Characterization and application of physiologically based pharmacokinetic models in risk assessment. IPCS harmonization project.* Vol. No.9. Ottawa, Canada: . 97pp

3. Clewell HJ. 2002. A consistent approach for the application of pharmacokinetic modeling in cancer and noncancer risk assessment. *Environmental Health Perspectives.* 110 : 85

4. Bus JS, Popp JA. 1987. Perspectives on the mechanism of action of the splenic toxicity of aniline and structurally-related compounds. *Food and Chemical Toxicology.* 25 : 619-26

5. Fowler LM, Moore RB, Foster JR, Lock EA. 1991. Nephrotoxicity of 4-aminophenol glutathione conjugate. *Human & Experimental Toxicology.* 10 : 451-9

6. Jenkins FP, Robinson JA, Gellatly JBM, Salmond GWA. 1972. The no-effect dose of aniline in human subjects and a comparison of aniline toxicity in man and the rat. *Food and Cosmetics Toxicology.* 10 : 671-9

7. Chhabra RS, Thompson M, Elwell MR, Gerken DK. 1990. Toxicity of p-chloroaniline in rats and mice. *Food and Chemical Toxicology.* 28 : 717-22

8. National Toxicology Program (NTP). 1990. *Toxicology and carcinogenesis studies of 2,6-xylidine (2,6-dimethylaniline) in charles river CD rats (feed studies). NTP Technical Report. Rep. No. 278,* US Department of Health and Human Services, Public Health Service, National Institutes of Health, Bethesda,

9. Caroline English J, Bhat VS, Ball GL, McLellan CJ. 2012. Establishing a total allowable concentration of o-toluidine in drinking water incorporating early lifestage exposure and susceptibility. *Regulatory Toxicology and Pharmacology.* 64 : 269-84

10. Newton JF, Kuo CH, Gemborys MW, Mudge GH, Hook JB. 1982. Nephrotoxicity of p-aminophenol, a metabolite of acetaminophen, in the fischer 344 rat. *Toxicology and Applied Pharmacology.* 65 : 336-44

11. R Core Team. 2012. R: A language and environment for statistical computing.

APPENDIX A

Glossary

$C =$ Blood concentration of model compound in each compartment (mM)

$V =$ Volume of tissue compartment (L)

$V^i_{Lumen} =$ Lumen volume of the ith small intestine compartment (L), calculated as function of the small intestine length, the fractional length, the proximal radius and the distal radium of the ith segment.

$k_s =$ Gastric emptying rate in fasted GI state constant (1/hr)

$k_{dissolve} =$ Dissolution constant, calculated using dissolution coefficient, drug particle radius, drug particle density and diffusion layer thickness.

$k_t =$ Intestinal transfer constant (1/hr)

$S_i =$ Solubility of the drug corresponding to the pH in the ith gastrointestinal compartment, calculated using the pKa of the compound, employing the Henderson-Hasselbach equation.

$k^i_a =$ Absorption rate constant in the ith gastrointestinal compartment, calculated as function of effective permeability ($\log P_{eff}$), surface area and lumen volume of each segment in the gastrointestinal tract.

$K_{B/P} =$ Blood to plasma ratio

$Kpu =$ Unbound tissue-to-plasma partition coefficient

$fu_p =$ Fraction protein unbound in plasma

$Q =$ Blood flow rate (L/hr)

$K_m =$ *In vivo* Michaelis constant (mM)

$V_{max} =$ *In vivo* maximal metabolic velocity (mmol/hr)

$f_{NAT} =$ Scale factor to account for acetylation pathway of metabolism

APPENDIX B

Differential equations of the ACAT model

Stomach:

$$V_{Lumen}^{Stomach} \cdot \frac{dC_{undissolved}^{Stomach}}{dt}$$

$$= -k_s \cdot C_{undissolved}^{Stomach} \cdot V_{Lumen}^{Stomach}$$

$$- k_{dissolve} \cdot C_{undissolved}^{Stomach} \left(S_{Stomach} - C_{dissolved}^{Stomach} \right) \cdot V_{Lumen}^{Stomach}$$

$$V_{Lumen}^{Stomach} \cdot \frac{dC_{dissolved}^{Stomach}}{dt}$$

$$= -k_s \cdot C_{dissolved}^{Stomach} \cdot V_{Lumen}^{Stomach}$$

$$+ k_{dissolve} \cdot C_{undissolved}^{Stomach} \left(S_{Stomach} - C_{dissolved}^{Stomach} \right) \cdot V_{Lumen}^{Stomach}$$

$$- k_a^{Stomach} \cdot C_{dissolved}^{Stomach} \cdot V_{Lumen}^{Stomach}$$

$$V_{Wall}^{Stomach} \cdot \frac{dC_{Wall}^{Stomach}}{dt}$$

$$= Q_{Wall}^{Stomach} \cdot \left(C_{Artery} - \frac{C_{Wall}^{Stomach} \cdot K_{B/P}}{fu_p \cdot Kpu^{Stomach}} \right) + k_a^{Stomach} \cdot C_{dissolved}^{Stomach} \cdot V_{Lumen}^{Stomach}$$

First segment of small intestine:

$$V_{Lumen}^{SI^1} \cdot \frac{dC_{undissolved}^{SI^1}}{dt}$$

$$= k_s \cdot C_{dissolved}^{Stomach} \cdot V_{Lumen}^{Stomach} - k_t \cdot C_{undissolved}^{SI^1} \cdot V_{Lumen}^{SI^1}$$

$$- k_{dissolve} \cdot C_{undissolved}^{SI^1} \left(S_{SI^1} - C_{dissolved}^{SI^1} \right) \cdot V_{Lumen}^{SI^1}$$

$$V_{Lumen}^{SI^1} \cdot \frac{dC_{dissolved}^{SI^1}}{dt}$$

$$= k_s \cdot C_{dissolved}^{Stomach} \cdot V_{Lumen}^{Stomach} - k_t \cdot C_{dissolved}^{SI^1} \cdot V_{Lumen}^{SI^1}$$

$$+ k_{dissolve} \cdot C_{undissolved}^{SI^1} \left(S_{SI^1} - C_{dissolved}^{SI^1} \right) \cdot V_{Lumen}^{SI^1}$$

$$- k_a^{SI^1} \cdot C_{dissolved}^{SI^1} \cdot V_{Lumen}^{SI^1}$$

$$V_{Wall}^{SI^1} \cdot \frac{dC_{Wall}^{SI^1}}{dt} = Q_{Wall}^{SI^1} \cdot \left(C_{Artery} - \frac{C_{Wall}^{SI^1} \cdot K_{B/P}}{fu_p \cdot Kpu^{SI^1}} \right) + k_a^{SI^1} \cdot C_{dissolved}^{SI^1} \cdot V_{Lumen}^{SI^1}$$

Other segments of small intestine:

$$V_{Lumen}^{SI^i} \cdot \frac{dC_{undissolved}^{SI^i}}{dt}$$

$$= k_t \cdot C_{undissolved}^{SI^{i-1}} \cdot V_{Lumen}^{SI^{i-1}} - k_t \cdot C_{undissolved}^{SI^i} \cdot V_{Lumen}^{SI^i}$$

$$- k_{dissolve} \cdot C_{undissolved}^{SI^i} \left(S_{SI^i} - C_{dissolved}^{SI^i} \right) \cdot V_{Lumen}^{SI^i}$$

$$V_{Lumen}^{SI^i} \cdot \frac{dC_{dissolved}^{SI^i}}{dt}$$

$$= k_t \cdot C_{dissolved}^{SI^{i-1}} \cdot V_{Lumen}^{SI^{i-1}} - k_t \cdot C_{dissolved}^{SI^i} \cdot V_{Lumen}^{SI^i}$$

$$+ k_{dissolve} \cdot C_{undissolved}^{SI^i} \left(S_{SI^i} - C_{dissolved}^{SI^i} \right) \cdot V_{Lumen}^{SI^i}$$

$$- k_a^{SI^i} \cdot C_{dissolved}^{SI^i} \cdot V_{Lumen}^{SI^i}$$

$$V_{Wall}^{SI^i} \cdot \frac{dC_{Wall}^{SI^i}}{dt} = Q_{Wall}^{SI^i} \cdot \left(C_{Artery} - \frac{C_{Wall}^{SI^i} \cdot K_{B/P}}{fu_p \cdot Kpu^{SI^i}} \right) + k_a^{SI^i} \cdot C_{dissolved}^{SI^i} \cdot V_{Lumen}^{SI^i}$$

Where i from 2 to 7.

Colon:

$$V_{Lumen}^{Colon} \cdot \frac{dC_{undissolved}^{Colon}}{dt}$$

$$= k_t \cdot C_{undissolved}^{SI^7} \cdot V_{Lumen}^{SI^7} - k_{t(CO)} \cdot C_{undissolved}^{Colon} \cdot V_{Lumen}^{Colon}$$

$$- k_{dissolve} \cdot C_{undissolved}^{Colon} \left(S_{Colon} - C_{dissolved}^{Colon} \right) \cdot V_{Lumen}^{Colon}$$

$$V_{Lumen}^{Colon} \cdot \frac{dC_{dissolved}^{Colon}}{dt}$$

$$= k_t \cdot C_{dissolved}^{SI^7} \cdot V_{Lumen}^{SI^7} - k_{t(CO)} \cdot C_{dissolved}^{Colon} \cdot V_{Lumen}^{Colon}$$

$$+ k_{dissolve} \cdot C_{undissolved}^{Colon} \left(S_{Colon} - C_{dissolved}^{Colon} \right) \cdot V_{Lumen}^{Colon}$$

$$- k_a^{Colon} \cdot C_{dissolved}^{Colon} \cdot V_{Lumen}^{Colon}$$

$$V_{Wall}^{Colon} \cdot \frac{dC_{Wall}^{Colon}}{dt} = Q_{Wall}^{Colon} \cdot \left(C_{Artery} - \frac{C_{Wall}^{Colon} \cdot K_{B/P}}{fu_p \cdot Kpu^{Colon}} \right) + k_a^{Colon} \cdot C_{dissolved}^{Colon} \cdot V_{Lumen}^{Colon}$$

APPENDIX 3 – Differential equations of the disposition model

Venous blood:
$$V_{Vein} \cdot \frac{dC_{Vein}}{dt} = Q_{Vein} \cdot \left(\frac{1}{\sum Q_{tis}} \sum \frac{Q_{tis} \cdot C_{tis} \cdot K_{B/P}}{fu_p \cdot Kpu^{tis}} - C_{Vein} \right)$$

Arterial blood:
$$V_{Artery} \cdot \frac{dC_{Artery}}{dt} = Q_{Artery} \cdot \left(\frac{C_{Lung} \cdot K_{B/P}}{fu_p \cdot Kpu^{Lung}} - C_{Artery} \right)$$

Adipose:
$$V_{Adipose} \cdot \frac{dC_{Adipose}}{dt} = Q_{Adipose} \cdot \left(C_{Artery} - \frac{C_{Adipose} \cdot K_{B/P}}{fu_p \cdot Kpu^{Adipose}} \right)$$

Muscle:
$$V_{Muscle} \cdot \frac{dC_{Muscle}}{dt} = Q_{Muscle} \cdot \left(C_{Muscle} - \frac{C_{Muscle} \cdot K_{B/P}}{fu_p \cdot Kpu^{Muscle}} \right)$$

Skin:
$$V_{Skin} \cdot \frac{dC_{Skin}}{dt} = Q_{Skin} \cdot \left(C_{Muscle} - \frac{C_{Skin} \cdot K_{B/P}}{fu_p \cdot Kpu^{Skin}} \right)$$

Lung:
$$V_{Lung} \cdot \frac{dC_{Lung}}{dt} = Q_{Lung} \cdot \left(C_{Lung} - \frac{C_{Lung} \cdot K_{B/P}}{fu_p \cdot Kpu^{Lung}} \right)$$

Pancreas:
$$V_{Pancreas} \cdot \frac{dC_{Pancreas}}{dt} = Q_{Pancreas} \cdot \left(C_{Pancreas} - \frac{C_{Pancreas} \cdot K_{B/P}}{fu_p \cdot Kpu^{Pancreas}} \right)$$

Spleen:
$$V_{Spleen} \cdot \frac{dC_{Spleen}}{dt} = Q_{Spleen} \cdot \left(C_{Spleen} - \frac{C_{Spleen} \cdot K_{B/P}}{fu_p \cdot Kpu^{Spleen}} \right)$$

Bone:
$$V_{Bone} \cdot \frac{dC_{Bone}}{dt} = Q_{Bone} \cdot \left(C_{Bone} - \frac{C_{Bone} \cdot K_{B/P}}{fu_p \cdot Kpu^{Bone}} \right)$$

Brain:

$$V_{Brain} \cdot \frac{dC_{Brain}}{dt} = Q_{Brain} \cdot \left(C_{Brain} - \frac{C_{Brain} \cdot K_{B/P}}{fu_p \cdot Kpu^{Brain}} \right)$$

Heart:

$$V_{Heart} \cdot \frac{dC_{Heart}}{dt} = Q_{Heart} \cdot \left(C_{Heart} - \frac{C_{Heart} \cdot K_{B/P}}{fu_p \cdot Kpu^{Heart}} \right)$$

Thymus:

$$V_{Thymus} \cdot \frac{dC_{Thymus}}{dt} = Q_{Thymus} \cdot \left(C_{Thymus} - \frac{C_{Thymus} \cdot K_{B/P}}{fu_p \cdot Kpu^{Thymus}} \right)$$

Liver:

$$V_{Liver} \cdot \frac{dC_{Liver}}{dt} = Q_{Liver} \cdot \left(C_{Liver\_in} - \frac{C_{Liver} \cdot K_{B/P}}{fu_p \cdot K_{pu}^{Liver}} \right) - f_{NAT} \cdot \frac{V_{max} \cdot \frac{C_{Liver}}{K_{pu}^{Liver}}}{K_m + \frac{C_{Liver}}{Kpu^{Liver}}}$$

$$C_{Liver\_in} = \frac{1}{Q_{Spleen} + Q_{Pancreas} + Q_{Hepatic\_Artery} + \sum_{i=1}^{9} Q_{Wall^i}} \cdot \left(\frac{Q_{Spleen} \cdot C_{Spleen} \cdot K_{B/P}}{fu_p \cdot Kpu^{Spleen}} \right.$$
$$+ \frac{Q_{Pancreas} \cdot C_{Pancreas} \cdot K_{B/P}}{fu_p \cdot Kpu^{Pancreas}} + Q_{Hepatic\_Artery} \cdot C_{Artery}$$
$$\left. + \sum_{i=1}^{9} \frac{Q_{Wall^i} \cdot C_{Wall^i} \cdot K_{B/P}}{fu_p \cdot Kpu^{Wall^i}} \right)$$

Kidney:

$$V_{Kidney} \cdot \frac{dC_{Kidney}}{dt} = Q_{Kidney} \cdot \left(C_{Artery} - \frac{C_{Kidney} \cdot K_{B/P}}{fu_p \cdot Kpu^{Kidney}} \right)$$